Optical Communication and Attitude Control Solutions for CubeSats

a project presented to
The Faculty of the Department of Aerospace Engineering
San José State University

in partial fulfillment of the requirements for the degree
Master of Science in Aerospace Engineering

by

Roberto Rosila Mares

December 2024

approved by

Dr. Periklis Papadopoulos
Faculty Advisor

ABSTRACT

Exploring Optical Communication and Attitude Control Solutions for CubeSats

Roberto Rosila Mares

This paper provides a preliminary exploration of existing optical communication approaches tailored for CubeSat platforms. We review fundamental principles, current system designs, and ongoing technological advancements in laser-based downlinks, inter-satellite links, and compact optical terminals. By examining existing hardware, modulation schemes, and pointing control methods, we highlight both the opportunities and challenges inherent to integrating optical communications into CubeSat missions. Since control on pointing is critical, we also explore a cold gas thruster nozzle design and tank configuration to improve attitude control and enhance communication stability. This exploration aims to inform future developments in miniaturized, high-bandwidth, and power-efficient optical communication solutions, ultimately enhancing CubeSat capabilities in Earth observation, deep space exploration, and scientific data return.

Acknowledgements

To fully acknowledge everyone who helped me reach this point would require far more than one acknowledgement section. From my family and friends to my professors, mentors, and colleagues, I am profoundly grateful to all who have supported me on my academic and professional journey—a journey that has never followed a straight path. This project has been no small undertaking, and I want to give proper recognition to those who have helped me time and time again.

To my parents, who came to this country and encouraged me to strive for greatness, supporting me unconditionally and understanding my journey more intimately than anyone: I love you, Mom, Maria Elena, and Dad, Prisciliano. To my siblings: Maria, Priscilla, and Jesus, who have proofread countless papers and even assisted me in some of my projects, thank you for always being there. To my partner Rosy, who has patiently weathered all of my ambitious endeavors—including the completion of this master's thesis—I appreciate your unwavering support.

To my professor, Dr. Periklis Papadopoulos, who understands better than anyone how challenging this project has been. I am deeply grateful for you sticking with me all these years. It may have taken me two thesis-level projects to reach graduation, but I will forever be thankful that you have always believed in my work.

Table of Contents

ABSTRACT iv
Acknowledgements v
Table of Contents vi
List of Figures x
List of Tables xii
Symbols and Abbreviations xiii
Chapter 1. Introduction 14
1.1 Motivation 14
1.2 Presentation of First Thesis 15
Chapter 2. Literature Review: Advancements in Optical Communication for CubeSats 16
2.1 Introduction 16
2.2 Background 16
2.3 Key Themes in CubeSat Optical Communication 17
2.3.1 High Data Rate Systems 17
2.3.2 Inter Satellite Links (ISLs), or Crosslinks 17
2.3.3 Quantum Communication Payloads 17
2.3.4 Miniaturized Optical Terminals 17
2.3.5 Moon Earth Optical Links 18
2.4 Challenges and Gaps in Research 18
2.4.1 Atmospheric Effects and Beam Stability 18
2.4.2 Integration Constraints 18
2.4.3 Quantum Communication Scalability 18
2.5 Conclusion 18
Chapter 3. Literature Review: Cold Gas Thruster for Cubesats 20
3.1 Introduction 20
3.2 Background 20
3.3 Design and Operational Principles 22
3.4 Performance Metrics and Applications 22
3.5 Technological Innovation and Challenges 23
3.6 Conclusion 24
Chapter 4. Optical Payload Trade Study 25
4.1 NICT Small Optical Transponder (SOTA) Socrates 25
4.1.1 Overview 25
4.1.2 Key Features 25
4.1.3 Experimental Setup and Results 26

4.1.4 Advantages and Implications 26
4.1.5 Future Prospects 26
4.2 DLS OSIRIS v1 Flying Laptop 27
4.2.1 Introduction 27
4.2.2 Performance Evaluation 27
4.2.3 Trade-Off Analysis 28
4.3 DLR OSIRIS v2 BiROS 28
4.3.1 Introduction 28
4.3.2 Overview of OSIRISv2 29
4.3.3 Technical Features 29
4.3.4 Operational Challenges 29
4.3.5 Achievements 30
4.3.6 Future Directions 30
4.4 Aerospace Corporation OCSD-B&C AeroCube-7 30
4.4.1 Introduction 30
4.4.2 Objectives 31
4.4.3 Key Results 31
4.4.4 Conclusion: Trade Space Analysis 31
4.5 NICT VSOTA RISESAT 32
4.5.1 Introduction 32
4.5.2 Objectives 32
4.5.3 Key Results 33
4.5.4 Conclusion and Trade Study Table Summary 33
4.6 Sony/JAXA SOLISS ISS 34
4.6.1 Introduction 34
4.6.2 Objectives 34
4.6.3 Key Results 35
4.6.4 Conclusion 35
4.7 DLR OSIRIS v4 CubeSat PIXL-1 36
4.7.1 Introduction 36
4.7.2 Objectives 36
4.7.3 Key Results 37
4.7.4 Conclusion 37
4.8 MIT CLICK-AB/C 38
4.8.1 Introduction 38
4.8.2 Objectives 39

4.8.3 Key Results 39
4.8.4 Conclusion 39
4.9 AAC Clyde Space CubeCat 40
4.9.1 Introduction 40
4.9.2 Objectives 40
4.9.3 3. Key Results 41
4.9.4 4. Conclusion 41
4.10 Trade Study Summary Table and Conclusion Statement 41
4.10.1 Key Trends and Outcomes 41
4.10.2 Conclusion 42
4.10.3 Summary Table of Trade Study Characteristics 42
Chapter 5. Cold Gas Thruster Design 44
5.1 Introduction and Motivation 44
5.2 Nozzle Geometry 44
5.3 Mesh Generation for the Nozzle Geometry 45
5.4 Physics and Fluid Model Data 47
5.5 Contour and Animations of the Resulting Model for Time Accurate 49
5.5.1 Mach 49
5.5.2 Pressure 50
5.5.3 Density 51
5.5.4 Temperature 53
Chapter 6. Cold Gas Propulsion Tank Proof of Concept 56
6.1 Propulsion – Rapid 3D Printed Prototype Characteristics 56
6.2 Propellant 57
6.3 Tank for Rapid Prototype 58
Chapter 7. Aluminum Alloy Space Grade Propulsion Tank Analysis 60
7.1.1 Summary of Deflection Base on Results 62
7.1.2 Summary of Stress and Strain 62
Chapter 8. Summary and Future Work 63
8.1 Summary 63
8.2 Future Work 63
References 64
Appendix A: TechEd Sat 8 Presentation 67
Appendix B: Simulation Data at 500 PSI 84
Model Information 84
Study Properties 85

Units 85
Material Properties 86
Loads and Fixtures 86
Contact Information 87
Mesh information 87
Mesh information - Details 87
Resultant Forces 88
Reaction forces 88
Reaction Moments 88
Free body forces 88
Free body moments 88
Study Results 89
Appendix C: Simulation Data at 1000 PSI 91
Model Information 91
Study Properties 92
Units 92
Material Properties 93
Loads and Fixtures 93
Contact Information 94
Mesh information 94
Mesh information - Details 94
Resultant Forces 95
Reaction forces 95
Reaction Moments 95
Free body forces 95
Free body moments 95
Study Results 96
Appendix D: Legend of Symbols, Units, and Abbreviations 99
Units of Measurement & Common Symbols 99
Thermodynamic and Gas Properties 99
Propulsion & Fluid Dynamics 99
Optical Communication and Related Terms 100
Satellite & Aerospace Systems 100
Organizations and Programs 100
Additional Technical Terms 100

List of Figures

Figure 1.1: TechEd Sat 8 Exploded View [1] 14
Figure 1.2: Deployment of TechEd Sat 8 from the ISS [1] 15
Figure 1.3: Presentation of First Thesis [2] 15
Figure 2.1: CubeSat Form Factor [3] 16
Figure 2.2: TBIRD Payload [4] 16
Figure 2.3: SelenIRIS Optical Subsystem [3] 18
Figure 3.1: Propulsion Block Diagram [12] 21
Figure 3.2: Schematic of a Cold Gas Propulsion System [9] 21
Figure 3.3: Exterior Tank Wall of CGP [10] 22
Figure 3.4: Thruster Alignment [12] 23
Figure 4.1: Small Optical Transponder SOTA [16] 25
Figure 4.2: Flying Laptop (FLP) – OSIRIS v1 [18] 27
Figure 4.3: OSIRIS v2 CAD Depiction [17] 29
Figure 4.4: Exploded schematic view of the AeroCube-OCSD CubeSat [20]. 31
Figure 4.5: RISESAT on vibe test table [21] 32
Figure 4.6: HD image transmitted from SOLISS via Laser Communication [23] 34
Figure 4.7:CubeLCT Laser Communication Terminal [24] 36
Figure 4.8: Click-B/C Terminals and Subassemblies [25] 38
Figure 4.9: Optical Bench with Components CAD [25] 38
Figure 4.10: Clyde Space CubeCat [26] 40
Figure 5.1: CGP Nozzle Geometry 44
Figure 5.2: 3D Model of Nozzle Geometry 45
Figure 5.3: Cross Section View of Nozzle Geometry 45
Figure 5.4: Domain Boundary 46
Figure 5.5: Nozzle Geometry and Segments 46
Figure 5.6: Snapshot of Results at 2.7E-004s Showing the Mesh Generation 47
Figure 5.7: Mach Transient State at Time 2.6815×10^-5s 49
Figure 5.8: Mach Transient State at Time 3.5103E00-5s 49
Figure 5.9: Mach Steady state at time 1.7280E-004s 50
Figure 5.10: Pressure Transient state at time 2.6815E00-5s 50
Figure 5.11: Pressure Transient state at time 3.5103E00-5s 51
Figure 5.12: Pressure Steady state at time 1.7280E-004s 51
Figure 5.13: Density Transient state at time 2.6815E00-5s 52
Figure 5.14: Density Transient state at time 3.5103E00-5s 52
Figure 5.15: Density Steady state at time 1.7280E-004s 53
Figure 5.16: Temperature Transient state at time 2.6815E00-5s 53

Figure 5.17: Temperature Transient state at time 2.6815E00-5s 54
Figure 5.18: Temperature Steady state at time 1.7280E-004s 54
Figure 6.1: Rapid prototype for a propulsion system mounting, vessel, and feed system. 58
Figure 6.2: 3D Cross Sectional View of the Prototype Proof of Concept 59
Figure 7.1: Visual Representation of the 1U structure Al 6061-T6 Tank 60
Figure 7.3: Shows 500 PSI results on the left and 1000 PSI results on the right 61

List of Tables

Table 3.1: Summary of notable CGP systems and their performance characteristics. 23
Table 4.1: OSIRIS v1 Performance Characteristics 28
Table 4.2: OSIRIS v2 Performance Parameters 30
Table 4.3: Optical vs RF vs Hybrid (RF + Optical) Approaches 33
Table 4.4: CubeLCT Characteristics 37
Table 4.5: Summary of Click A, B and C Mission 39
Table 4.6: Key Features of Click A, B, and C 39
Table 4.7: Key Tradeoffs between Click A, B, and C 40
Table 4.8: Clyde Space Performance Characteristics 41
Table 4.9: Comparison of SOTA, OSIRIS v1 and v3, CubeLCT, Click, and CubeCAT 42
Table 5.1: Meshe Generation Table 46
Table 5.2: Physics and Fluid Model 47
Table 5.3: Mesh Volume and Boundary Conditions. 48
Table 5.4: Solver, Algorithm, Numerical Integration, Stead State and/or Transient 48
Table 6.1: Requirements for the propulsion subsystem 56
Table 7.1: Aluminum Alloy 6061-T6 Properties 60
Table 7.2: Min and Max Results at for both 500 and 1000 PSI for Displacement 61
Table 7.3: Stress and Strain Results 62

Symbols and Abbreviations

Nomenclature

Acronyms and Abbreviations

BB84 = Quantum key distribution protocol
COTS = Commercial off-the-shelf
CPG = Cold Gas Propulsion
CUBE = CubeSat Unit (1U = 10 cm × 10 cm × 10 cm)
DLR = German Aerospace Center (Deutsches Zentrum für Luft- und Raumfahrt)
ESA = European Space Agency
FSO = Free-Space Optical
HPLD = High-Power Laser Diode
ISS = International Space Station
JAXA = Japan Aerospace Exploration Agency
LEO = Low Earth Orbit
LDGM = Low-Density Generator Matrix
MEMS = Microelectromechanical Systems
NASA = National Aeronautics and Space Administration (U.S.)
NICT = National Institute of Information and Communications Technology (Japan)
OCSD = Optical Communications and Sensor Demonstration
OSIRIS = Optical Space Infrared Downlink System
QKD = Quantum Key Distribution
RF = Radio Frequency
SJSU = San José State University
SOLISS = Small Optical Link for International Space Station
SOTA = Small Optical Transponder
SWaP = Size, Weight, and Power
TBIRD = TeraByte InfraRed Delivery
VSOTA = Very Small Optical Transponder

Roman Symbols

A = Constant in Sutherland's law
B = Constant in Sutherland's law
C_p = Specific heat at constant pressure
C_v = Specific heat at constant volume
I_sp = Specific impulse
M = Mach number
N = Number of cycles or grid points (context dependent)
P = Pressure
Pr = Prandtl number
R = Gas constant
Re = Reynolds number
T = Temperature
t = Time
V = Velocity

Greek Symbols

γ = Ratio of specific heats (C_p/C_v)
μ = Dynamic viscosity
ρ = Density

Units

Pa = Pascal l (N/m^2)
psi = Pounds per square inch

Other Terms

CFD = Computational Fluid Dynamics
LVDS = Low-Voltage Differential Signaling
UART = Universal Asynchronous Receiver-Transmitter

Chapter 1. Introduction

1.1 Motivation

I can pinpoint the exact moment I realized that I wanted to do aerospace engineering. I was sitting in a physics class in high school, and my professor provided us with an example of projectile motion, showing that by applying math and physics, one could accurately calculate where an object would land. Fast forward over a decade since that experience, and I have now gone to school, worked in industry, taken a break from my master's program, and returned—while still working in industry—to finish my degree. Since that moment in high school, I have had the chance to work on numerous projects: going to Mexico to serve as a wind tunnel design advisor, working for a startup out of Moffett Field where we attempted to develop telecommunications in remote areas for truck drivers (the project failed), developing CubeSats at NASA Ames, helping with power system designs at R&D facilities, and working on large satellites in geostationary orbit.

Furthermore, my original thesis project flew from the ISS a few years ago, but I never completed the thesis itself. After many years of working in the industry, one thing always lingered in my mind—an incomplete master's degree. So, here I am, a few years since my original project flew from the ISS, shown in Figure 1.1 and Figure 1.2. completing a new trade study project to fulfill my master's degree requirements. However, the advantage of prolonging this milestone—a master's degree in aerospace engineering—has its benefits. The perspective and knowledge I've gained over time can now be applied directly to this new project.

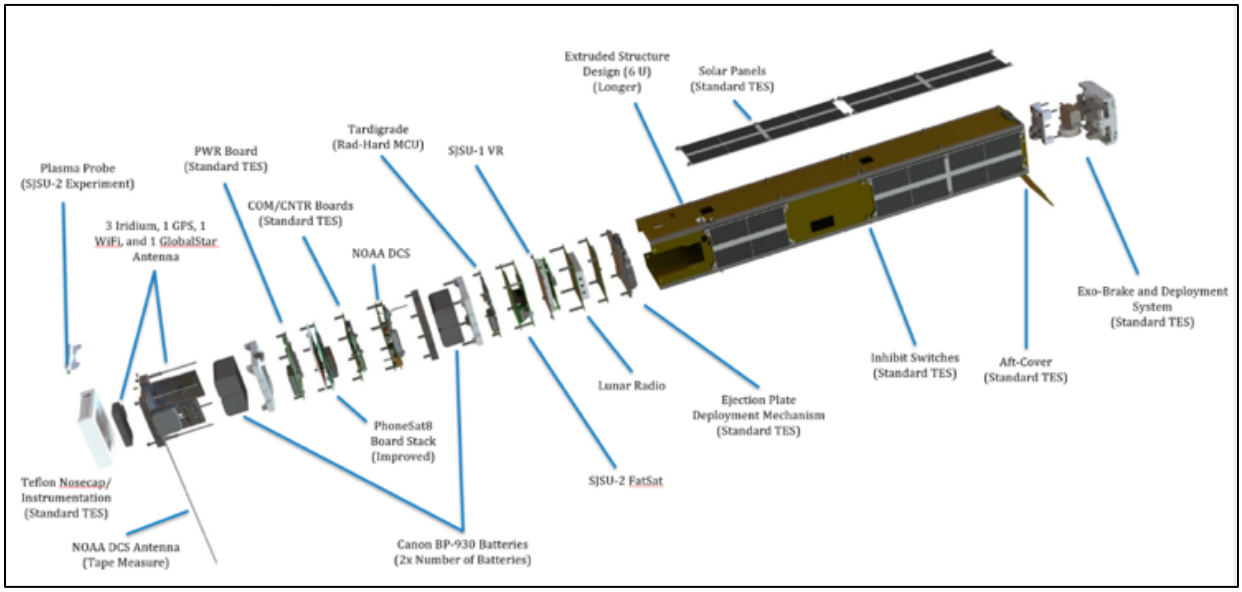

Figure 1.1: TechEd Sat 8 Exploded View [1]

Figure 1.2: Deployment of TechEd Sat 8 from the ISS [1]

1.2 Presentation of First Thesis

I am including this up front for the faculty because my first thesis experiment was conducted and flown within 1 year, SJSU VR experiment. The charts were presented at a conference in Cal Poly, title page is shown in Figure 1.3. This first thesis serves as my motivation to complete my degree at SJSU. It was a very rare experience to get to work on something while in college and have it jettison from the ISS. Lastly, I do want to highlight that my brother presented this package at Cal Poly as he was a mentee[2]. For the complete presentation chart package please refer to Appendix A: SJSU Virtual Reality, View from a CubeSat.

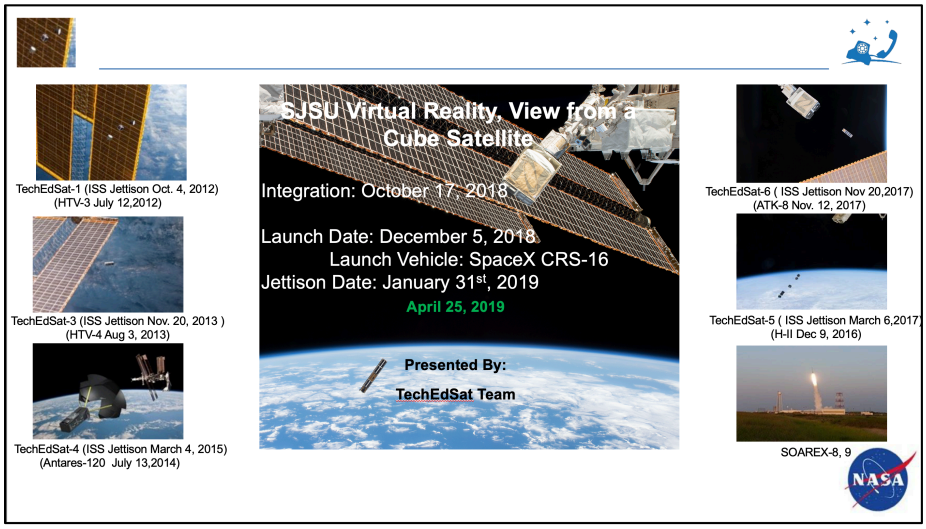

Figure 1.3: Presentation of First Thesis [2]

Chapter 2. Literature Review: Advancements in Optical Communication for CubeSats

2.1 Introduction

Cubesats are small satellites that are built on a 10cm x 10cm x 10cm structure form factor called a 1U. This form factor can expand by 5 or 10 cm in either x, y, or z direction to increase the U-factor of a CubeSat (i.e. 10x10x20 cm is equal to a 2U), as shown in Figure 2.1. These small form factor satellites have made space more accessible to rapid developments in technology and research. One area where they have been utilized for is optical communication payload design – Free Space Optical communication (FSO). Optical communication is an alternative to traditional RF communication. Some of its advantages over RF communication lie in more efficient use of power and volume, superior data rates, and stronger data protection. Furthermore, this section aims to highlight some of the recent developments in optical communication tailored for CubeSat platform.

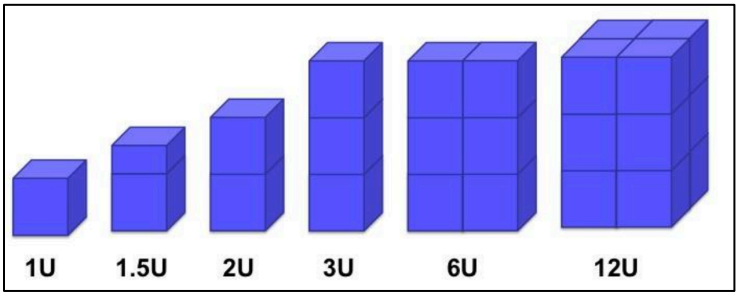

Figure 2.1: CubeSat Form Factor [3]

2.2 Background

Optical communication systems differ from RF systems in one very distinct way, they use laser beams to perform data transfer. In this section we will look at a few examples that cover some achievement in the FSO. For example, NASA's TBIRD, shown in Figure 2.2, mission established a record-breaking 200 Gbps optical downlink from a CubeSat [4]. Another advancement has been the miniaturization of optical terminals to fit within the tight form factor and resource constraints of CubeSats [5].

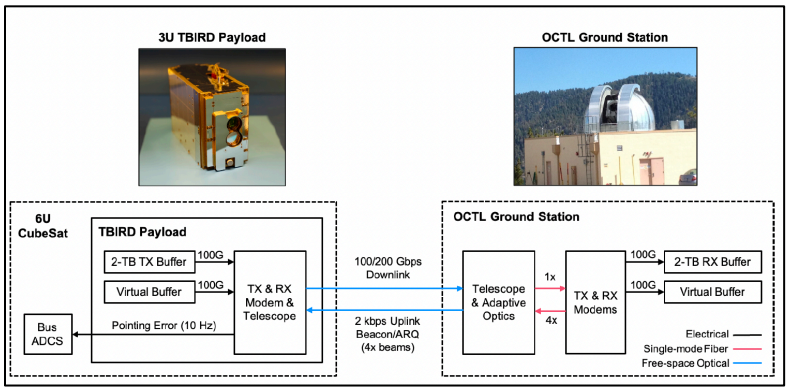

Figure 2.2: TBIRD Payload [4]

2.3 Key Themes in CubeSat Optical Communication

2.3.1 High Data Rate Systems

High data-rate systems are critical for applications for Earth observation and scientific data transmission. In addition, these data rates require more throughput and faster data rates to get information down for critical missions. The TBIRD payload is one example of demonstrating the capabilities of achieving a high data transfer, 200 Gbps downlink over 1 terabyte of data in 5 minutes [4]. Another example is the OSIRIS v4 CubeSat Payload that was created by the German Aerospace Center (DLR). This payload was capable of supporting data rates up to 100 Mbps at 8.5 W [5].

2.3.2 Inter Satellite Links (ISLs), or Crosslinks

ISLs, or crosslinks, facilitate data relay and constellation-level communication. Crosslinks are extremely important because as satellites become smaller with lower orbits, they sometimes will need to relay data information to another satellite to allow for data to be downlinked in an adequate time at a desired ground station. Therefore, they need a stable optical communication crosslink to be able to relay the information. An example of that is the CubeSat Laser Infrared Crosslink (CLICK) mission, which showcased a dual-channel optical system capable of maintaining links over distances up to 580 km while achieving a precision ranging of better than 50 cm [6]. Such advancements in this technology will enable faster communication across satellites in different orbits to allow for a data downlink to be established at ground station to the closest satellite in view.

2.3.3 Quantum Communication Payloads

Quantum communication is a growing field aimed at leveraging CubeSats for secure key distribution prototyping. We currently live a time where encryption is becoming more important due to that fact that cyber security is constantly in jeopardy by new technological advancement. For example, your private message and sensitive date could be more easily accessible by people with mal-intent. Quantum communication with quantum key distribution is one future technology that can provide more secure communication to mitigate security threats to data.

Therefore, systems like the Micius satellite have demonstrated feasibility where CubeSats could offer a cost-efficiency for scaling these technologies. A recent study proposed a CubeSat payload capable of implementing quantum key distribution (QKD) using the BB84 protocol, achieving a secret key rate of 80 kHz at zenith [7]. Such designs emphasize the role of CubeSats in advancing quantum networks to maintain more secure communication and data protection.

2.3.4 Miniaturized Optical Terminals

Miniaturization is pivotal point for CubeSat applications. Miniaturization contributes to lower cost, weight, energy consumption, and material which are all highly important when developing a space mission. An experiment that aims to echo the importance of miniaturization is DLR’s OSIRIs v4 Cubesat. It is the smallest optical terminal, occupying just 1/3 of a CubeSat unit while delivering robust downlink capabilities [5].

2.3.5 Moon Earth Optical Links

However not every mission that we design for space is meant to stay within Earth's orbits. Missions like SelenIRIS are adapting CubeSat optical systems for lunar applications. Figure 2.3 shows a CAD model of the SelenIRIS optical subsystem. These systems aim to deliver high-speed data rates over the Moon-Earth distance, leveraging innovations in fine pointing assemblies and optical amplifiers [8].

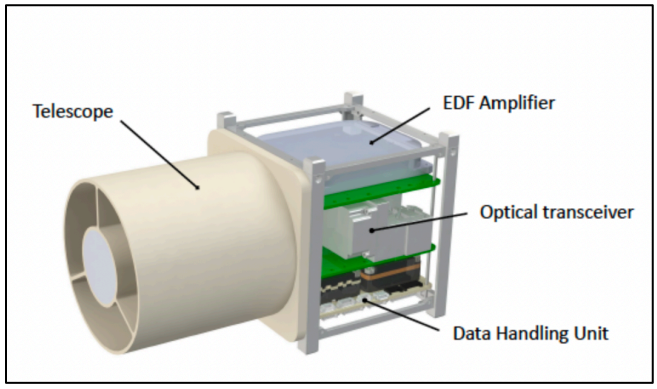

Figure 2.3: SelenIRIS Optical Subsystem [3]

2.4 Challenges and Gaps in Research

2.4.1 Atmospheric Effects and Beam Stability

Optical communication systems are highly susceptible to atmospheric conditions, which can distort beams and degrade signal quality. Mitigation strategies, including adaptive optics and error correction protocols, have been explored, but more robust solutions are needed for consistent performance under these harsh varying conditions [4].

2.4.2 Integration Constraints

Designing payloads to be within a CubeSats form factor poses significant challenges. For optical payloads key design trade-offs between aperture size, power consumption, and thermal management often limit system performance. Studies like Lin [6] highlight the need for more efficient designs that optimize optical and mechanical integration. However, it is important to remember as a design miniaturizes, complexity for performance tends to increase.

2.4.3 Quantum Communication Scalability

While QKD systems show promise, scaling quantum communication protocols for CubeSat constellations requires further innovation. Issues such as photon loss, limited onboard resources, and synchronization need addressing for broader adoption [7]. Emerging trends and innovations recent research is exploring hybrid communication systems combining RF and optical technologies to leverage the strengths of both. Advances in material science and fabrication techniques are also enabling more efficient optical components, further pushing the limits of CubeSat optical communication capabilities [5; 6].

2.5 Conclusion

CubeSat optical communication systems have advanced significantly, with milestones such as the 200-Gbps TBIRD downlink and the development of modular, miniaturized optical

terminals. These innovations pave the way for applications ranging from Earth observation to inter-satellite networking and quantum communication. However, challenges such as atmospheric distortion, integration constraints, and the scalability of quantum protocols remain. Future research should focus on overcoming these barriers while leveraging emerging technologies to enhance system/performance. By addressing these gaps, CubeSats will play a transformative role in global communication networks and space exploration.

Chapter 3. Literature Review: Cold Gas Thruster for Cubesats

3.1 Introduction

CubeSats, as we have discussed earlier, have revolutionized, space exploration by offering cost-effective and accessible platforms for a wide range of missions. However, a challenge that is not only applied to launch vehicles (rockets) is also applied to satellites – the propulsion system. However, unliked launch vehicles, CubeSats can utilize a type of propulsion system known as Cold Gas Propulsion (CPG). Cold gas propulsion systems on satellites are extremely valuable because they remove the added complexity of managing "controlled explosions." This means they can provide a solution that is simple, safe, and reliable for CubeSats.

A cold gas propulsion system operates by expelling compressed gas through a nozzle to produce through – it does not require any ignition. Due to its simplicity, this technology has become increasingly attractive for CubeSat missions, particularly for tasks such as station-keeping, attitude control, and orbital transfers.

Furthermore, this literature review explores the principles, technological advancements, and applications of CGP systems, with a focus on their implementation in CubeSats. The significance of CGP lies in its ability to provide controlled propulsion for small satellite missions, enabling capabilities previously restricted to larger spacecraft. Challenges in efficiency will be addressed in different ways: materials development, manufacturing techniques, general performance, and how they are considered for different mission needs.

3.2 Background

Cold gas propulsion systems generate thrust through the controlled ejection of pressurized gas – they do not have a combustion phase. The core components include a tank, valves, standard plumbing, and a nozzle. Figure 3.1 shows an example of what a detailed block diagram for a cold gas propulsion system looks like [12]. . A simplified version of a cold gas propulsion system is shown in Figure 3.1. Its driving performance parameters: type of propellant, propellant pressure, and nozzle geometry to name a few. For example, gases like nitrogen, argon, and butane are commonly used as propellants due to their inert properties and ease of storage.

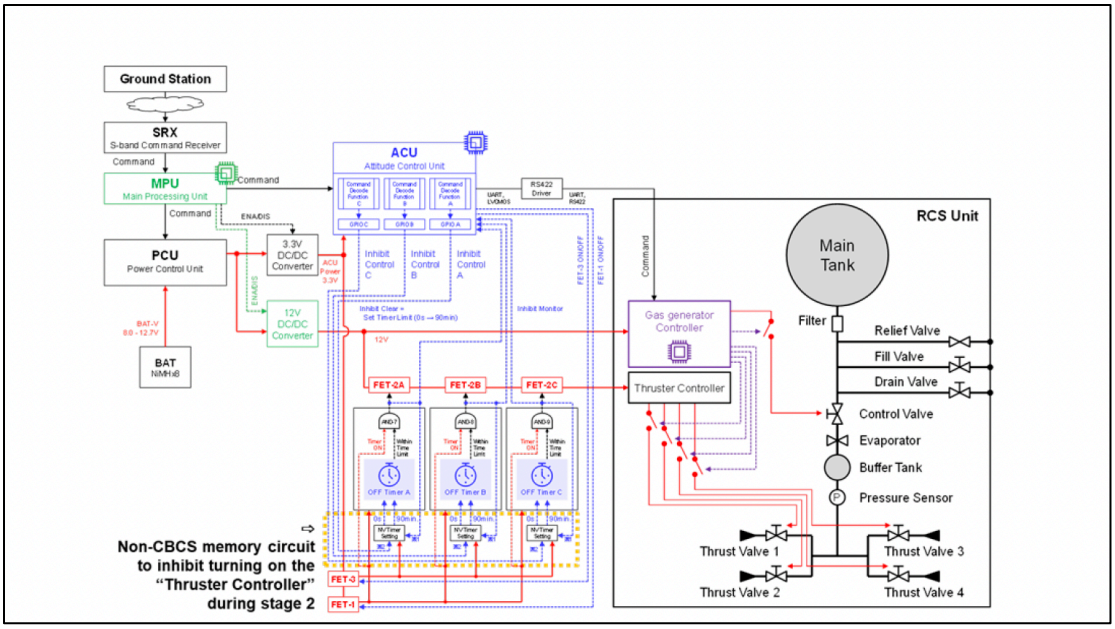

Figure 3.1: Propulsion Block Diagram [12]

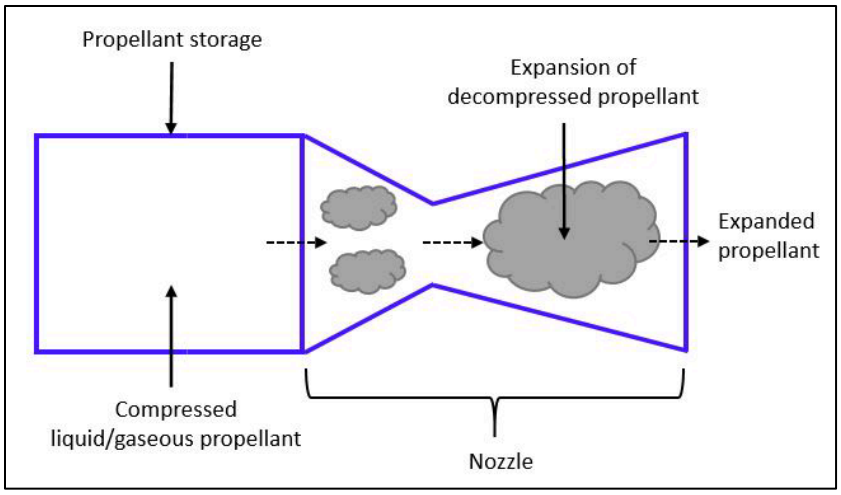

Figure 3.2: Schematic of a Cold Gas Propulsion System [9]

Innovative designs have improved the efficiency and integration of CGP systems within CubeSats architecture framework. As an example, innovation in 3D-printed components that integrate tanks, feed pipes, and nozzles into a single unit have provided easier cubesat form factor compliance. 3D printing not only not only reduces the overall mass of the system but also minimizes the risk of leaks and optimizes the use of limited space within the satellite.

Another significant innovation is the development of cubic-shaped tanks that maximize the storage capacity within the standard CubeSat dimensions. Research has shown that these designs can increase the delta-V, or velocity change, available to the satellite by up to 35 percent compared to traditional spherical tanks, although at the cost of increased structural mass [10]. Figure 3.2, shows how shell portion of a CGP tank handles pressure loads. It also provide a reference on how to save mass on a design by creating a rib like structure.

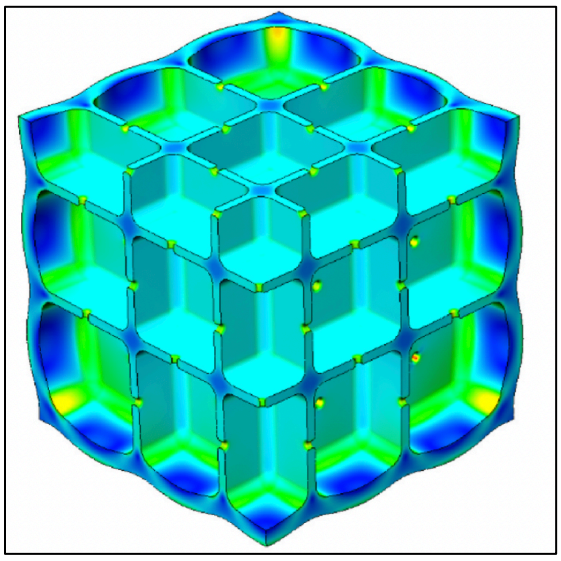

Figure 3.3: Exterior Tank Wall of CGP [10]

3.3 Design and Operational Principles

Cold gas propulsion systems working principles from physics is gas expansion through a nozzle to generate thrust. The primary method to achieve this in a CPG propulsion system is by storing high-pressure gas in a tank, and then releasing it through a nozzle. As the gas moves through the nozzle it will expand and accelerate, creating a reactive force. System performance is influence by propellant's molecular weight, storage pressure, and the design of the nozzle. For example, gases like nitrogen, argon, and butane are commonly used as propellants due to their inert properties and ease of storage.

3.4 Performance Metrics and Applications

The effectiveness of a CGP system is typically evaluated based on key performance metrics, including thrust, specific impulse, and delta-V. Specific impulse, a measure of the efficiency of a propulsion system, typically ranges between 40 and 50 seconds for most CGP systems. While this is lower than that of electric or chemical propulsion systems, it is adequate for the modest propulsion needs of CubeSats The effectiveness of a CGP system is typically evaluated based on key performance metrics, including thrust, specific impulse, and delta-V. Specific impulse, a measure of the efficiency of a propulsion system, typically ranges between 40 and 50 seconds for most CGP systems. While this is lower than that of electric or chemical propulsion systems, it is adequate for the modest propulsion needs of CubeSats [9; 11; 12]. For instance, the HOKUSHIN-1 CubeSat, equipped with a 1U-sized CGP system, achieved sufficient thrust for orbit maintenance and attitude control in a low Earth orbit mission [12].

Applications of CGP systems in CubeSats include but are not limited to:

- Station-keeping, where the propulsion system counteracts orbital decay
- Attitude control, where precise thrust is used to stabilize or reorient the satellite;
- Orbital transfers, where the satellite changes its trajectory within or between orbits.

In interplanetary missions, such as NASA's BioSentinel CubeSat, CGP systems have been employed for momentum management and small-scale maneuvers, demonstrating their adaptability to diverse mission profiles [13].

Table 3.1: Summary of notable CGP systems and their performance characteristics.

System	Thrust (mN)	Specific Impulse (s)	Delta-V (m/s)	Propellant	Mission	Reference
BioSentinel CGP	40-70 (mN)	~50	0.4	Refrigerant	Interplanetary	Lightsey, (2018)
HOKUSHIN-1 RCS	18 – 90 µN (per nozzle)	~40	~15	Butane	ISS Deployment	Komachi (2024)
CanX-2	50	45	2	Nitrogen	Earth Observation	Kvell (2014)

Table 3.1 illustrates the thrust, specific impulse, delta-V, and propellant used by different CubeSat missions employing cold gas propulsion systems.

Figure 3.3 is an example of how one could incorporate canted thrusters to support attitude control (i.e. stabilization or reorientation).

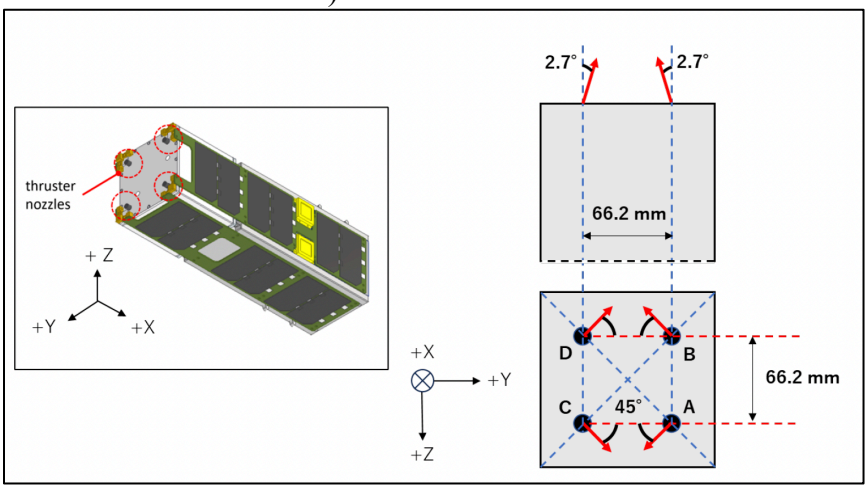

Figure 3.4: Thruster Alignment [12]

3.5 Technological Innovation and Challenges

Recent technological advancements have significantly enhanced the capabilities of CGP systems. The use of 3D printing has allowed for the production of custom-designed components that optimize the system's efficiency and compatibility with CubeSat architectures. Similarly, the integration of MEMS technology has enabled precise control of gas flow, making CGP systems suitable for high-accuracy applications such as scientific measurements or formation flying [14]. Furthermore, high-temperature ceramics and advanced materials have allowed for the development of robust systems capable of withstanding extreme environmental conditions [11].

However, several challenges remain. The low specific impulse of CGP systems limits their efficiency compared to other propulsion technologies. Additionally, the design of propellant tanks that maximize storage while maintaining structural integrity within the CubeSat's dimensions is an ongoing engineering challenge. Finally, while CGP systems have proven

effective in low Earth orbit, their performance in the harsher conditions of deep space missions requires further validation [10].

3.6 Conclusion

Cold gas propulsion systems have established themselves as a reliable and practical solution for CubeSat propulsion needs. Their simplicity, safety, and adaptability make them an ideal choice for small satellite missions, enabling capabilities such as station-keeping, attitude control, and orbital transfers. Technological innovations, including 3D-printed components and MEMS technology, have further enhanced their efficiency and applicability. However, addressing the challenges of low specific impulse and optimizing propellant storage will be crucial for expanding their use in more demanding missions, such as interplanetary exploration. Future research should focus on these areas, alongside long-term performance testing in diverse orbital and space environments, to unlock the full potential of CGP systems in advancing CubeSat technology.

Chapter 4. Optical Payload Trade Study

4.1 NICT Small Optical Transponder (SOTA) Socrates

4.1.1 Overview

The Small Optical Transponder (SOTA), shown in Figure 4.1, was developed by the National Institute of Information and Communications Technology (NICT) as part of the Space Optical Communications Research Advanced Technology Satellite (SOCRATES) project. It is a compact optical communication payload designed for low-earth orbit (LEO) satellites to evaluate satellite-to-ground laser communication links. The system emphasizes resolving challenges like atmospheric turbulence and signal fading through advanced error-correction methodologies [15].

Figure 4.1: Small Optical Transponder SOTA [16]

4.1.2 Key Features

1. System Design and Payload:
   - Mass: 5.9 kg (optical and electrical components).
   - Power consumption: <16W during communication.
   - Operates on a 50 kg-class small satellite with a size of ~50 cm and power availability of approximately 100W.
2. Laser System:

Equipped with four lasers for communication and measurement:

- TX1: 976 nm.
- TX4: 1549 nm for communication.
- TX2 & TX3: 800 nm band for polarization measurements.
- Receiver operates at 1064 nm with beam tracking capabilities via quadrant detectors and fast-pointing mirrors.

3. Modulation and Error Correction:

- Modulation: On-Off Keying (OOK) and Non-Return-to-Zero (NRZ).
- Error-correcting codes: Reed-Solomon and Low-Density Generator Matrix (LDGM) codes.

4. Link Characteristics:
   - Data rates: 1 Mbps or 10 Mbps.
   - Transmission range: Up to 1000 km.
   - Beam divergence: approximately 223 μrad for TX4.

4.1.3 Experimental Setup and Results

1. Mission Objectives:
   - Conduct laser communication experiments to analyze atmospheric effects on signal transmission and validate error correction techniques.
   - Evaluate the system's performance against theoretical link budget and Rytov approximation.
2. Success Criteria:
   - Minimum: Equipment startup and sensor verification.
   - Success: Tracking tests and bit error rate (BER) measurements.
   - Full: Data transmission and error correction validation.
   - Extra: Polarization measurements and collaborations with international ground stations.
3. Performance Metrics:
   - Received power validated theoretical predictions within ~2 dB accuracy under Rytov approximation, with minor discrepancies due to atmospheric and tracking errors.
   - LDGM coding demonstrated robust error correction, recovering data with error rates as high as 35%.
4. Progress and Partnerships:
   - International experimental campaigns included collaborations with ESA, DLR, CNES, and CSA.
   - Initial experiments began in August 2014, with the system proving functional and stable.

4.1.4 Advantages and Implications

- The SOTA demonstrates a scalable and efficient platform for future optical communication in small satellites, providing significant advancements in handling atmospheric challenges and enabling high-speed data transfer.
- The integration of advanced error-correction codes like LDGM enhances reliability in data transmission over laser links.

4.1.5 Future Prospects

Future research aims to expand on experimental success by conducting tests under diverse atmospheric conditions and environments, enhancing the understanding of atmospheric turbulence effects on optical communication systems. This project represents a milestone in advancing space-to-ground laser communication, showcasing the potential of compact optical payloads in modern satellite missions.

4.2 DLS OSIRIS v1 Flying Laptop

4.2.1 Introduction

The OSIRISv1 laser communication system, installed on the Flying Laptop satellite Figure 4.2, was developed to demonstrate high-speed optical downlinks from small LEO satellites. The system is notable for its compact design, weighing only 1.3 kg and consuming 26 W of power. It features an Erbium-Doped Fiber Amplifier (EDFA) and a High-Power Laser Diode (HPLD) capable of delivering data rates up to 200 Mbps. The system employs open-loop body pointing, relying on star trackers for alignment, and achieves a beam divergence of 1.2 mrad to accommodate pointing inaccuracies. Its compactness and reliance on Commercial Off-The-Shelf (COTS) components make it well-suited for small satellite platforms, enabling cost-effective deployment and rapid integration [17].

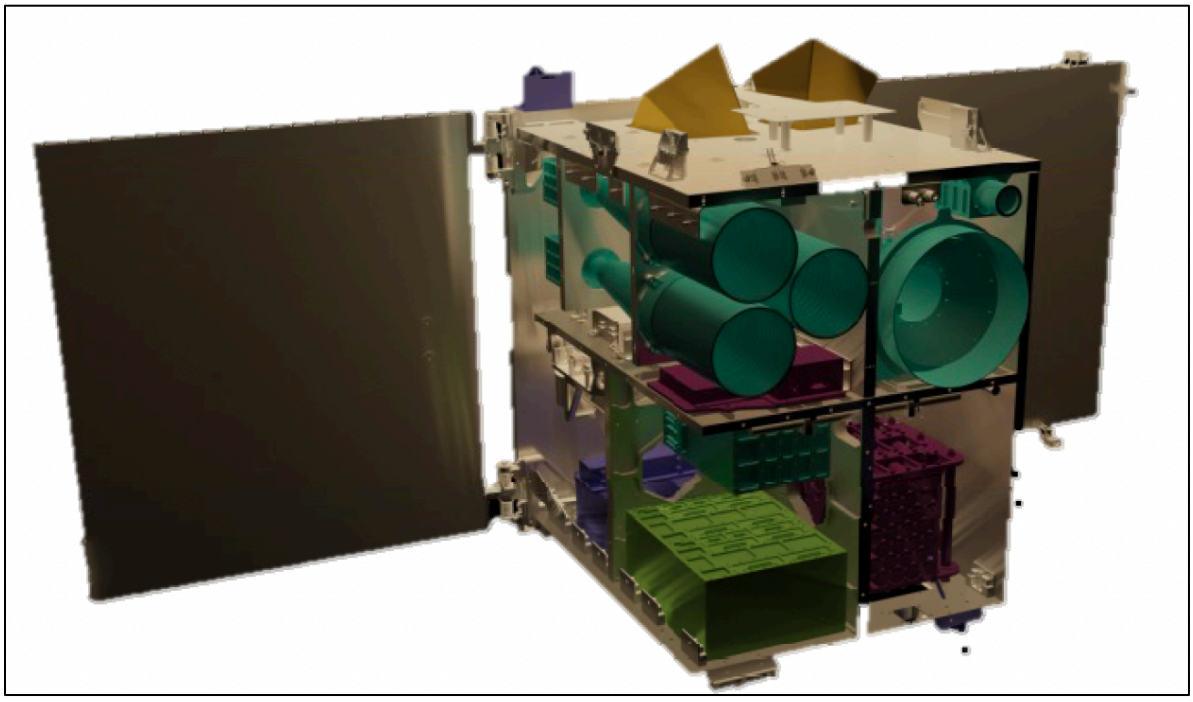

Figure 4.2: Flying Laptop (FLP) – OSIRIS v1 [18]

4.2.2 Performance Evaluation

OSIRISv1 demonstrated significant achievements during its operational phase, including successful downlinks with data rates up to 39 Mbps. Multiple ground stations, such as DLR's Optical Ground Station and the Grasse Station, verified its functionality and stability. The system achieved a Bit Error Rate (BER) below 10E-4 at optical power levels above 10 nW, showcasing the viability of laser communication for small satellites. However, the reliance on open-loop pointing introduced challenges, such as frequent beam-wander-induced fading caused by calibration limitations and atmospheric disturbances [19]. Atmospheric variability, including turbulence and cloud cover, also impacted signal strength and BER, underscoring the environmental sensitivity of laser communication [18].

4.2.3 Trade-Off Analysis

The design of OSIRISv1 represents a trade-off between technological complexity and deployment readiness Table 4.1 shows the performance characteristics based off those trade offs. By using simpler, cost-effective technologies, the system achieves lower production costs and rapid deployment, but it lacks the precision of advanced beam-steering mechanisms. While its compactness and low power consumption make it ideal for small satellites, its performance depends heavily on accurate attitude control and optimal atmospheric conditions. This limitation highlights the need for enhanced beam-stability mechanisms, such as hybrid pointing assemblies, and broader strategies to mitigate atmospheric interference [18; 19].

Table 4.1: OSIRIS v1 Performance Characteristics

Parameter	**Value/Details**	**Notes**
Satellite Platform	110 kg	Flying Laptop
Data Rate	Up to 200 Mbps demonstrated 39 Mbps in experiments	
Optical Power Output	1 W	EDFA mean
	100 mW	HPLD mean
Beam Divergence	1.2 mrad (Full Width at Half Maximum)	Full Width half at Maximum
Pointing Mechanism	Open-loop body pointing controlled via star trackers	
Bit Error Rate (BER)	Less than 10^-4	at power above 10 nW
Power Consumption	26 W during operation	In Operation Mode
System Mass	1.3 kg, optimized for small satellites	For CubeSats
Wavelength	EDFA: 1545 nm; HPLD: 1550 nm	
Pointing Accuracy	150 arcseconds (~727 µrad)	With star trackers
Ground Stations Used	DLR OGS in Oberpfaffenhofen; Grasse Station in France	France

4.3 DLR OSIRIS v2 BiROS

4.3.1 Introduction

The OSIRIS program by the German Aerospace Center (DLR) develops optical communication payloads optimized for small satellites. It aims to enhance data transmission capabilities, leveraging optical communication's unregulated spectrum and compact design. This summary focuses on OSIRISv2, the second-generation system, highlighting its technical features, operational performance, and associated challenges. Figure 4.3 is a CAD depiction of OSIRIS v2.

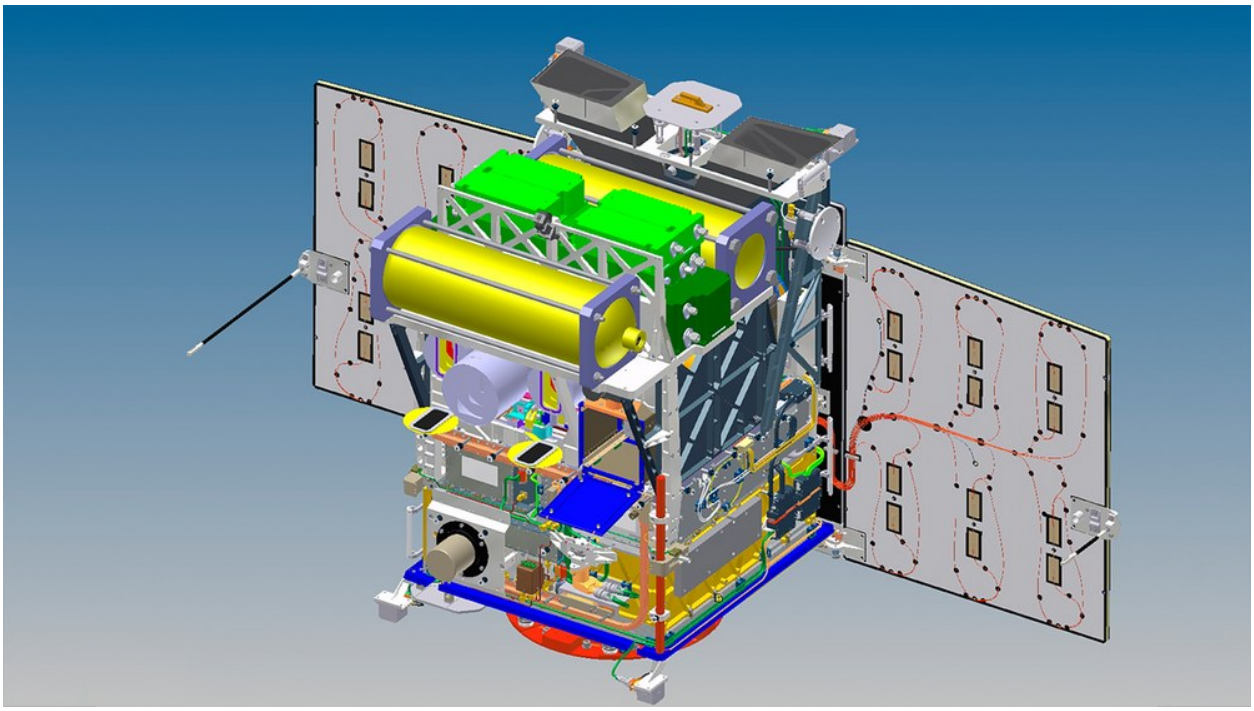

Figure 4.3: OSIRIS v2 CAD Depiction [17]

4.3.2 Overview of OSIRISv2

OSIRISv2 was integrated into the BiROS satellite, an Earth observation platform focused on fire detection. Designed to support data-intensive missions, OSIRISv2 offered significant improvements in data rates and pointing accuracy over its predecessor, OSIRISv1. However, operational challenges with the satellite's attitude control system limited its full functionality in demonstrating optical communication links [17].

4.3.3 Technical Features

- Data Rate and Power: OSIRISv2 achieved a theoretical data rate of 1 Gbps, with a consistent 1 W optical output power. Power consumption increased to 37 W due to advanced tracking systems.
- Pointing Accuracy: A key enhancement was the integration of a tracking sensor to improve attitude control. The sensor detected angular offsets using a beacon from the ground station, relaying corrections to the satellite's attitude control system.
- System Design: The payload consisted of an optical bench, laser modules, and tracking electronics, adding 1.65 kg to the satellite's mass. This modularity and design optimization made OSIRISv2 a scalable platform for high-data-rate applications.

4.3.4 Operational Challenges

- Attitude Control Limitations: While the tracking sensor improved pointing accuracy, the BiROS satellite's attitude control system did not meet the precision required for successful optical downlinks.
- Operational Constraints: BiROS prioritized its primary fire-detection mission, limiting opportunities for extensive OSIRISv2 testing and improvements.
- Weather Sensitivity: As with all optical communication systems, atmospheric conditions impacted link reliability, necessitating robust ground station networks.

4.3.5 Achievements

Despite operational limitations, telemetry confirmed OSIRISv2's functionality in orbit. Its advanced tracking sensor successfully demonstrated enhanced pointing capability, paving the way for future high-data-rate optical systems [17]. Furthermore, a summary of OSIRIS v2's performance characteristics are found in Table 4.2.

Table 4.2: OSIRIS v2 Performance Parameters

Parameter	**OSIRISv2 (BiROS)**
Platform	BiROS satellite (Earth observation, fire detection)
Data Rate	1 Gbps
Power Consumption	37 W
Optical Output Power	1 W
Wavelength Modulation	Not explicitly mentioned
Mass Addition	1.65 kg
Launch Date	2016
Key Features	Tracking sensor for angular offset correction
Challenges	Attitude control limitations, weather dependency
Achievements	Demonstrated enhanced pointing precision in orbit

4.3.6 Future Directions

Lessons from OSIRISv2 inform subsequent designs, such as OSIRISv3, which addresses attitude control challenges by incorporating satellite-independent beam steering mechanisms. OSIRISv3 also scales data rates up to 10 Gbps, leveraging advancements in coarse-pointing assemblies and onboard data handling.

4.4 Aerospace Corporation OCSD-B&C AeroCube-7

4.4.1 Introduction

The Optical Communications and Sensors Demonstration (OCSD) project aimed to validate the feasibility of using compact CubeSats equipped with optical communication systems for high-data-rate downlinks. The study examined the trade-offs involved in designing and operating such systems, focusing on cost, complexity, performance, and scalability [20]. Figure 4.4, shows an exploded view of the assembly of the AeroCube-OCSD cubesat.

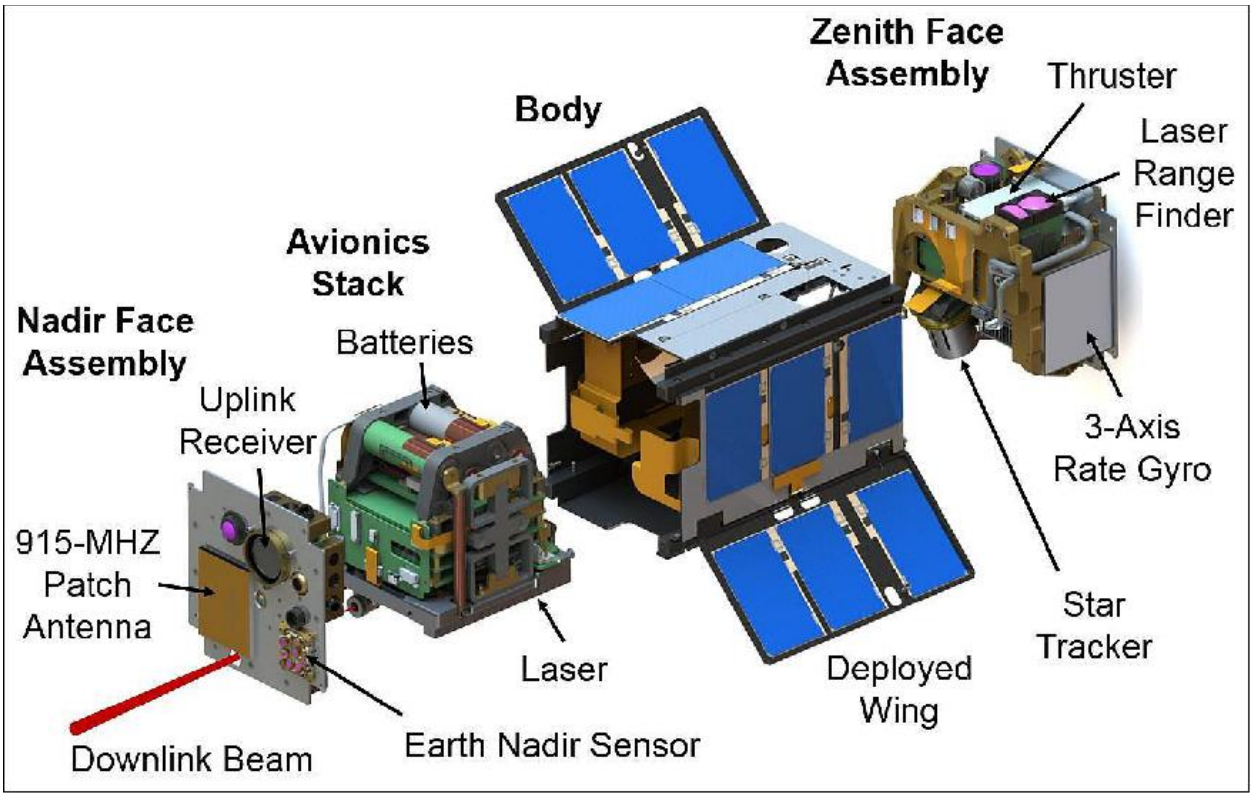

Figure 4.4: Exploded schematic view of the AeroCube-OCSD CubeSat [20].

4.4.2 Objectives

- Develop a cost-effective optical communication platform for small satellites.
- Demonstrate high-speed downlink capabilities (≥200 Mbps) without relying on traditional uplink beacons or gimbal mechanisms.
- Validate the use of body-pointed star trackers for precision alignment and data transmission.

4.4.3 Key Results

- Performance Achieved: Data rates of up to 200 Mbps were achieved, with 78% of the communication window being error-free without forward error correction.
- Technological Advances: Precision pointing was achieved with star trackers, eliminating the need for complex gimbal systems.
- Challenges: Thermal management, pointing accuracy, and atmospheric effects posed operational limitations.

4.4.4 Conclusion: Trade Space Analysis

The OCSD project demonstrated a novel optical communication system, offering a cost-effective and high-performance alternative to traditional RF systems for CubeSat platforms. Below is a trade space analysis highlighting the comparative advantages and challenges of optical communication [20].

4.5 NICT VSOTA RISESAT

4.5.1 Introduction

The integration of the Very Small Optical Transponder (VSOTA) into the RISESAT microsatellite marks a significant step in advancing cost-effective and reliable satellite-to-ground optical communication. Developed at Tohoku University in collaboration with the National Institute for Information and Communications Technology (NICT), VSOTA emphasizes lightweight design, minimal power consumption, and simplified communication architecture. Unlike traditional systems, VSOTA relies on body pointing for ground station tracking, supported by the High Precision Telescope (HPT) for laser detection [21]. Shown in Figure 4.5 is a the RISESAT on a vibe test table.

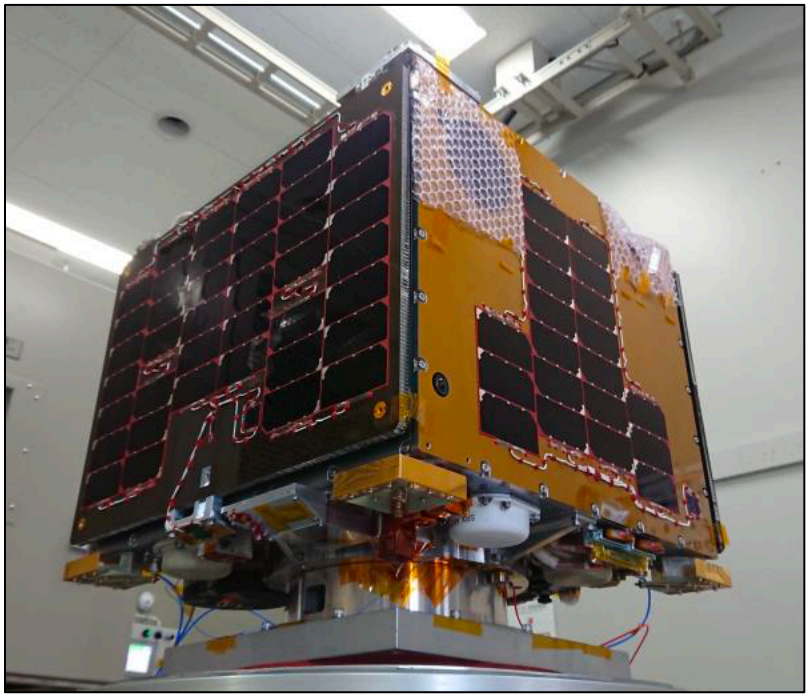

Figure 4.5: RISESAT on vibe test table [21]

4.5.2 Objectives

The primary objectives of the RISESAT project include:

- Demonstrate Lightweight Communication Systems: Show the feasibility of integrating VSOTA, a lightweight (<1 kg) and energy-efficient communication system, on a microsatellite platform.
- Establish Body Pointing Accuracy: Replace traditional gimbal mechanisms with satellite attitude control for optical alignment with ground stations.
- Collect Scientific Data: Enable one-way laser communication for Earth observation and provide reference data for future adaptive optics and quantum communication systems.
- Evaluate Optical Tracking Systems: Assess the performance of VSOTA and HPT in achieving precise ground station alignment using open-loop and closed-loop controls.

4.5.3 Key Results

The project achieved the following significant milestones:

1.0 Optical Communication Tests:
Verified data transmission with a Bit Error Rate (BER) of 0 at variable data rates (PRBS-11 and PRBS-15 modes). Demonstrated dual-band optical communication (980 nm and 1550 nm). Achieved minimum success criteria of demonstrating lightweight optical communication.

2.0 Body Pointing Feasibility:
Combined open-loop and closed-loop attitude control for satellite alignment with ground stations. Supported tracking accuracy within 0.04°, ensuring reliable ground station communication.

3.0 Energy and Mass Efficiency:
Achieved significant reductions in system mass (<1 kg) and power consumption (4.33 W max) compared to SOTA (5.9 kg, 15.74 W max).

4.0 Scientific and Technological Impact:
Enabled adaptive optics validation for future high-throughput satellite systems. Established baseline data for quantum communication experiments using superconducting nanowire single-photon detectors (SSPD).

4.5.4 Conclusion and Trade Study Table Summary

The VSOTA and RISESAT project highlights trade-offs between performance, complexity, and efficiency in microsatellite optical communication. These tradeoffs in performance are shown in Table 4.5.1. By eliminating gimbal mechanisms and adopting body pointing, the system achieves significant reductions in weight and power at the expense of simpler, though effective, tracking mechanisms [21].

Table 4.3: Optical vs RF vs Hybrid (RF + Optical) Approaches

Parameter	**OCSD Optical Approach**	**Traditional RF Approach**	**Hybrid (RF + Optical)**
Data Rate	High – Up to 200 Mbps (scalable).	Low – Typically ≤10 Mbps for small satellites.	Moderate – RF for reliability; optical for bursts of high data.
Pointing Mechanism	Body-pointing with star trackers (0.024° accuracy).	No precise pointing required due to wide beamwidth.	Requires integration of pointing-free RF and precise optical.
Cost	Lower – No gimbals, compact design.	Medium – Established, reliable technology.	Higher – Integration challenges for dual systems.
SWaP (Size, Weight, Power)	Compact – 2.3 kg, 10–20 W power.	Medium – Requires larger antennas and more power.	Larger footprint due to dual components.
Reliability	Moderate – Susceptible to atmospheric conditions.	High – Reliable under most conditions.	Moderate – Hybrid systems face integration risks.

Parameter	OCSD Optical Approach	Traditional RF Approach	Hybrid (RF + Optical)
Scalability	High – Modular design for inter-satellite links or higher rates.	Limited by RF spectrum availability and bandwidth.	Moderate – Complexity increases with mission scope.

4.6 Sony/JAXA SOLISS ISS

4.6.1 Introduction

The Small Optical Link for International Space Station (SOLISS) is a compact optical communication terminal designed to demonstrate high-speed, bi-directional laser communication between the ISS and a ground station. Developed by Sony and JAXA, SOLISS incorporates miniaturized optical technology inspired by consumer-grade optical disk mechanisms. Figure 4.6 shows an image that was transmitted from SOLISS. This study evaluates SOLISS's technical performance, including pointing accuracy, communication success, and environmental resilience [21; 22].

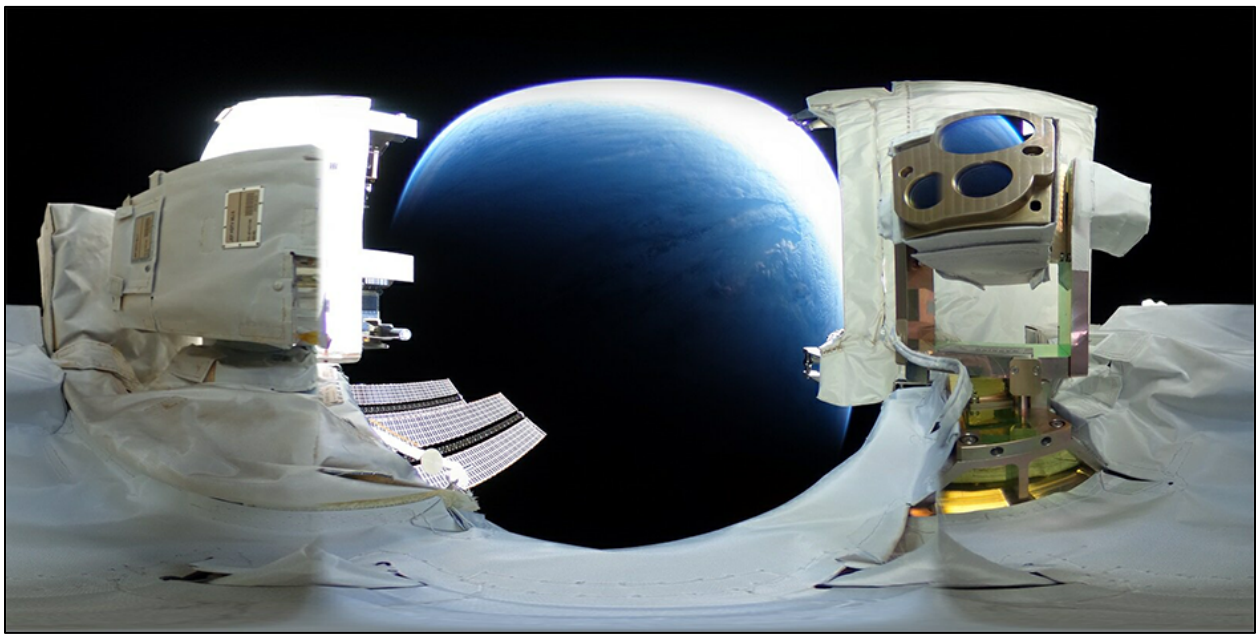

Figure 4.6: HD image transmitted from SOLISS via Laser Communication [23]

4.6.2 Objectives

- To validate the feasibility of a 100 Mbps Ethernet-based optical communication link between the ISS and ground.
- To demonstrate the robustness of SOLISS's pointing mechanism in low-Earth orbit (LEO).
- To assess SOLISS's performance under varied atmospheric and operational conditions.
- To identify the strengths and limitations of the current implementation for future advancements [21].

4.6.3 Key Results

- Performance Metrics: Achieved a data rate of 100 Mbps with a pointing accuracy of 39.2 µrad and communication range of up to 1000 km [22]
- Operational Success: Successfully captured uplink beams in 18 out of 22 operations and downlink beams in 17 operations, with 2 full-duplex Ethernet links established [21].
- Environmental Resilience: Performed well under clear skies but faced challenges in foggy and cloudy conditions [22].
- System Design: Demonstrated effective thermal management (0.4 µrad distortion) and resistance to ISS platform vibrations [21; 22].
- Limitations: Lacked scalability for higher data rates, no point-ahead correction, and dependency on optimal atmospheric conditions [21].

4.6.4 Conclusion

The SOLISS experiment successfully validated the practicality of compact optical communication systems for space applications, proving its capability in achieving bi-directional links with sufficient accuracy and robustness. However, the study highlighted areas for improvement, such as increasing scalability, integrating advanced tracking features, and enhancing performance under adverse weather conditions, a summary is provided in Table 4.6.1. These insights provide a foundation for developing next-generation space optical communication systems [21; 22].

Table 4.6.1: SOLISS Performance Summary and Considerations

Criteria	**SOLISS Performance**	**Strengths**	**Weaknesses**
Data Rate	100 Mbps (Ethernet-based)	High data throughput for a compact system	Limited scalability for higher speeds
Pointing Accuracy	39.2 µrad total error	Adequate accuracy for low-Earth orbit links	Does not include point-ahead correction
Communication Range	Up to 1000 km	Effective at planned communication distances	Restricted to low-Earth orbit operations
Success Rate	77% (uplink capture), 75% (downlink capture)	Reasonable performance under varying conditions	Dependent on atmospheric clarity
Atmospheric Challenges	Clear skies optimal, partial success in fog/clouds	Demonstrated ability in challenging weather	Fog significantly reduces effectiveness
Thermal Challenges	Minimal thermal distortion (0.4 µrad)	Thermal management well handled	Thermal errors not zero
Vibration Challenges	Low vibration influence in orbit	Resilient to mild vibrations of ISS platform	Potential limits in extreme vibration settings
Power Consumption	36 W during communication	Efficient power use for its functionality	May limit higher power applications
Hardware Design	Compact with fine and coarse pointing mechanisms	Innovative, miniaturized, and modular	Reliant on specific ISS platform interfaces

Criteria	SOLISS Performance	Strengths	Weaknesses
Operational Success	18 uplink successes, 17 downlink successes, 2 full-duplex links	Proof of concept demonstrated effectively	Few bidirectional full-duplex links established

4.7 DLR OSIRIS v4 CubeSat PIXL-1

4.7.1 Introduction

The CubeLCT (Cube Laser Communication Terminal) is a compact laser communication solution specifically designed for CubeSat applications. Figure 4.7 shows how compact the payload is relative to a pen. Developed by Tesat-Spacecom GmbH in collaboration with the DLR Institute of Communications and Navigation, the CubeLCT is tailored for low-earth orbit (LEO) to ground communications, optimizing size, weight, and power consumption (SWaP). It represents a pioneering step in miniaturized laser communication systems with its debut on the PIXL-1 mission in January 2021 [41].

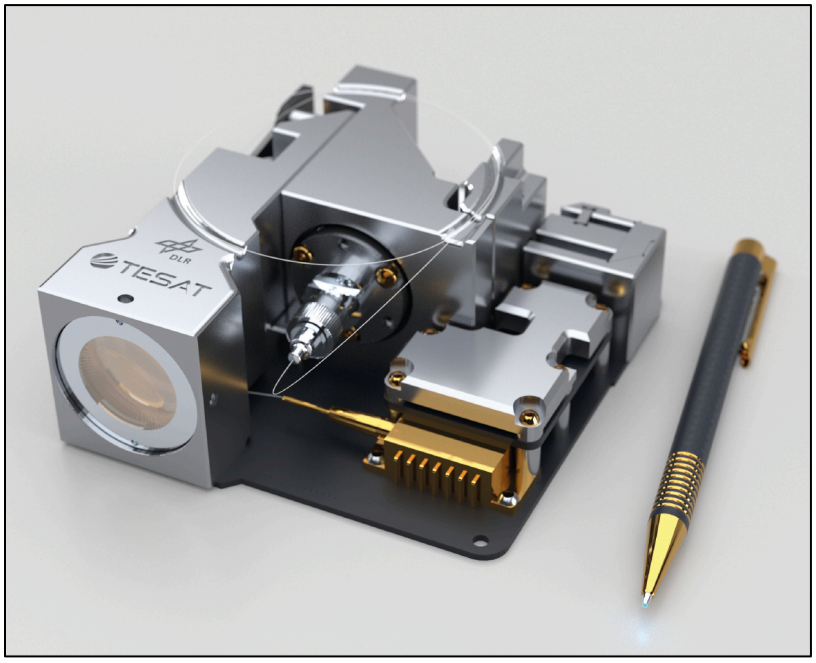

Figure 4.7:CubeLCT Laser Communication Terminal [24]

4.7.2 Objectives

- The primary objectives of this study are:
- To evaluate the performance capabilities of CubeLCT, including data rate, power, size, and durability.
- To assess its suitability for CubeSat missions requiring high-speed optical communications.

- To identify trade-offs between performance, cost, and scalability for inter-satellite and air-to-ground communications.

4.7.3 Key Results

The CubeLCT is a cutting-edge technology in LEO satellite communication. Its specifications are summarized below:

Table 4.7.1: Summary of Specification of CubeLCT

Parameter	Value
Channel Data Rate	100 Mbps (LEO to ground), 1 Mbps (ground to LEO)
Mass	397 g
Size	9 x 9.5 x 3.5 cm^3
Power Consumption	10 W (Peak)
Field of Regard	±1° (integrated Fine Steering Mirror capability with spacecraft pointing)
Lifetime	3 years in LEO orbit
Data Interface	LVDS for data; UART for telemetry and telecommand (TM/TC)
Wavelength	Telecom C-band (CCSDS standard implementation)
Range	Up to 1,500 km LEO to ground
Technical Features	IM/DD technology, CCSDS O3K implementation, expandable to 1 Gbps
Applications	CubeSat LEO to ground laser communications, inter-satellite links

Key highlights include:

- High-speed laser communications at 100 Mbps for CubeSats.
- Ultra-compact design optimized for space applications, requiring minimal SWaP resources.
- Proven reliability with TRL9 (Technology Readiness Level 9), validated in space.

4.7.4 Conclusion

The CubeLCT offers a state-of-the-art solution for optical communications in LEO CubeSat missions. Its compact size, lightweight design, and efficient power consumption make it ideal for constrained small satellite platforms. A summary of its key characteristics is summarized in table 4.7.2. While currently optimized for LEO-to-ground communications, the technology is expandable for higher data rates and inter-satellite links, demonstrating potential for broader applicability in satellite constellations and aerospace communications [24].

Table 4.4: CubeLCT Characteristics

Parameter	CubeLCT Characteristics
Innovation	Smallest laser communication transmitter
Data Transfer Rate	100 Mbps (LEO to ground), 1 Mbps (TC Channel)
SWaP Efficiency	Low mass (397 g), size (9 x 9.5 x 3.5 cm^3), power
Lifetime	3 years in LEO
Application	CubeSat LEO-ground communications, inter-satellite

4.8 MIT CLICK-AB/C

4.8.1 Introduction

The CubeSat Laser Infrared Crosslink (CLICK) mission is a multi-phase initiative designed to demonstrate advanced optical communication technologies for CubeSats. By reducing Size, Weight, and Power (SWaP) requirements, CLICK aims to address the growing needs for high-speed data transfer, intersatellite connectivity, and secure communication in nanosatellite constellations. Figure 4.8 shows optical payloads terminals and subassesmblies from a CAD drawing, and Figure 4.9 provides a view of how all the components come together and are laid out in the design. The mission progresses through two key phases: CLICK-A and CLICK-B/C [25].

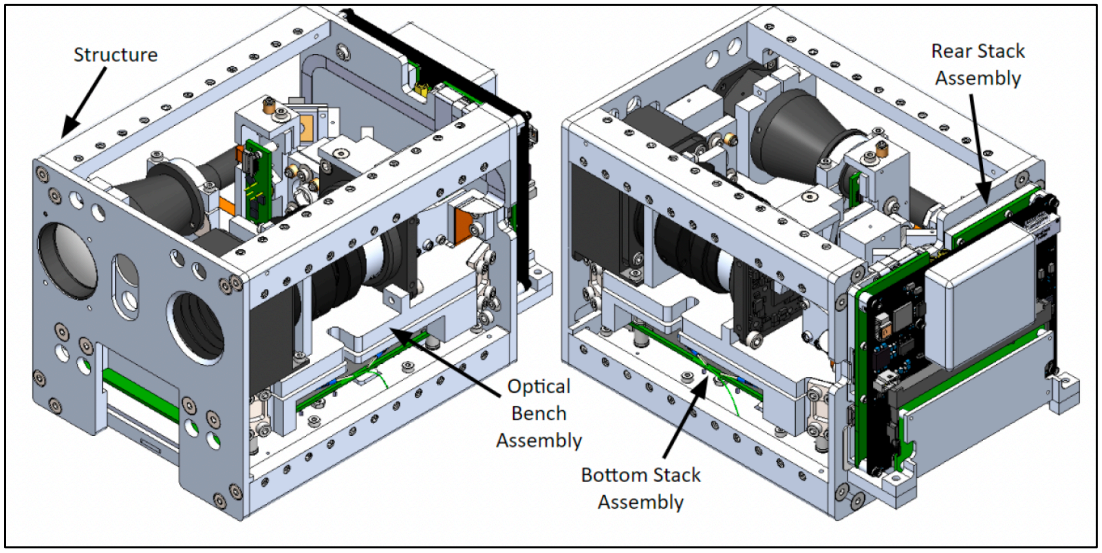

Figure 4.8: Click-B/C Terminals and Subassemblies [25]

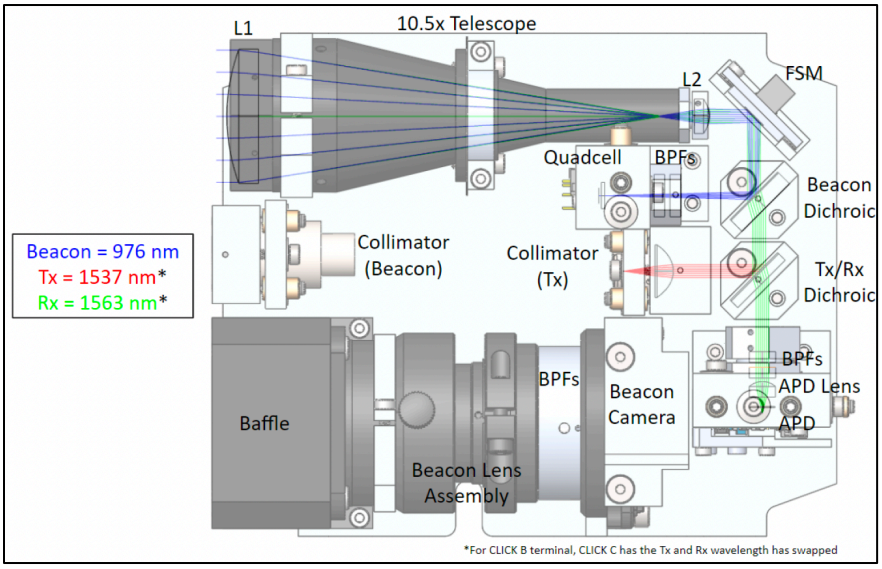

Figure 4.9: Optical Bench with Components CAD [25]

4.8.2 Objectives

Table 4.5 provides a high-level summary of the mission for CLICK A/B/C.

Table 4.5: Summary of Click A, B and C Mission

Aspect	CLICK-A	CLICK-B/C
Purpose	Risk reduction and technology validation	Demonstrate intersatellite optical links and high-precision ranging
Primary Objective	≥10 Mbps optical downlink to ground	Establish 20 Mbps intersatellite communication
Additional Objective	None	Ranging accuracy of 50 cm
Communication Mode	Downlink-only	Full-duplex (downlink and crosslink)

4.8.3 Key Results

Table 4.6 provides a high-level summary of the key features from CLICK A/B/C, and what their results where.

Table 4.6: Key Features of Click A, B, and C

Feature/Phase	CLICK-A	CLICK-B/C
Design	1.2U terminal in a 3U spacecraft	1.5U terminal with modular optical bench
Communication Type	Optical downlink only	Optical downlink and intersatellite crosslink
Data Rate	≥10 Mbps	20 Mbps
Precision Ranging	Not Applicable	≤50 cm
Beam Divergence	2 mrad	121 μrad
Thermal Management	Integrated design with limited isolation	Separate optical bench with advanced isolators
Power Consumption	<15 W	<35 W
Testing Results	Fully validated during environmental tests	Prototype tested; beam divergence achieved at 154 μrad
Launch Status	Launched and deployed from ISS in 2022	Planned for late 2023

4.8.4 Conclusion

The phased approach of the CLICK mission highlights trade-offs between simpler risk-reduction systems (CLICK-A) and the complexity of multifunctional designs (CLICK-B/C). CLICK-A successfully validated key technologies, paving the way for the more advanced technology implementations on CLICK-B/C systems. These differences in complexity captured in the tradeoff's summary Table 4.7. By addressing beam precision, power efficiency, and thermal challenges, CLICK-B/C achieves higher data rates and intersatellite communication [25].

Table 4.7: Key Tradeoffs between Click A, B, and C

Trade-Off	CLICK-A	CLICK-B/C
Complexity	Lower, focused on a single function	Higher, modular design with advanced features
Development Cost	Lower	Higher due to precision requirements
Operational Capability	Limited to ground communication	Ground and intersatellite communication
Application	Foundational technology demonstration	Advanced optical networking in constellations

4.9 AAC Clyde Space CubeCat

4.9.1 Introduction

The CubeCAT laser communication module, shown in Figure 4.10, is a cutting-edge optical communication system for CubeSats and small satellites. It enables high-speed data transfer between satellites and ground stations without the need for radio frequency licensing. Developed by AAC Clyde Space and TNO, it boasts a compact design, low power usage, and high performance, tailored to the needs of modern space missions [26].

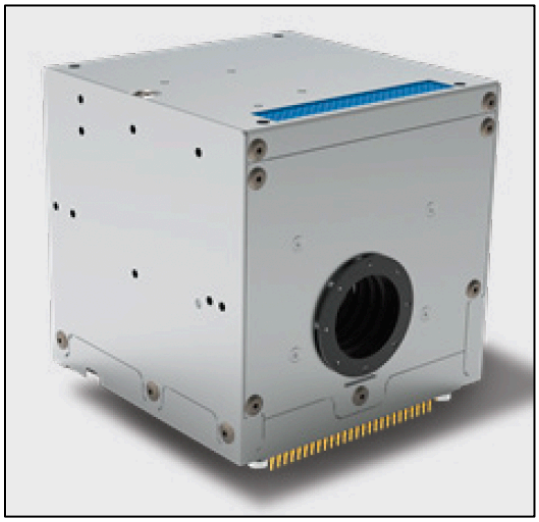

Figure 4.10: Clyde Space CubeCat [26]

4.9.2 Objectives

- Deliver a high-speed, optical communication solution for small satellites.
- Eliminate regulatory hurdles by bypassing radio frequency licensing.
- Simplify integration with plug-and-play compatibility.
- Provide a reliable and robust system for diverse satellite applications.

4.9.3 3. Key Results

Since this module is commercially available, Table 4.8 summarizes the characteristics and performance parameters of the payload.

Table 4.8: Clyde Space Performance Characteristics

Category	Performance Characteristics	Notes
Performance	-100 Mbps, 300 Mbps, 1 Gbps - 200 Kbps - Max000 km - On-board buffer: >64 GB	Downlink Uplink Max Range On Board Buffer
Design Features	- <1U (96 x 96 x 96 mm) - <1.33 kg - 15W; <1W - -20°C to +40°C	Size Mass Power Peak and Average Operating Temps
Advantages	- ITAR-free - No regulatory certification required - Cost-effective with low cost-per-bit	
Integration	- Interfaces: USB 3.0, I2C - Plug-and-play system with built-in data coding/sync	
Robustness	- High precision pointing and vibration tolerance - Compatible with a variety of platforms	

4.9.4 4. Conclusion

The CubeCAT laser communication module is a transformative innovation in CubeSat communications, addressing the need for high-speed data transmission with minimal regulatory hurdles, compact design, and cost efficiency. It is well-suited for both commercial and scientific satellite missions, offering reliability and simplicity for satellite developers and operators.

4.10 Trade Study Summary Table and Conclusion Statement

The collected body of evidence from recent small satellite optical communication trials captured in Chapter 4, reveals a field in active maturation, transitioning from nascent proofs-of-concept to increasingly standardized, higher-performance systems. Several key trends and outcomes emerge from this trade and will be highlighted below.

4.10.1 Key Trends and Outcomes

Performance Gains and Data Rates:

Optical terminals have demonstrated a clear progression from early Mbps-level downlinks to present-day systems achieving or targeting Gbps-scale throughput. This upward trend responds to escalating data demands in Earth observation, scientific instrumentation, and emerging commercial constellations.

Size, Weight, and Power (SWaP) Constraints:

There is a concerted push toward miniaturization. Early systems, though functional, were often bulky and power intensive. More recent payloads integrate sophisticated optical

technologies into minimal form factors suitable for CubeSats, enabling high-capacity links without substantial mass or power penalties.

Pointing and Acquisition Techniques:

The complexity of pointing solutions spans from open-loop body pointing using star trackers to fine steering mirrors and beacon-based acquisition. Continued improvements in precision pointing and closed-loop control have significantly mitigated link instability and beam-wander-induced fading.

Atmospheric and Environmental Sensitivities:

Although atmospheric turbulence, cloud cover, and environmental variability remain key impediments to reliably achieving high link availability, error-correction codes and network-level redundancy (e.g., multiple ground stations) are increasingly employed to ensure data integrity and mission resiliency.

Cost, Complexity, and Deployment Trade-offs:

Systems balance complexity, cost, and performance. While simpler, cost-effective designs yield moderate throughput and stability, more advanced systems demand higher investment in tracking technology and attitude control. This scenario highlights a strategic decision point for mission planners, balancing ambition against budget and risk tolerance.

Maturity and Standardization:

With growing adoption of standardized wavelengths, interfaces, and CCSDS protocols, optical communication is evolving beyond bespoke prototypes. These trends indicate an increasingly commercialized and interoperable environment, reducing integration barriers and accelerating technology uptake.

4.10.2 Conclusion

The evolution of optical payloads for small satellites indicates that high-data-rate laser downlinks and inter-satellite links are rapidly becoming practically achievable and increasingly reliable. Ongoing developments emphasize refining pointing solutions, mitigating atmospheric effects through adaptive strategies, and consolidating standards. In aggregate, these trends presage a future in which optical communication is a routine, if not essential, component of small satellite mission architectures, responding to the pressing need for efficient, scalable, and high-throughput data exchange.

4.10.3 Summary Table of Trade Study Characteristics

Table 4.9: Comparison of SOTA, OSIRIS v1 and v3, CubeLCT, Click, and CubeCAT

Characteristic	**Early Demonstrations (e.g., SOTA)**	**Intermediate Systems (e.g., OSIRISv1/v2, OCSD)**	**Advanced/Recent Systems (e.g., CubeLCT, CLICK, CubeCAT)**
Typical Data Rates	~1–10 Mbps	~10–200 Mbps	100 Mbps–1 Gbps (or higher)
SWaP Requirements	Moderate mass & power (>5 kg, ~15 W)	Reduced mass & power (~1–2 kg, 20–30 W)	Highly optimized (<1 kg, <15 W), suitable for CubeSats

Characteristic	Early Demonstrations (e.g., SOTA)	Intermediate Systems (e.g., OSIRISv1/v2, OCSD)	Advanced/Recent Systems (e.g., CubeLCT, CLICK, CubeCAT)
Pointing & Acquisition	Open-loop body pointing, star trackers	Hybrid: star trackers + partial fine control	Closed-loop tracking, fine steering mirrors, beacon tracking
Atmospheric Sensitivity	Significant performance variability	Improved with error correction & scheduling	Advanced mitigation (error-correcting codes, multiple ground stations)
Complexity & Cost	Lower complexity, lower initial cost	Moderate complexity; balanced cost & performance	Higher complexity & cost for maximum throughput and stability
Maturity & Standardization	Experimental prototypes	Some CCSDS compliance, standardized wavelengths	High TRL, CCSDS protocols, modular “plug-and-play” architectures
Scalability (Constellations)	Limited applicability	Emerging feasibility (some inter-satellite tests)	Mature scalability: inter-satellite links, constellation-ready
Technology Readiness Level	TRL ~4–5 (lab to early flight)	TRL ~6–7 (in-orbit demonstrations)	TRL 8–9 (fully operational, commercially available)

Chapter 5. Cold Gas Thruster Design

5.1 Introduction and Motivation

A cold gas thruster design was explored as a next step to support a key finding from the trade study on optical payloads. From our trade study it was indicated that precision pointing and acquisition techniques were one of the key drivers for improvement. Therefore, a potential method that could help resolve precision satellite orientation from a cubesat could be a cold gas propulsion system. Therefore, this section will cover our nozzle design for a cold gas propulsion system and computational fluid dynamic results.

5.2 Nozzle Geometry

As shown in Figure 5.1 CAD drawing, the nozzle geometry consists of a compact, axisymmetric, converging-diverging design tailored to a cold gas thruster for small spacecraft, all dimensions are in inches. In this configuration, the flow accelerates from subsonic speeds at the inlet to sonic conditions at the throat, and then expands to supersonic velocities as it passes through the divergent section. This modest expansion ratio and relatively short nozzle length offer a careful balance of performance, reliability, and integration efficiency within the tight volume and mass constraints of CubeSat-class platforms.

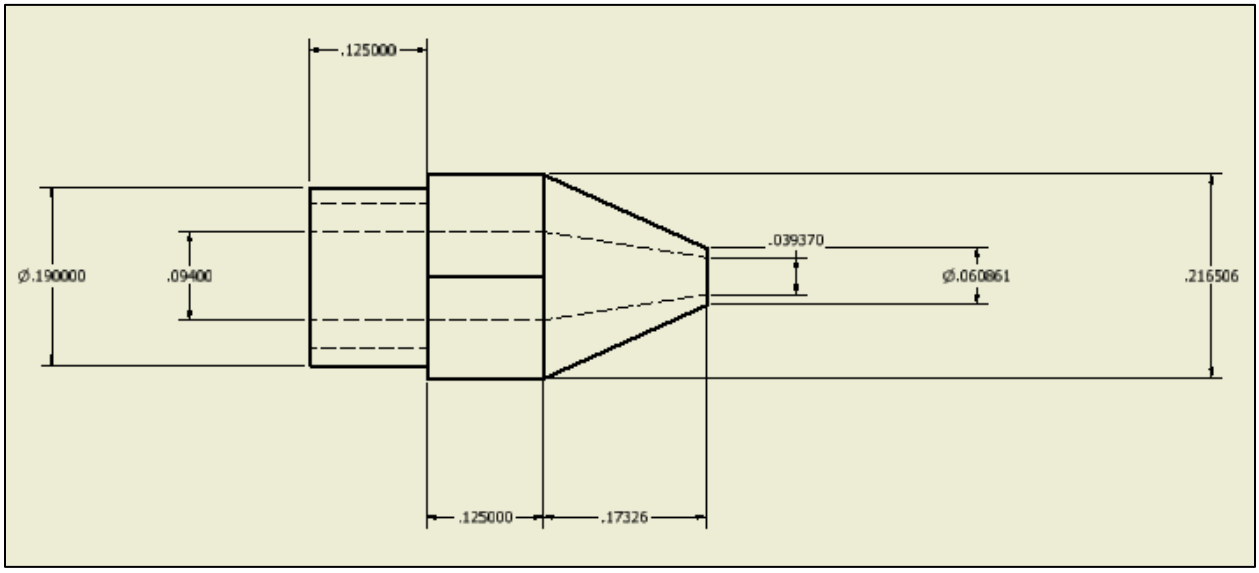

Figure 5.1: CGP Nozzle Geometry

The simplicity of the conical profile is depicted in Figure 5.1, Figure 5.2 highlights a 3D view of the nozzle, and Figure 5.3 highlights the cross-section view of the model. This design approach facilitates manufacturing and assembly, ensuring that the nozzle can be readily integrated into the propulsion subsystem. Once operational, the controlled acceleration of inert propellant gas through this geometry provides a stable, low-thrust, supersonic jet well-suited for fine attitude adjustments or small orbital corrections. While the resulting specific impulse may be modest, the configuration leverages the inherent safety and reduced complexity of cold gas propulsion, making it ideal for missions where reliability and straightforward implementation are paramount.

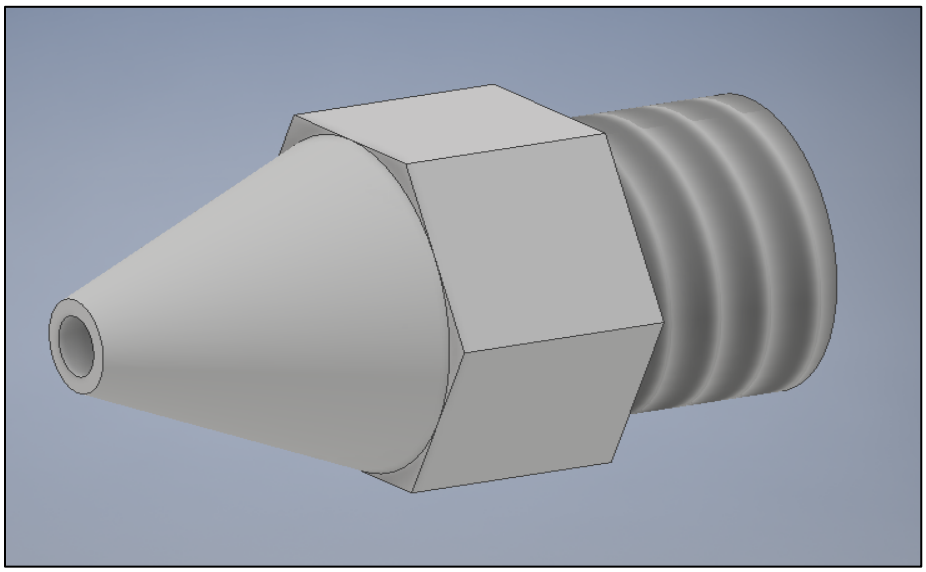

Figure 5.2: 3D Model of Nozzle Geometry

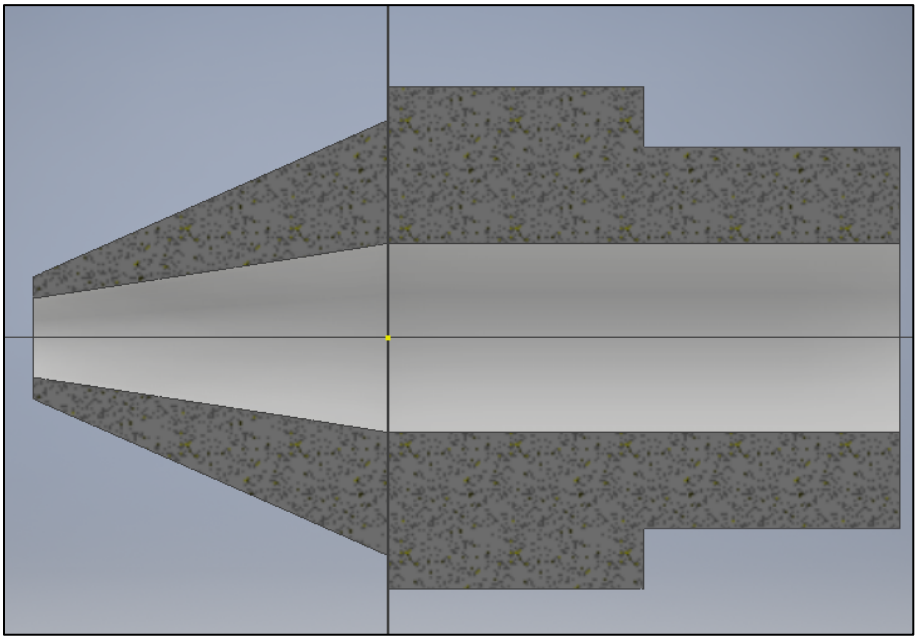

Figure 5.3: Cross Section View of Nozzle Geometry

5.3 Mesh Generation for the Nozzle Geometry

In Figure 5.4, we define the computation domain boundary conditions into multiple segments: including a curved far-field arc (1) and ground line (2), ensuring that freestream conditions and boundary effects are correctly captured. Its layout allows for an extended solution space that prevents artificial reflections or distortions at the domain edges.

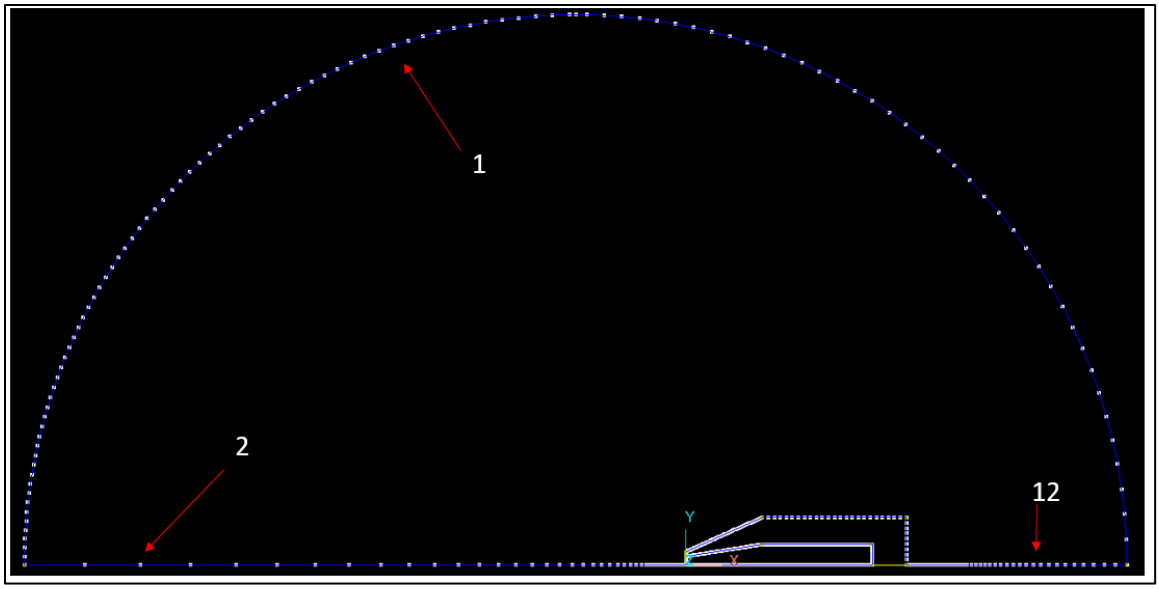

Figure 5.4: Domain Boundary

Figure 5.5 provides a close-up view highlighting the nozzle geometry and adjacent boundary segments, including the outlet (3), nozzle outer walls (4-7), and the flow downstream from (10, 9, 8) until it reaches the outlet. which together define the core flow region. Such careful segmentation ensures that mesh refinement can be strategically applied where velocity, pressure, and temperature gradients are most significant. Lastly, segment 11 shows that axisymmetric line.

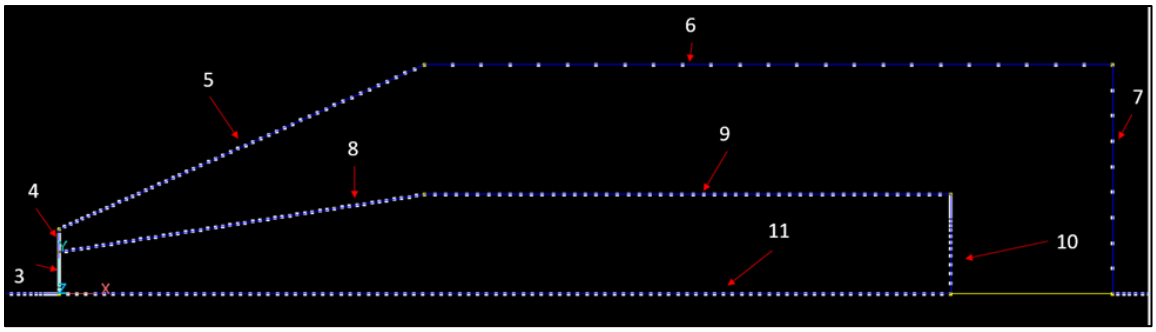

Figure 5.5: Nozzle Geometry and Segments

Table 5.1 details the discretization strategy for each boundary segment, specifying the number of grid points, distribution type (Geometric or Power Law), and a transition factor that controls mesh spacing growth. By carefully selecting these parameters, the mesh can be optimized for accuracy, stability, and computational efficiency.

Table 5.1: Meshe Generation Table

Segment	Num. Grid Points	Type	Transition Factor
1	111	Geometric	1.01
2	50	Geometric	1.1

Segment	Num. Grid Points	Type	Transition Factor
3	20	Geometric	1.1
4	10	Geometric	1.2
5	50	Geometric	1.01
6	25	Geometric	1.0
7	10	Geometric	1.0
8	50	Power Law	1.0
9	50	Power Law	1.0
10	20	Geometric	1.1
11	99	Power Law	1.0
12	50	Geometric	1.05

Figure 5.6 shows what the mesh results were during a computational run at 2.7E-004 seconds.

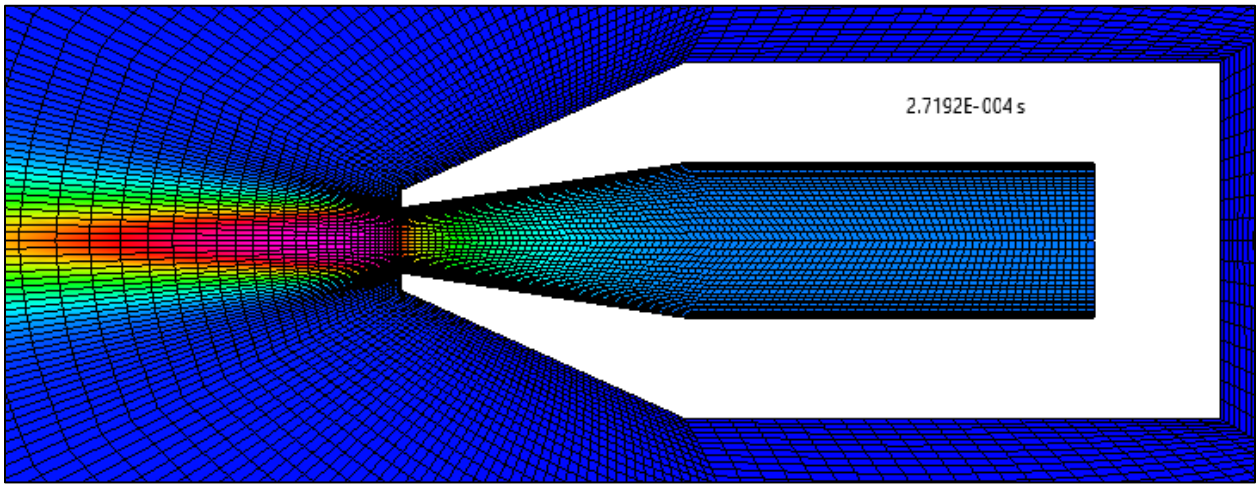

Figure 5.6: Snapshot of Results at 2.7E-004s Showing the Mesh Generation

5.4 Physics and Fluid Model Data

The fluid model used, and its details are shown in Table 5.2.

Table 5.2: Physics and Fluid Model

Problem Type	Compressible Flow
Polar	Axisymmetric about the x-axis
Gas Model	Ideal Gas

Problem Type	Compressible Flow
Viscous Model	Turbulent (Navier-Stokes)
Ideal Gas Molecular Weight (g/mol)	28.97
Gamma (C_p/C_v)	1.4
Viscosity	Sutherland's Law
A (K^1/2 kg/ms)	1.4605E-006
B (K)	112
Conductivity (Prandtl Number)	0.7
Turbulent Conductivity (Pr_T)	0.9
Turbulence Model	K Epsilon: Compressibility Correction

After defining the fluid model and physics model, we then defined the mesh volume conditions. Table 5.3 details what was used for the Mesh Volume and Boundary Conditions.

Table 5.3: Mesh Volume and Boundary Conditions.

	Free Stream	**Cold Gas Thruster**
Velocity (m/s)	0	0
Temperature (K)	N/A	2000000
Pressure (Pa)	0	290
BC Subtype	Extrapolated	Fixed Total P and T

Lastly, we defined our solver, algorithm, numerical integration, stead state and/or transient parameters for our model in Table 5.4

Table 5.4: Solver, Algorithm, Numerical Integration, Stead State and/or Transient

Max No. of Cycles	**Zonal Sub cycles**	**Convergence Criteria**	**Discretization**	**Integration**	**Initial CFL**	**Final CFL**	**Ramping Cycles**
100,000	1	1E-6	Backward Euler	Implicit	0.1	1	100

5.5 Contour and Animations of the Resulting Model for Time Accurate

5.5.1 Mach

Figure 5.7 shows the Mach profile at 2.6815×10^-5s. At this very early stage, the Mach number distribution within the nozzle and its near field is still forming. The flow is accelerating from rest, but uneven velocity regions and incomplete expansions indicate the jet has not yet reached a stable, fully developed pattern

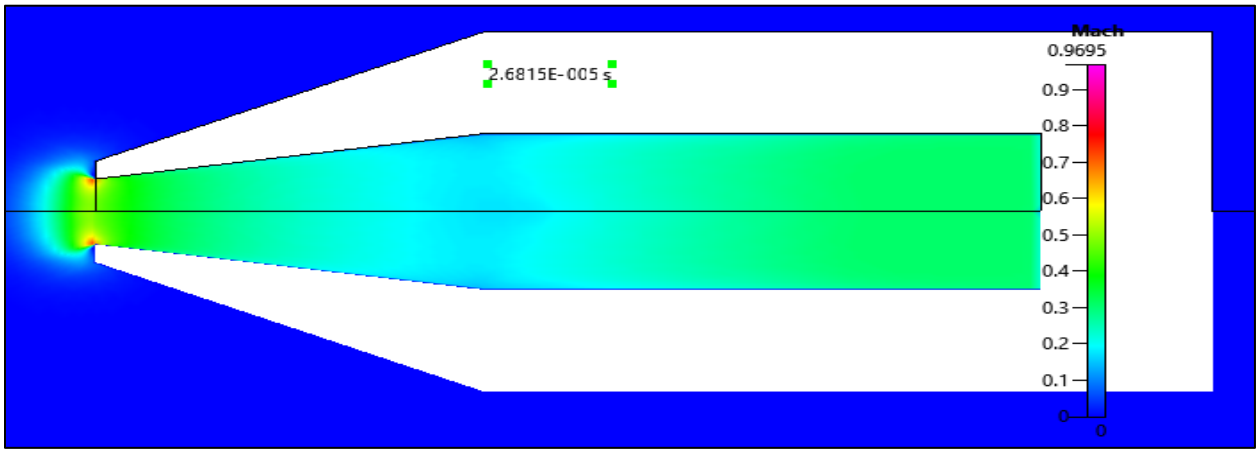

Figure 5.7: Mach Transient State at Time 2.6815×10^-5s

Figure 5.8 shows the Mach profile at 3.5103E00-5s (Mach profile slightly later). The Mach number contours show a more coherent acceleration through the throat and an expanding supersonic region downstream. While the flow structure is still settling, the previously uneven regions are becoming more uniform, signaling that the nozzle flow is progressing toward a steadier supersonic jet.

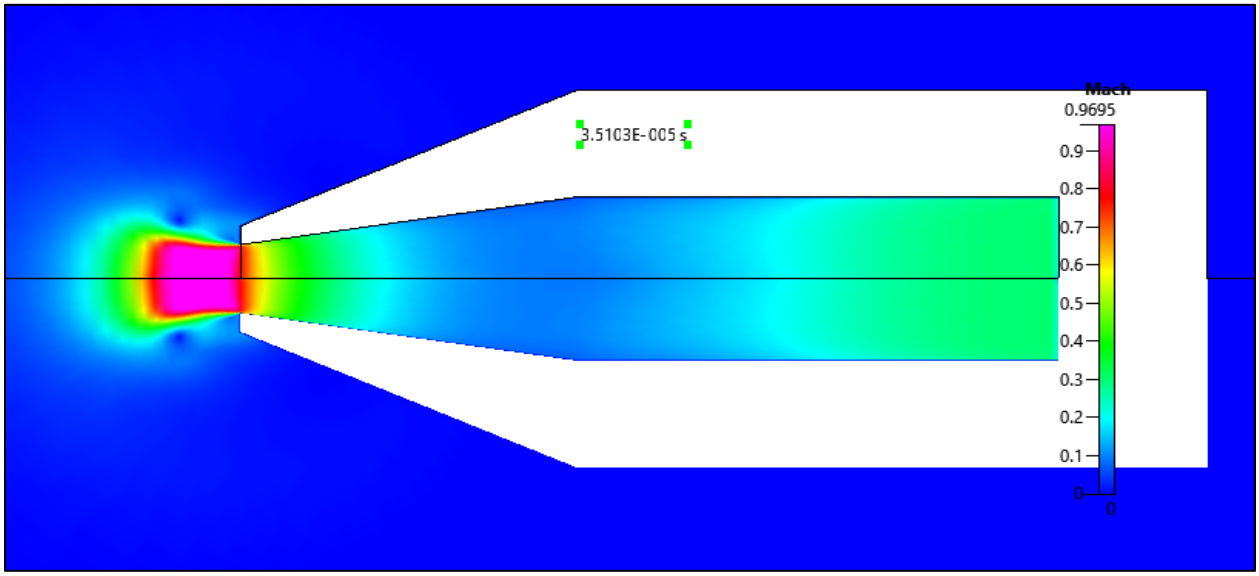

Figure 5.8: Mach Transient State at Time 3.5103E00-5s

Figure 5.9, shows the steady state Mach field. By this time, the Mach number field has stabilized into a smooth, predictable pattern. The flow now exhibits a well-defined, fully

expanded supersonic jet emerging from the nozzle, indicating that the transient startup effects have diminished, and the nozzle is operating at its intended steady-state conditions.

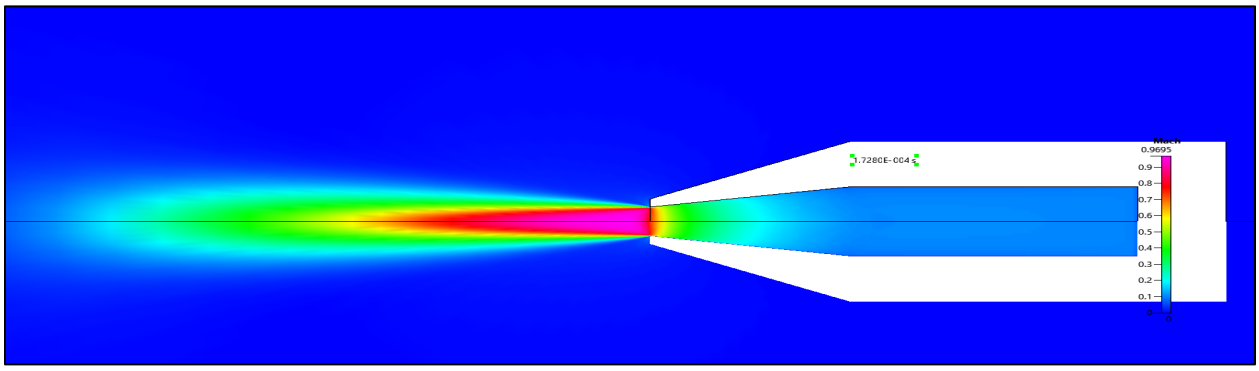

Figure 5.9: Mach Steady state at time 1.7280E-004s

5.5.2 Pressure

Figure 5.10 shows pressure at time = 2.6815×10^-5s in a transient state. At this early stage, the pressure field within and just beyond the nozzle is still adjusting from the initial startup conditions. Higher pressures near the inlet rapidly transition downstream, but localized variations and incomplete expansions indicate the flow has not yet formed a stable pressure profile.

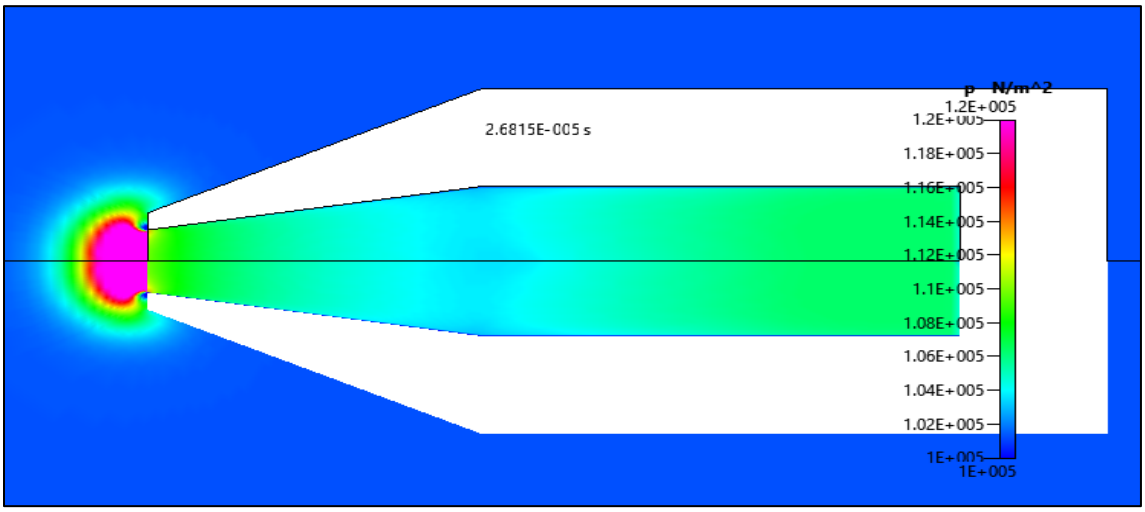

Figure 5.10: Pressure Transient state at time 2.6815E00-5s

Figure 5.11 shows pressure at time 3.5103×10^-5s in a transient state. As the flow evolves, the pressure distribution begins to smooth out, showing a more coherent drop in pressure along the nozzle centerline. While still not fully steady, the gradients are less abrupt, and the downstream region is starting to reflect a more organized expansion and consistent pressure levels.

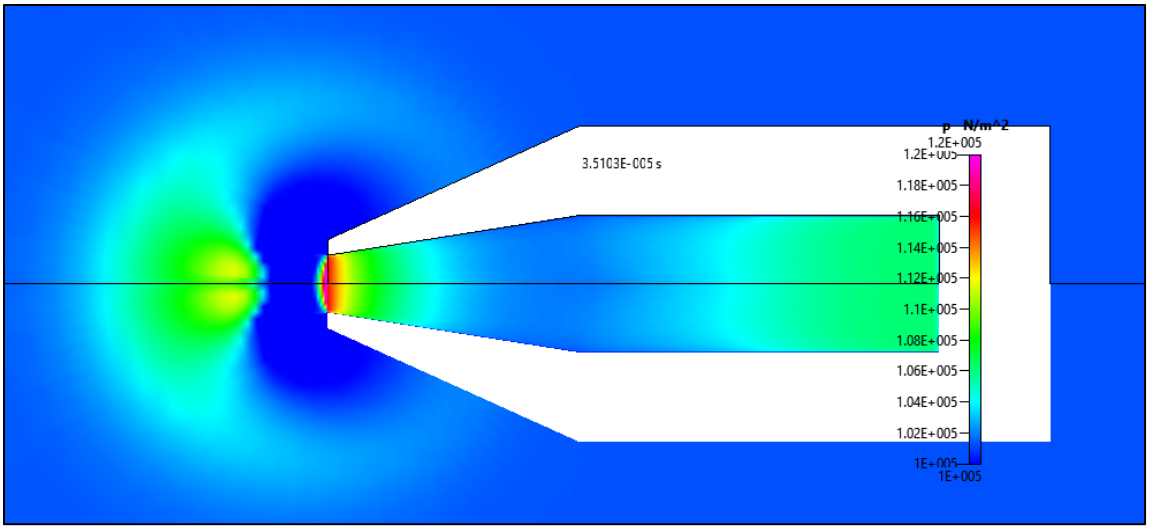

Figure 5.11: Pressure Transient state at time 3.5103E00-5s

Figure 5.12 shows pressure at time 1.7280×10^-4s in steady state: By this point, the pressure field has stabilized into a steady, predictable pattern, with a smooth and gradual pressure decrease from inlet to exit. The well-defined, stable pressure distribution indicates the nozzle has reached its intended operating condition, enabling a uniform and controlled expansion of the cold gas into the ambient environment.

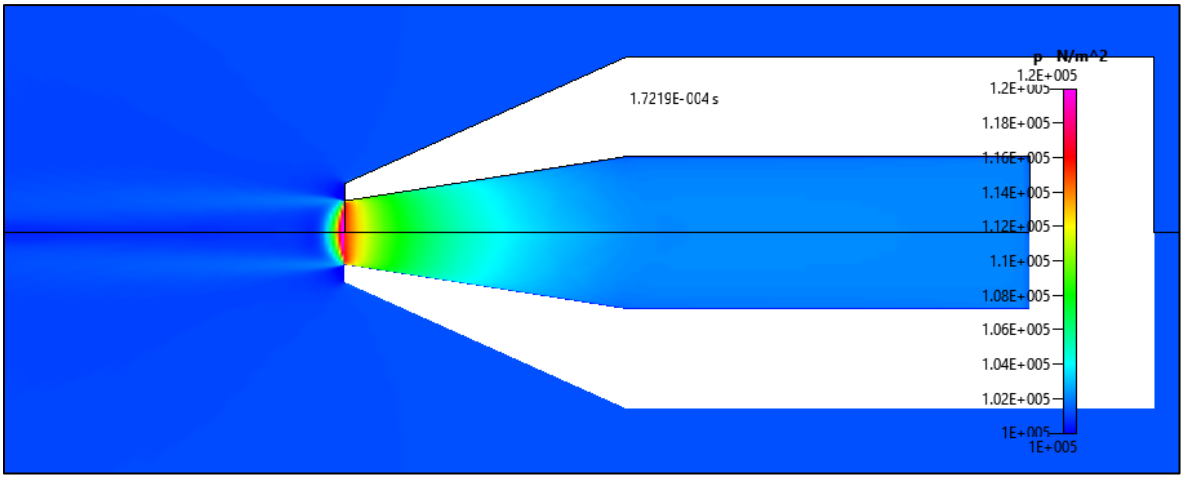

Figure 5.12: Pressure Steady state at time 1.7280E-004s

5.5.3 Density

Figure 6.12 shows density at time 2.6815×10^-5 s in transient state. At this very early transient stage, the density field within and just downstream of the nozzle is still adjusting from initial conditions. The gas near the inlet remains relatively dense, while regions farther into the divergent section show a gradual decrease in density that is not yet uniform, indicating that the flow is still establishing its expected density gradient.

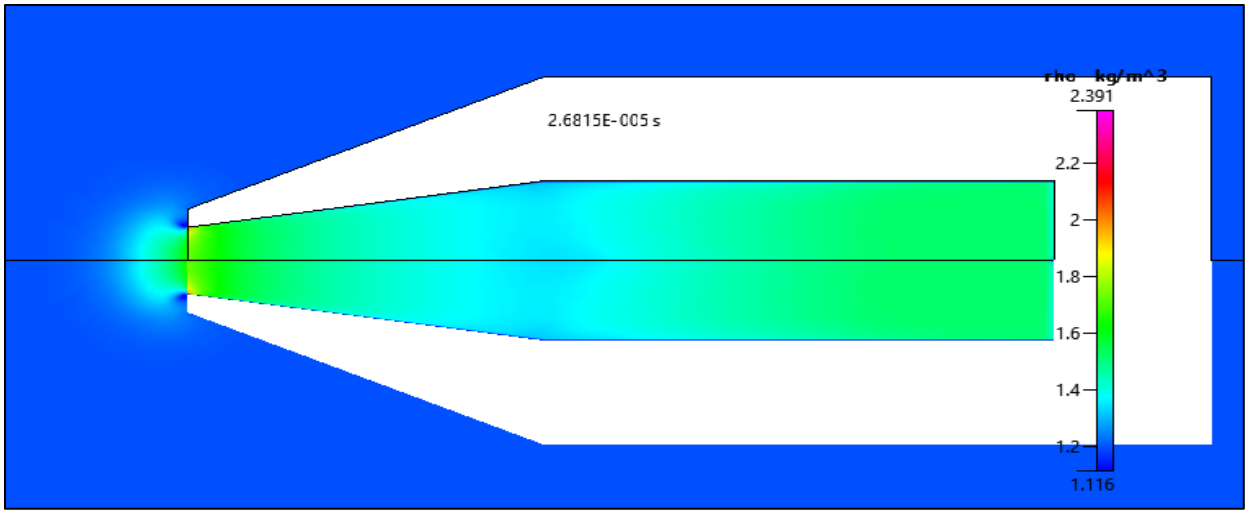

Figure 5.13: Density Transient state at time 2.6815E00-5s

Figure 5.14 shows density at time 3.5103×10^-5s in transient state. A bit later in the transient, the density distribution becomes more coherent, with a more pronounced decline from the inlet to the nozzle exit. Although not fully settled, the gradient is smoother, and the density variations along the core flow are less irregular, suggesting that the flow is moving closer to a stable expansion regime.

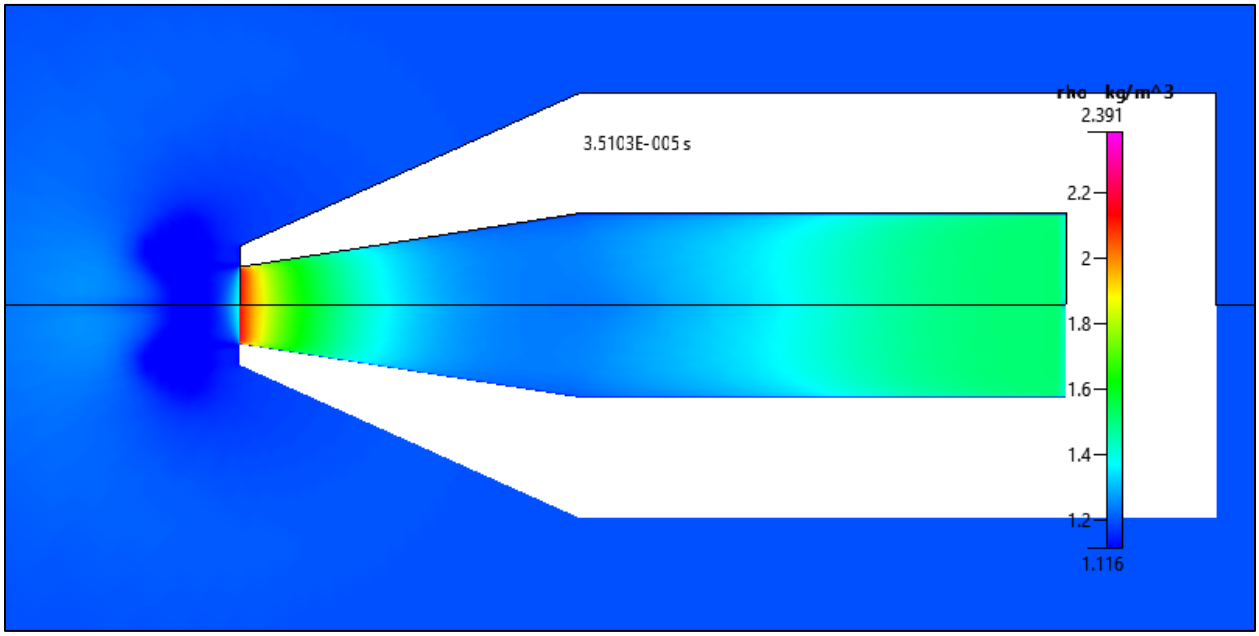

Figure 5.14: Density Transient state at time 3.5103E00-5s

Figure 5.15 shows density at time 1.7280×10^-4s in steady state. By steady state, the density field has reached a stable and predictable pattern, with a clear, uniform gradient from high density at the inlet to lower density at the nozzle exit. The well-defined density distribution

now reflects the expected isentropic expansion through the nozzle, signifying that the transient startup effects have passed and the flow is operating as designed.

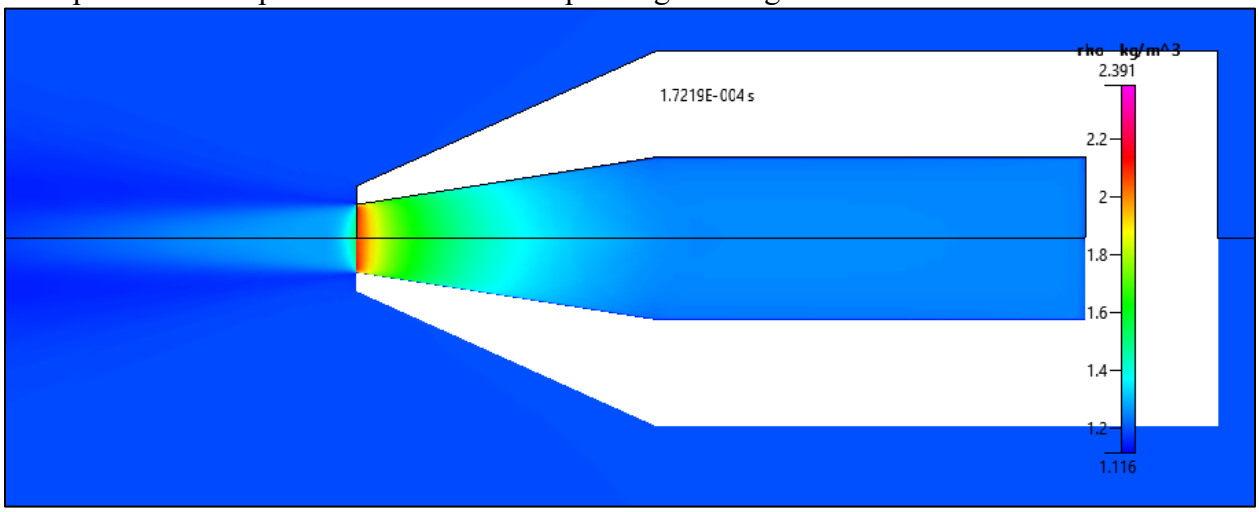

Figure 5.15: Density Steady state at time 1.7280E-004s

5.5.4 Temperature

Figure 5.16 temperature at time 2.6815×10^-5s in transient state. At this very early transient stage, the temperature field shows a high-temperature region near the nozzle inlet gradually extending downstream but still relatively uneven. Warmer gas is entering the nozzle, but the expansion process is not yet fully developed, resulting in a non-uniform thermal gradient that indicates the flow is still transitioning from initial startup conditions.

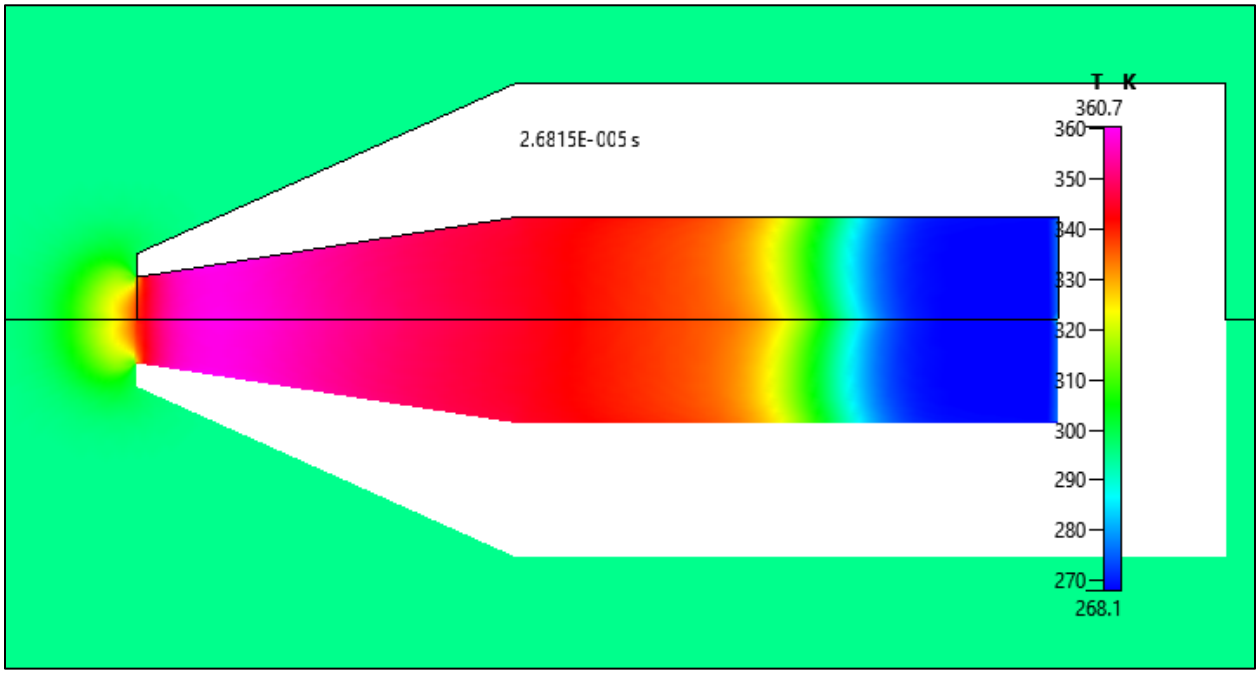

Figure 5.16: Temperature Transient state at time 2.6815E00-5s

Figure 5.17 shows temperature at time 3.5103×10^-5s in transient state. A short time later, the temperature distribution becomes more coherent, with a clearer gradient along the nozzle axis. The once uneven thermal field is smoothing out as the gas continues to expand and cool, reflecting a flow that is moving closer to the stable temperature profile expected in steady-state operation.

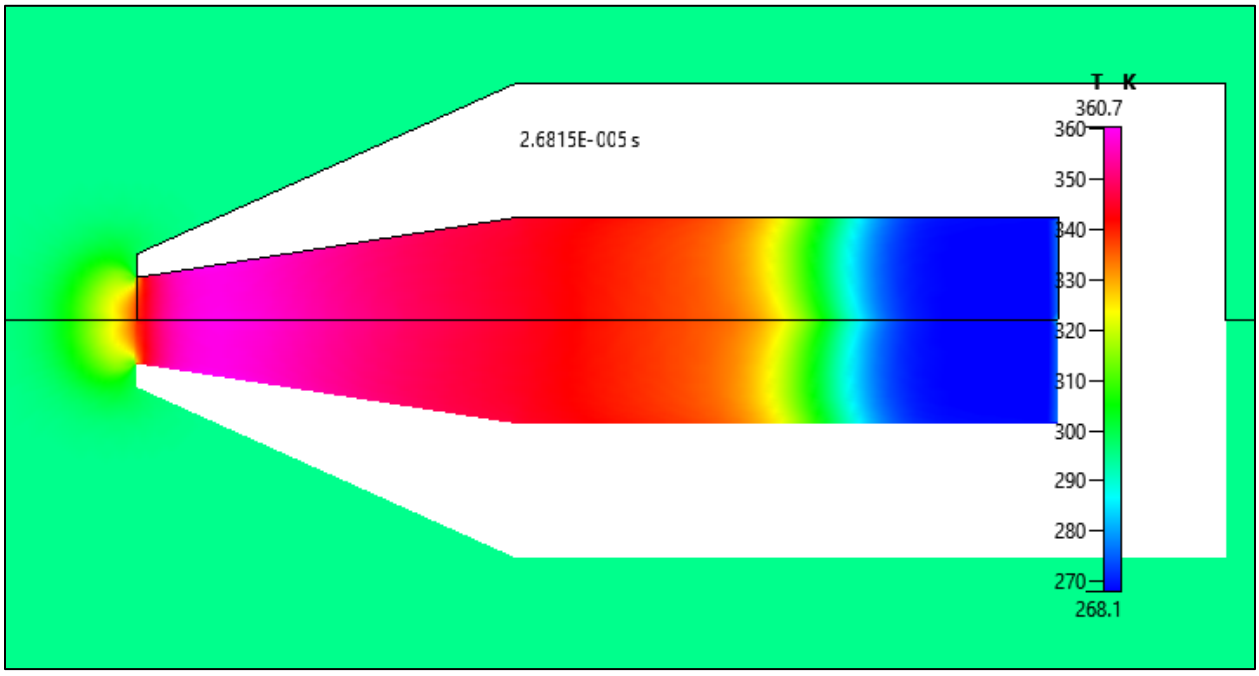

Figure 5.17: Temperature Transient state at time 2.6815E00-5s

Figure 5.18 temperature at time 1.7280×10^-4s in steady state. By the steady-state point, the temperature field has fully stabilized, presenting a well-defined thermal gradient from the warmer inlet region to the cooler nozzle exit. The gas has now undergone a nearly ideal, isentropic expansion through the nozzle, resulting in a consistent, predictable temperature distribution that matches the nozzle's intended design conditions.

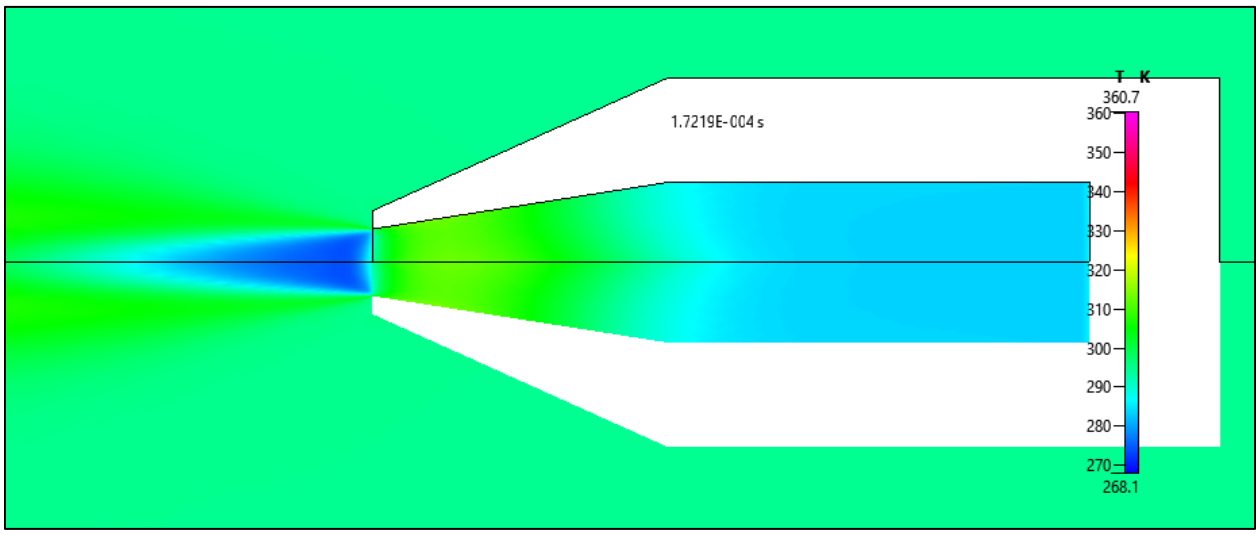

Figure 5.18: Temperature Steady state at time 1.7280E-004s

Chapter 6. Cold Gas Propulsion Tank Proof of Concept

6.1 Propulsion – Rapid 3D Printed Prototype Characteristics

Attitude control for the spacecraft will be actuated with a cold gas thrusting system. Cold gas systems are simple, precise, and accurate; ideal for an attitude control system for spacecraft which require specific orientations. Cold gas systems provide several benefits over alternative propulsion or attitude control systems, as well as several drawbacks. In comparison to other propulsive systems, a cold gas system does not require high voltage electronics, such as with ion propulsion, nor are extreme thermal loads a concern, such as with pressure fed combustion systems.

The reliability of pressure-fed, inert gas systems rivals those of pump-fed, combusting systems. However, the benefits provided with reliability and precision are offset with efficiency and longevity. Cold gas systems have significantly lower specific impulses, requiring additional propellant for equivalent longevity or velocity. Cold gas systems operate at lower temperatures and pressures than combusting counterparts, and consequently have lower internal propellant energies. This hinders the maximum linear momentum change of the propellant, resulting in lower exhaust velocities. While the system is capable of precise control, high reaction speeds, and reliability, it suffers in requiring more propellant or shorter endurance for equivalent performance or mass, respectively.

Table 6.1: Requirements for the propulsion subsystem

Requirement	Parameters	Justification
Configuration	4 nozzles, 2 pairs	Roll Control (3DOF capable: 1 orientation, 2 translation)
Thrust	50 mN-100 mN	Low thrust for low impulse bit and low rate changes and accelerations. Thrust must be enough to provide high reaction time to perturbation, however.
Minimum impulse bit	0.1 mN*s	Low impulse bit results in higher control precision.
Propellant	CO_2	Propellant is cheap, widely available and inert.
Storage	860 psig liquid	Liquid storage for high density, and cartridges of varying propellant masses are available at this pressure.
Regulation	0-60 psig manual	Manual adjustment to set ideal pressure. Lower pressure to lower stress of propulsion components.
Feed	1/8" ID vinyl	Tubing is flexible, strong, and must provide enough mass flow rate for the nozzles while having a small volume and wide availability.

Requirement	Parameters	Justification
Recharge/Refuel	Disposable CO_2 cartridges	Widely availability and easy to use.
Quantity/Endurance	10 mins	Long enough duration for frequency analysis and to observe steady state performance of prototype
Valve actuating speed	100-500Hz	Higher actuation speed decreases impulse bit of the nozzle, but has drawbacks in cost and manufacturability. Desired range is functional with electronics and cost constraints.
Number of valves	4 to 5 DC Solenoid	A valve for each nozzle, and an optional expansion tank valve to provide a buffer for long duration thrusting. Optional valve can be replaced with manually adjustable passive regulator for simplicity and reliability.

6.2 Propellant

Cold gas systems do not add any more energy through chemical reactions, or electric power, and are powered only by the internal energy of the pressurized gas at a specific temperature. The qualities of the gas greatly affect the performance of the system. The gas constant of the propellant determines the maximum theoretical specific impulse of the thruster, with higher gas constants resulting in higher performance, given all other conditions are ideal. However, due to the expansion of the gas in the divergent section of the nozzle, it is important to consider the phase transition lines of the propellant. Hydrogen propellant has a gas constant of $R = 4124\ \frac{J}{kg \cdot K}$, so with a given pressure and temperature, the specific impulse will be the highest of any cold gas propellant. However, hydrogen is difficult to store over long periods, highly flammable, and stores at lower density than other propellants. Nitrogen was also considered a propellant. Nitrogen is strongly inert, harmless if inhaled (unless inhaled to the exclusion of oxygen), provides acceptable performance and storage characteristics ($R = 289\ \frac{J}{kg \cdot K}$), and is easily interchangeable with other propellants. At very low pressures (>.1 atm) the transition temperature of gaseous N_2 is -210°C, defining the expansion ratio envelope.

However, CO_2 was chosen as the propellant for the rapid prototype due to the availability of compatible parts and low expense, allowing for testing room within the budget. CO_2 propellant characteristics do not provide the same characteristics as other propellants' characteristics ($R = 188.9\ \frac{J}{kg \cdot K}$), but will be sufficient for testing the attitude control system and basic propulsion configuration. The transition temperature at low pressures is higher than nitrogen, -105°C, which limits the expansion ratio.

6.3 Tank for Rapid Prototype

For this project we will only focus on the tank design but have included what a full mounting configuration could look like for a complete feed system for a cold gas propulsion system. Figure 6.1 highlights all the key features that are used in a rapid prototype solution for proof of concept cold gas propulsion tank using inexpensive parts prior to investing in more space grade quality material and components.

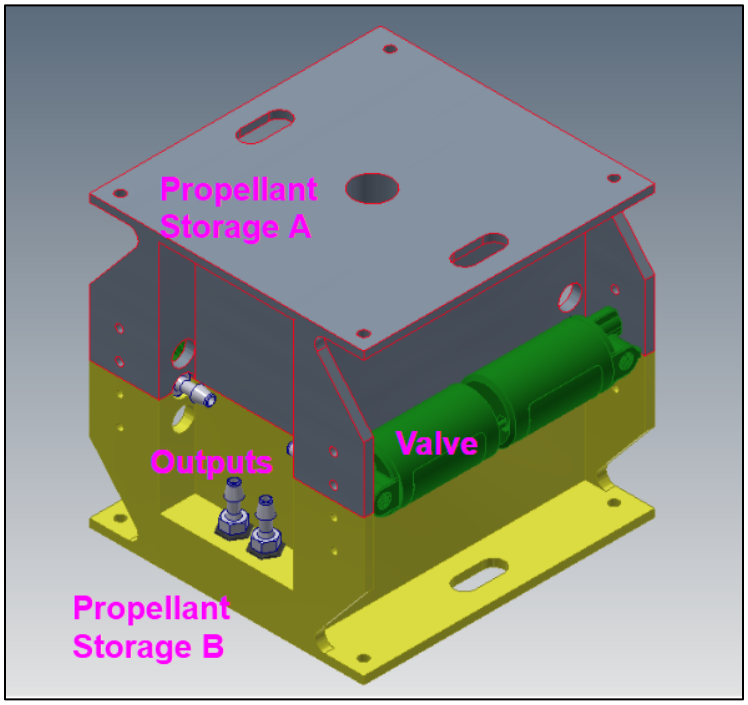

Figure 6.1: Rapid prototype for a propulsion system mounting, vessel, and feed system.

Figure 7.3: Is a cross section view of the entire pressure vessel, showing the top half without the outputs. In this figure note that deformation is not to scale. For this tank we modeled it using common 3D printed material, PLA, and got a yield strength result of 8 ksi. If in a test environment the tank were to be filled only to 60 Psi, we would obtain a maximum stress result of 3.43 ksi, giving a safety factor of greater than 2.

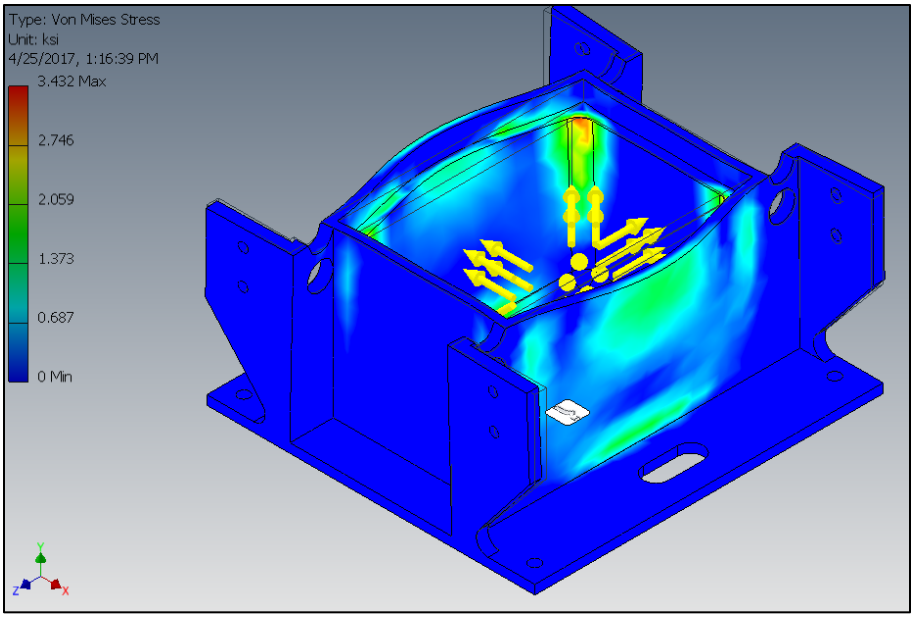

Figure 6.2: 3D Cross Sectional View of the Prototype Proof of Concept

Chapter 7. Aluminum Alloy Space Grade Propulsion Tank Analysis

After testing some initial conditions and methodology approach we then went ahead and re-ran the results simulating actual space requirement parameters. We simplified the design of it for manufacturability and incorporate Aluminum Alloy 6061-T6 as the structure material. Table 7.1 contains the material properties for the alloy. Furthermore, assumed that we would have Nitrogen readily available so therefore used it as our working fluid. Figure 7.5 is the representation of the new 3D model for the tank we used to simplify the new simulation.

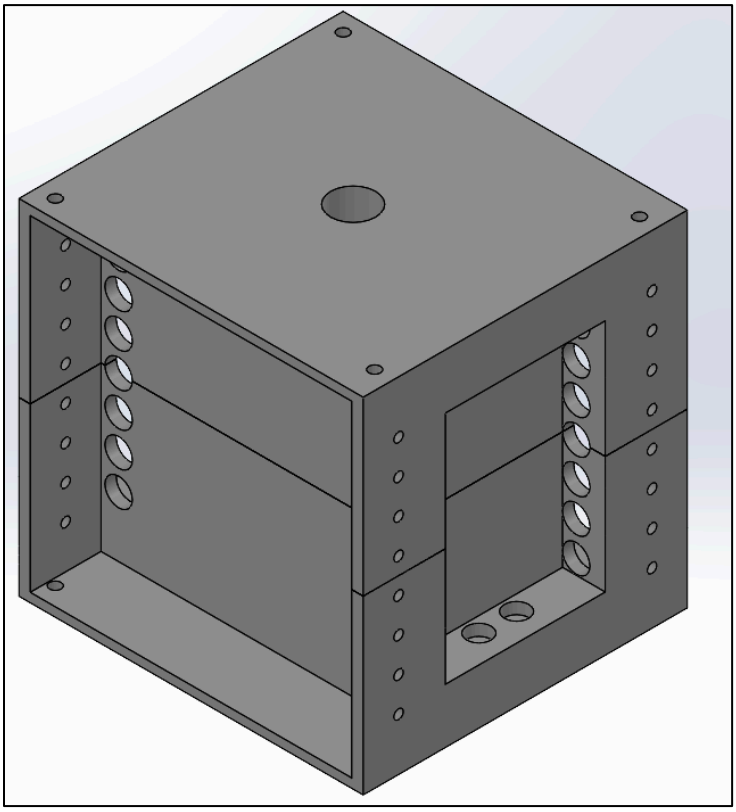

Figure 7.1: Visual Representation of the 1U structure Al 6061-T6 Tank

Table 7.1: Aluminum Alloy 6061-T6 Properties

Name:	Properties
Name:	6061-T6 (SS)
Model type:	Linear Elastic Isotropic
Default failure criterion:	Max von Mises Stress
Yield strength:	2.75e+08 N/m^2
Tensile strength:	3.1e+08 N/m^2
Elastic modulus:	6.9e+10 N/m^2
Poisson's ratio:	0.33
Mass density:	2,700 kg/m^3
Shear modulus:	2.6e+10 N/m^2
Thermal expansion coefficient:	2.4e-05 /Kelvin

The propulsion tank structure has a 1U footprint, with an interior tank dimension area of 4cm x 5cm x 6cm. Furthermore, the tank has a wall thickness of 5.00 mm. One test case was done at 500 psi an another test case at1000 psi. Figure 7.4 shows how we set up the pressure profile.

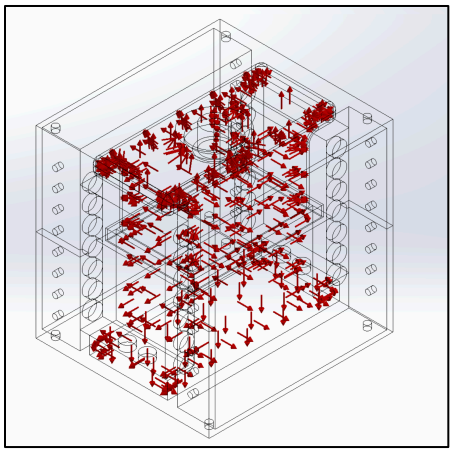

We ran two different test cases to see if our results would have significant variance in structural integrity and deformation. As mentioned, one test was done at 500 psi and another at 1000 psi. Figure 7.5 illustrates the results of both test cases focusing on structural deformation.

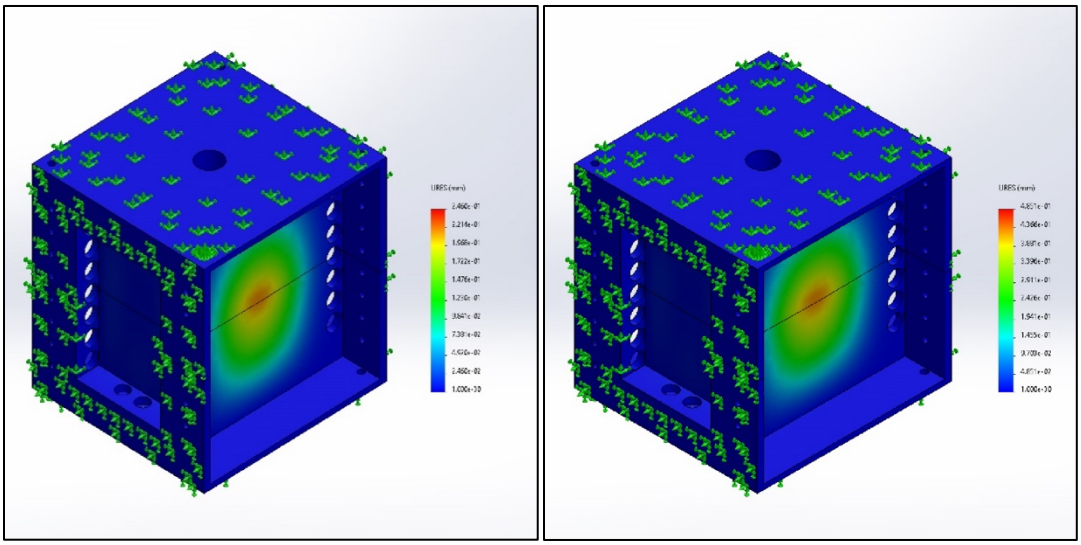

Figure 7.2: Shows 500 PSI results on the left and 1000 PSI results on the right

The max and min displacements of the displacement results are summarized in Table 7.2.

Table 7.2: Min and Max Results at for both 500 and 1000 PSI for Displacement

Displacement	**500 PSI**	**1000 PSI**
Min	0.000e+00mm	0.000e+00mm
Max	2.460e-01mm	4.851e-01mm

7.1.1 Summary of Deflection Base on Results

At 500 PSI, the maximum displacement is about 0.246 mm. Compared to a 5.08 mm thick wall, this displacement is roughly 4.8% of the wall thickness. At 1000 PSI, the maximum displacement is about 0.4851 mm, about 9.5% of the wall thickness. Although these displacements are not negligible, we do have a relatively stiff panel structure with good material properties from Aluminum 6061-T6. Furthermore, we do observe some bending in the simulation but given that we are well below 1 mm of deflection, this puts us in a healthy, robust design with plenty of margin.

7.1.2 Summary of Stress and Strain

When we apply a pressure of about 500 psi, the highest stress in the part is around 200 MPa. Since the yield strength of 6061-T6 aluminum is around 275 MPa, this means the part should be fine and only deform elastically at 500 psi, with no lasting damage. But when we go up to 1000 psi, the stress hits about 399 MPa, which is above the yield strength. That suggests the material might start to permanently bend or even fail if it stays at that higher pressure. Results show in in table 7.3.

At 500 psi, the strain we see (about 0.001854) makes sense and fits with the idea that the material is only bending a little bit and staying elastic. This is totally reasonable given the thickness of the part (about 0.2 inches or 5.08 mm). But at 1000 psi, we got a weird result with the strain numbers being the same for both minimum and maximum strain. Normally, if you double the pressure, you'd expect the strain to go up too, not stay the same. This might mean there was some kind of mistake in how we ran the model or processed the data. To be sure, we'd probably want to re-check the calculations or even do a physical test to confirm what really happens at 1000 psi. Results show in in table 7.3.

Table 7.3: Stress and Strain Results

	500 PSI	**1000 PSI**
Stress		
Min	4.313e-04N/m^2	1.565e-03N/m^2
Max	2.004e+08N/m^2	3.987e+08N/m^2
Strain		
Min	3.505E-09	5.27E-09
Max	0.001854	0.003693

Given some uncertainty in our results for 1000 psi, please reference the appendix for further details on how the simulation was set up. However, the results for the tank design do meet at a minimum 500 PSI and our CFD nozzle design. Further work is required to understand the tanks upper pressure limits.

Chapter 8. Summary and Future Work

8.1 Summary

Over the course of this project, I conducted a comprehensive literature review and trade study on cutting-edge optical communication technologies tailored for CubeSats, while simultaneously investigating a cold gas propulsion system intended to support precise spacecraft orientation and improve communication link stability. The literature reviews encompassed a range of CubeSat laser communication payloads—such as NASA's TBIRD, DLR's OSIRIS series, and commercial terminals like CubeLCT and CubeCAT—demonstrating a clear trend toward higher data rates, improved SWaP efficiencies, and more robust pointing and tracking methods. This knowledge was integrated to highlight both the rapid technological maturation of optical communication systems and the persistent challenges posed by atmospheric effects, miniaturization constraints, and inter-satellite link complexities.

In addition to the communications trade study, I designed and analyzed a cold gas propulsion nozzle and conceptual propulsion tank system. Using computational fluid dynamics (CFD) simulations, I characterized the nozzle's flow field evolution from transient to steady-state operation, capturing the development of Mach, pressure, density, and temperature fields. I then did a structural analyses to further examine a propellant tank design, ranging from initial 3D-printed prototypes to aluminum alloy tanks suitable for higher pressures.

8.2 Future Work

For future work on the optical communication system, a logical next step would be conducting a focused ground-based or lab-based test campaign that replicates anticipated orbital conditions. This could involve simulating atmospheric turbulence, employing adaptive optics techniques, and validating key performance parameters—such as data rate and pointing stability—under controlled, repeatable scenarios. Such testing would provide valuable feedback that refines models, informs hardware modifications, and builds confidence prior to any flight demonstrations.

For the cold gas thruster, moving from analysis to physical prototyping would yield the most immediate benefit. Fabricating a small-scale test article and conducting static fire tests would allow for direct measurement of thrust, specific impulse, and valve response times. Gathering empirical data would enable validation of CFD models, identification of manufacturing or design refinements, and ultimately guide the development of a flight-ready propulsion unit that can be integrated into future CubeSat missions.

References

[1] Figliozzi, G., and Tavares, F., “What are NASA’s Technology Educational Satellites?,” *NASA Ames Research Center*.[online article], URL: [retrieved 09 December 2024].

[2] Rosila-Mares, J., “CubeSat development and testing: An overview,” CalPoly Cube Developers Workshop 2019 [Presentation], URL: http://mstl.atl.calpoly.edu/~workshop/archive/2019/Spring/Day%203/Session%204/JesusRosilaMares.pdf [retrieved 09 December 2024]

[3] “What are smallsats and CubeSats?,” *NASA* [online article], URL: https://www.nasa.gov/what-are-smallsats-and-cubesats/ [retrieved 09 December 2024]

[4] Schieler, C. M., Riesing, K. M., Bilyeu, B. C., Chang, J. S., Garg, A. S., Gilbert, N. J., Horvath, A. J., Reeve, R. S., Robinson, B. S., Wang, J. P., Piazzolla, S., Roberts, W. T., Kovalik, J. M., and Keer, B., "On-orbit demonstration of 200-Gbps laser communication downlink from the TBIRD CubeSat," *Proc.SPIE*. Vol. 12413, 2023, p. 1241302.

[5] Rödiger, B., Menninger, C., Fuchs, C., Grillmayer, L., Arnold, S., Rochow, C., Wertz, P., and Schmidt, C., “High data-rate optical communication payload for CubeSats," *Proc.SPIE*. Vol. 11506, 2020, p. 1150604.

[6] Lin, S.F., "Compact dual channel free space optical communication for CubeSat inter-satellite links," *Proc.SPIE*. Vol. 12691, 2023, p. 126910U.

[7] Mendes, P. N., Teixeira, G. L., Pinho, D., Rocha, R., André, P., Niehus, M., Faleiro, R., Rusca, D., and Zambrini Cruzeiro, E., “Optical payload design for downlink quantum key distribution and keyless communication using CubeSats,” *arXiv.* [online database], doi: *https://arxiv.org/abs/2310.16017*

[8] Nonay, J. R., Fuchs, C., Orsucci, D., Schmidt, C., and Giggenbach, D., “SelenIRIS: A Moon-Earth optical communication terminal for CubeSats,” *2022 IEEE International Conference on Space Optical Systems and Applications (ICSOS), 186–195.* doi*: https://doi.org/10.1109/ICSOS53063.2022.9749725*

[9] Tummala, A. R., and Dutta, A. “An overview of Cube-satellite propulsion technologies and trends,[online journal] *Aerospace,* Vol.4 No. 4, 58. 2017. doi:*https://doi.org/10.3390/aerospace4040058*

[10] Shcheglov, G. A., and Mordovskii, A. V., "Design optimization of cubic-shaped pressurant tank for CubeSat propulsion system," *Acta Astronautica* Vol. 224, 2024, pp. 48-56. doi: https://doi.org/10.1016/j.actaastro.2024.07.037

[11] Ranjan, R., Chou, S. K., Riaz, F., and Karthikeyan, K., "Cold gas micro propulsion development for satellite application," *Energy Procedia* Vol. 143, 2017, pp. 754-761. doi: https://doi.org/10.1016/j.egypro.2017.12.758

[12] Komachi, S., Fujita, S., Takeda, K., Nakaoka, H., Kuwahara, T., Yoshida, K., and Kawaguchi, J., Safe Attitude and Orbit Control for ISS-Deployed CubeSat HOKUSHIN-1 with Cold-Gas Propulsion System," *2024 IEEE/SICE International Symposium on System Integration (SII)*. 2024, pp. 1445-1451. doi:10.1109/SII58957.2024.10417713

[13] Lightsey, E. G., Stevenson, T., and Sorgenfrei, M., "Development and Testing of a 3-D-Printed Cold Gas Thruster for an Interplanetary CubeSat," *Proceedings of the IEEE* Vol. 106, No. 3, 2018, pp. 379-390.
doi: 10.1109/JPROC.2018.2799898

[14] Kvell, U., Puusepp, M., Kaminski, F., Past, J.-E., Palmer, K., Grönland, T.A., and Noorma, M., Nanosatellite orbit control using MEMS cold gas thrusters. *Proceedings of the Estonian Academy of Sciences*, Vol.63, No. 2S, 2014, pp. 279–285.
doi:https://doi.org/10.3176/proc.2014.2S.09

[15] Takenaka, H., Koyama, Y., Kolev, D., Akioka, M., Iwakiri, N., Kunimori, H., Carrasco-Casado, A., Munemasa, Y., Okamoto, E., and Toyoshima, M., ("In-orbit verification of small optical transponder (SOTA): evaluation of satellite-to-ground laser communication links," *Proc.SPIE*. Vol. 9739, 2016, p. 973903.
doi: https://doi.org/10.1117/12.2214461

[16] "Small Optical TrAnsponder (SOTA)," *National Institute of Information and Communications Technology (NICT)* [online article] URL: https://www2.nict.go.jp/spacelab/en/pj_sota.html [retrieved 10 December 2024]

[17] Fuchs, C., Schmidt, C., Keim, J., Molla, F., Rödigera, B., Lengowski, M., Gaißer, S., and Giggenbach, D., "Update on DLR's OSIRIS program and first results of OSIRISv1 on Flying Laptop," *Proc.SPIE*. Vol. 10910, 2019, p. 109100S.
doi:https://doi.org/10.1117/12.2514349

[18] Schmidt, C., and Fuchs, C., "The OSIRIS program at DLR," *Proc.SPIE*. Vol. 10524, 2018, p. 105240R.
doi:https://doi.org/10.1117/12.2290726

[19] Giggenbach, D., Fuchs, C., Schmidt, C., Rödigera, B., Gaißer, S., Klinkner, S., Phung, D.-H., Chabé, J., Courde, C., Maurice, N., Mariey, H., Samain, E., and Artaud, G., "Downlink communication experiments with OSIRISv1 laser terminal onboard Flying Laptop satellite," *Applied Optics* Vol. 61, No. 8, 2022, pp. 1938-1946.
doi: 10.1364/AO.446771

[20] Rose, T. S., Rowen, D. W., LaLumondiere, S. D., Werner, N. I., Linares, R., Faler, A. C., Wicker, J. M., Coffman, C. M., Maul, G. A., Chien, D. H., Utter, A. C., Welle, R. P., and Janson, S. W., (2019). "Optical communications downlink from a low-earth orbiting 1.5U CubeSat," *Optics Express* Vol. 27, No. 17, 2019, pp. 24382-24392.
doi: 10.1364/OE.27.024382

[21] Iwamoto, K., Komatsu, H., Ohta, S., Kubo, Y., Nakao, T., Yamazoe, H., Kamata, T., Munemasa, Y., Kunimori, H., Toyoshima, M., Koda, D., and Sawada, H., "Experimental results on in-orbit technology demonstration of SOLISS," *Proc.SPIE*. Vol. 11678, 2021, p. 116780D.
doi:https://doi.org/10.1117/12.2578089

[22] Komatsu, H., Ohta, S., Yamazoe, H., Kubo, Y., Nakao, T., Ito, T., Koda, D., Sawada, H., Ikeda, T., Munemasa, Y., Kunimori, H., Toyoshima, M., and Iwamoto, K., "The pointing performance of the optical communication terminal, SOLISS in the experimentation of bidirectional laser communication with an optical ground station," *Proc.SPIE*. Vol. 11678, 2021, p. 116780F.
doi:https://doi.org/10.1117/12.2577067

[23] "Small Optical Link for International Space Station (SOLISS) Succeeds in Bidirectional Laser Communication Between Space and Ground Station," Japan Aerospace Exploration Agency (JAXA). 2020. URL: https://global.jaxa.jp/press/2020/04/20200423-1_e.html. [retrieved 10 December 2024]

[24] Tesat., "CubeLCT: Smallest laser communication transmitter worldwide," *Tesat-Spacecom GmbH & Co. KG.* URL: https://satcatalog.s3.amazonaws.com/components/568/SatCatalog_-_Tesat-Spacecom_-_CubeLCT_100M_-_Datasheet.pdf?lastmod=20210803070119. [retrieved 09 December 2024)

[25] Kammerer, W., Grenfell, P., Hyest, L., Serra, P., Tomio, H., Belsten, N., Lindsay, C., Čierny, O., Cahoy, K., Clark, M., Coogan, D., Conklin, J., Mayer, D., Stupl, J., and Hanson, J. (2023)., "CLICK mission flight terminal optomechanical integration and testing," *Proc.SPIE*. Vol. 12777, 2023, p. 1277730.
doi:https://doi.org/10.1117/12.2690321

[26] "CubeCAT: Laser communication module for CubeSats," *AAC Clyde Space.* URL: https://www.aac-clyde.space/wp-content/uploads/2021/10/CUBECAT.pdf. [retrieved 09 December 2021]

Appendix A: TechEd Sat 8 Presentation

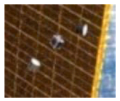

TechEdSat-N and SOAREX Flight Series

SOAREX-6
2008

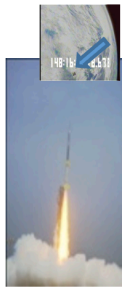

SOAREX-7
2009

TES-1
Oct 4, 2012

First US Nanosat deployed off ISS
PSRP process mastered
Rad-tolerant processor demo

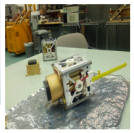

TES-2
Iridium test
Aug 21, 2013

First Iridium in-space COM demonstration

First Exo-Brake Deployed from a cubesat

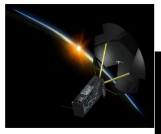

TES-3
Aug 3, 2013
(6 wk deorbit)

Evolution of TES-3 Iridium modem Uplink/via email demonstrated Exo-Brake II

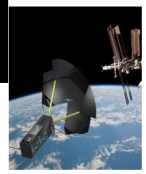

TES-4
Mar 3, 2015
(4 wk deorbit)

WSM1, AIM Camera X-Band, ISM-Band, P5 alpha, ISM-Camera and Full ExoBrake

SOAREX-8 During test (WFF)
July 7, 2015

WSM2, AIM Camera ISM-Band, P5 alpha, ISM-Camera

SOAREX -9 (WFF)
March 3, 2016

Modulated Exo-Brake
Improved positional/target accuracy
Improved Targeting, WSM2, ISM Band

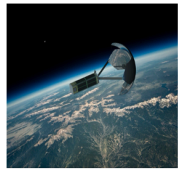

TechEdSat5/PhoneSat5
March 6, 2017

First cubesat commanded and target for re-entry, ISM band, WSM2

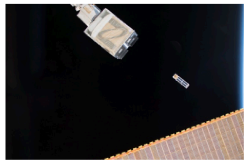

TechEdSat-6 (ISS Jettison Nov 20,2017)
(ATK-8 Nov. 12, 2017)

Recent Years of Flight Experiments (2008-2015):
6 Flights +1(SOAREX8&9) +PhoneSats 1-4

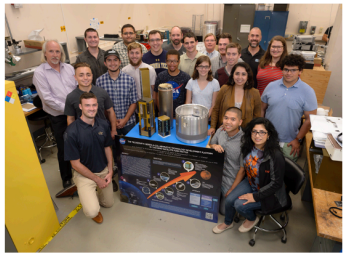

First Lunar and Mars radio, control board with magnetorquers, VR and Nvidia board, rad-tolerant power board.

Launch Date: December 5, 2018; Launch Vehicle: SpaceX CRS-16; Jettison Date: January 31st, 2019

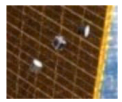

Let's Load and Go

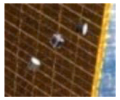

TechEdSat-8

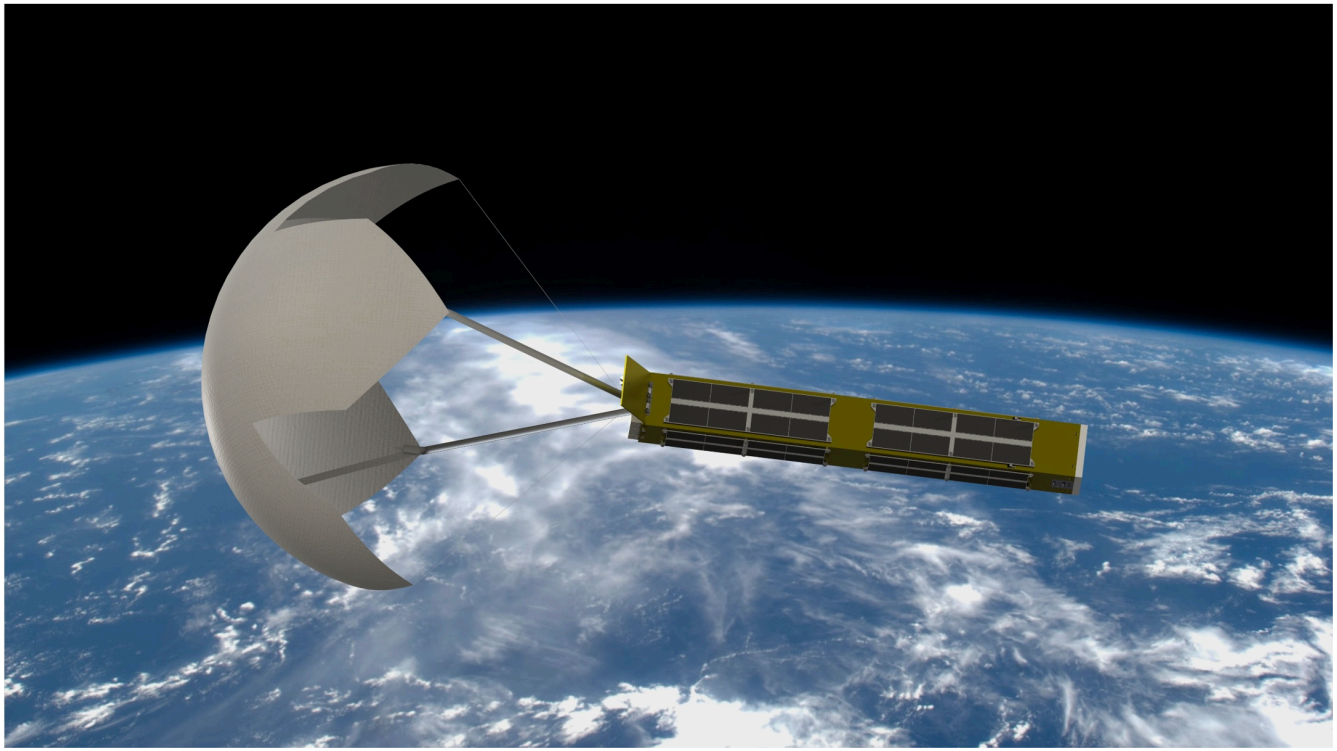

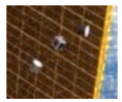

Background

ISS EDL Capabilities For Future Missions

SPQR-Small Payload Quick Return

- 3 stage concept
- Rapid Development and Test of **science and technology**

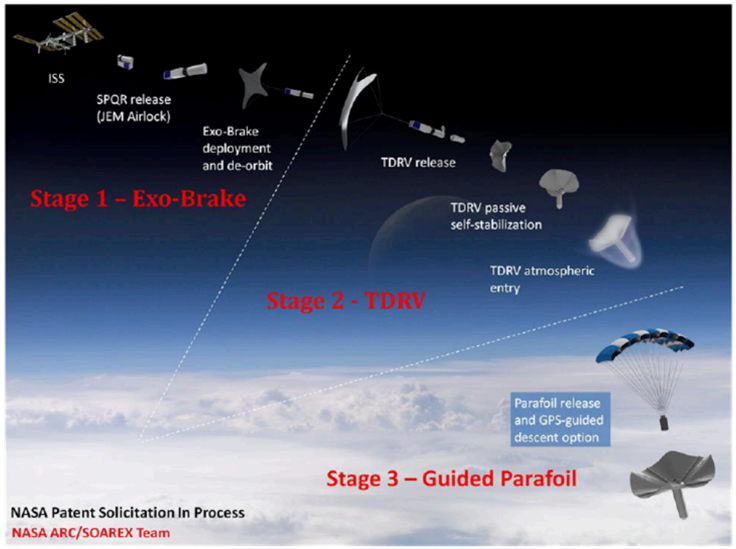

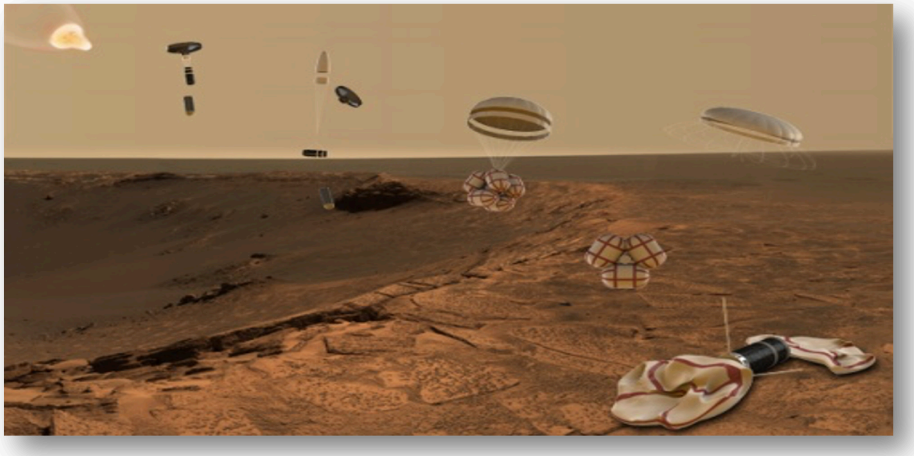

Atromos: Cubesat Mission to the Surface of Mars

- **Mission Attributes**
  - Self-stabilizing re-entry probe (TDRV-Tube Deployed Re-Entry Vehicle)
  - EDL Technique for small probes
  - Nuclear option for mission longevity

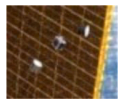

TES-8 Exploded View

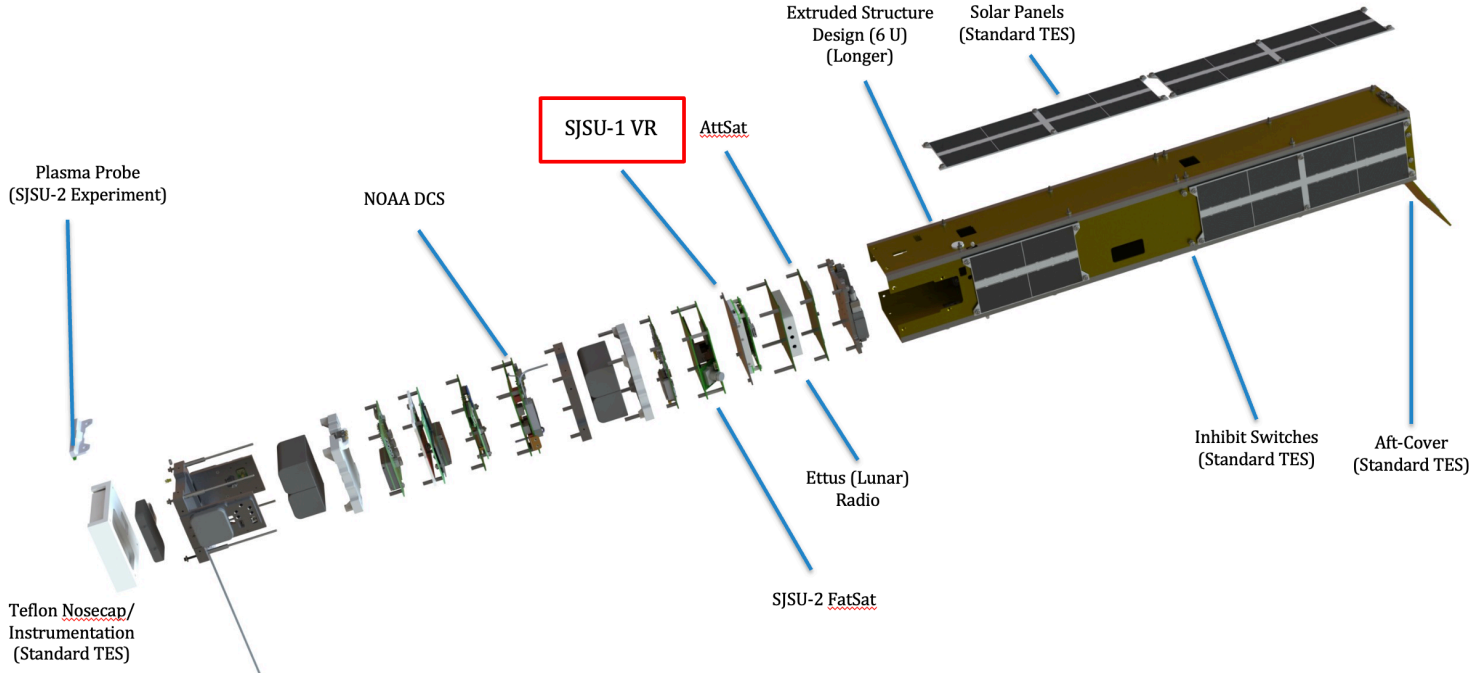

Nano-Orbital Workshop: **8 radios** (3 Iridium; 1 Globalstar; GOES/DCS/Mars Radio, Wifi-to-ground; Internal Zigbee sensor network; Lunar Radio/SDR), **4 cameras** (including VR), banjo-magnetorquer, Plasma experiment; **8 processors** (including NVIDIA/TX2), modulated **Exo-Brake**.

TES8/PS8

VR (SJSU Experiment)

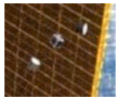

VR Research Experiment

Mission Goal of VR Team

- Obtain **Stereoscopic video** of the exterior of ISS as TES-8 was jettisoned from the NanoRacks Deployer (NRCSD).
- Command TES-8 via Iridium to turn on PhoneSat and command VR to record videos.
- VR provides the ability for millions to experience space missions remotely in 3D.
- Combined with **NVIDIA's TX2 AI compute engine**, it can become a powerful next-gen tool for local real-time **analysis and decision making**.
- Transfer image data to Intel Edison Board
- Analyze packets send via Iridium vs. SBAND
- **Validate NVIDIA** TX2 edge (local) onboard computing capabilities
  - Measure system performance
  - Capture, encode, packetize stereo HD video

Bernardo and Austin working on TechEdSat 8

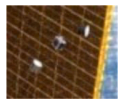

SJSU Software Diagram

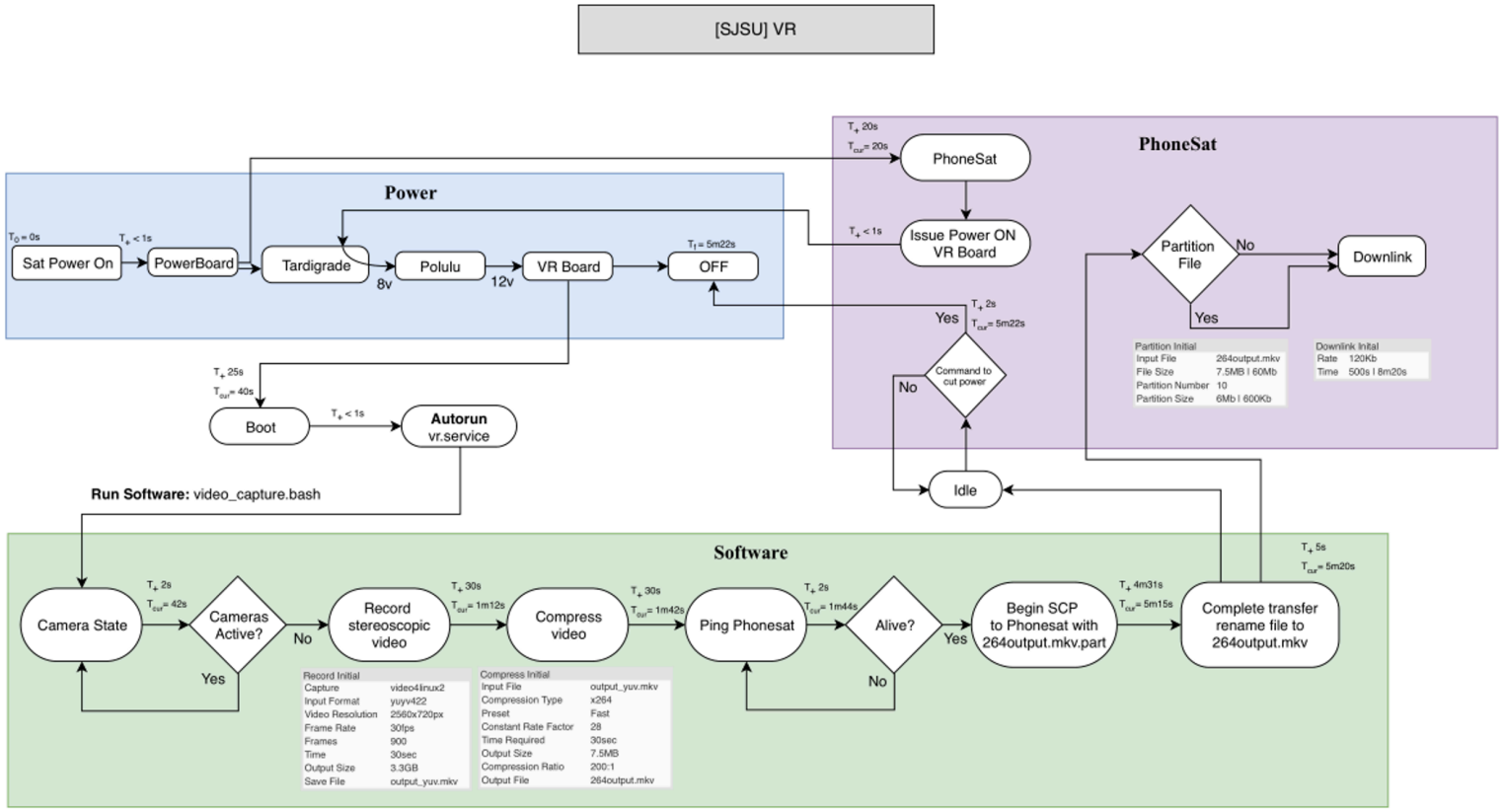

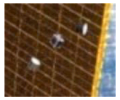

Environmental Testing

Computing

Raspberry PI 3, ODROID-N2, NVidia TX2

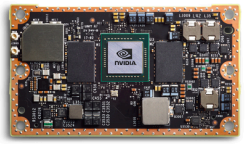

Daughter board

AVerMedia's EX731-AA/N1, Connect Tech's Orbitty Carrier

Camera

ZED Stereo Camera, LI-OV580-STEREO

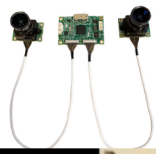

Choices between software.

C++, Shell/Unix, Bash script.

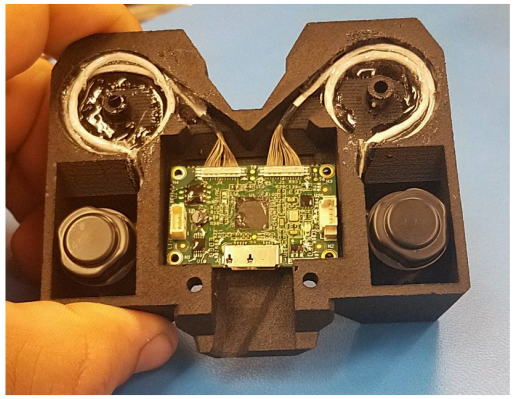

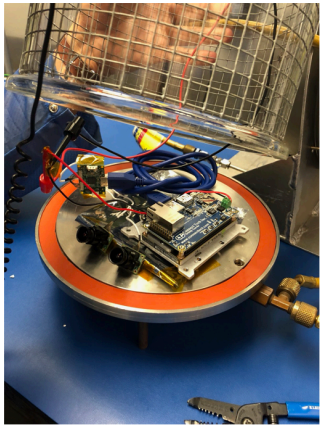

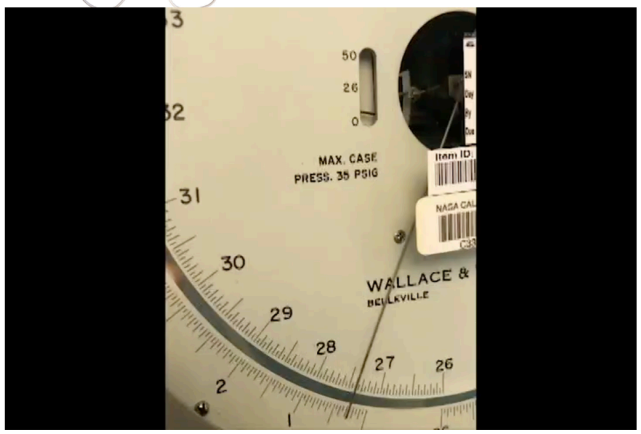

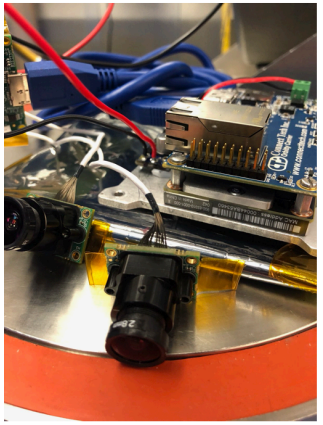

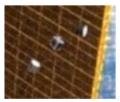

Pre-flight validation test

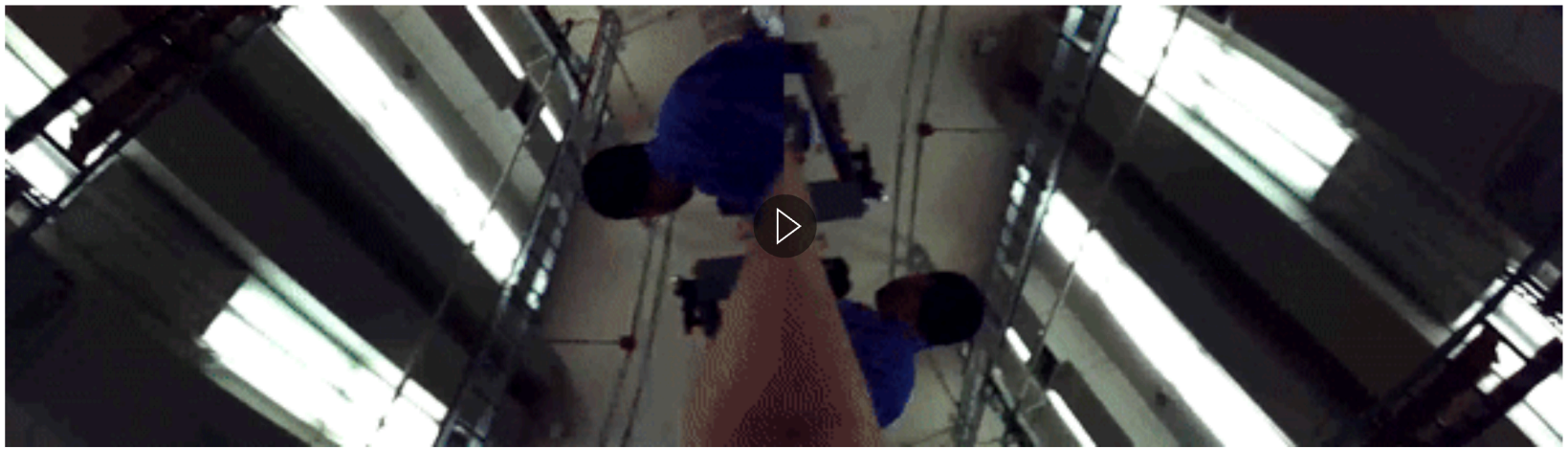

Pre-flight test validation with more than 200:1 compression ratio.

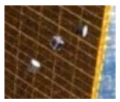

Transmitting from Space

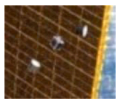

How to bring data down for VR Experiment

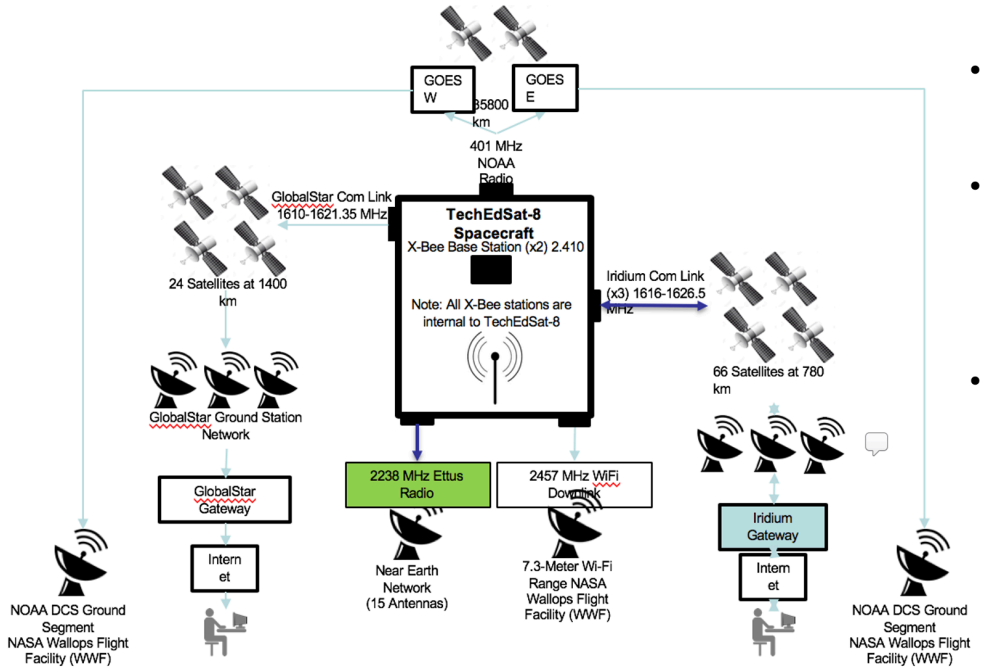

- **NEN-compatible S-band**
  - uses SDR transmitter (ETTUS) intended for use in one of the EM-1 nanosat payloads
- **LEO applications**
  - ~15 ground antennas scattered over the globe
  - Increase of the downlink capability of current generation nano-sats
- **TechEdSat-8 experiment**
  - transmit data gathered from the VR (Virtual Reality) experiment, during which >200:1 compression techniques would be used
  - validate the COM system of a 'pathfinder' EM-1 payload
  - high volumes of optical data would be processed on-board with the NVIDIA TX2 system, compressed, and downlinked.

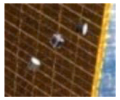

CONOPS

- Nanosat is jettisoned from the ISS/NRCSD
- TES-8 powers the core microprocessors/Iridium/VR/ Cameras
- Records for 30sec (after 42 sec latency)
  - 30 Frames/sec
  - Video resolution 2560x720pixels
  - Total data 3.3GB
- NVIDIA/TX2 performs 200:1 compression to result in 7.5MB (60 Mb)
- Wifi transmission to the PhoneSat/Intel-Edison
- Phonesat partitions compressed file 10x resulting in 6Mb/file
- Wait for Iridium-1,2 command to downlink compressed data to NEN(Near Earth Network) antennas at 125Kb/s
- Repeat 10 times

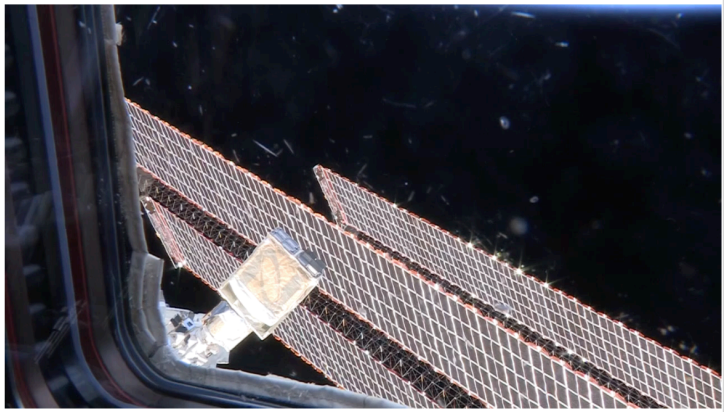

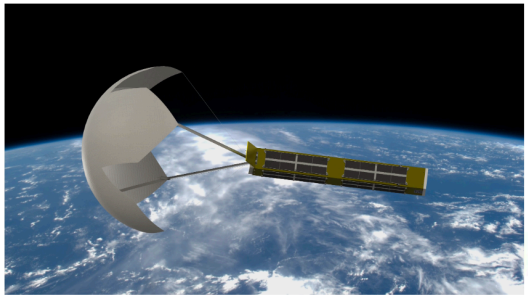

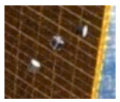

Future Considerations & Iterations

- **More functions** to the Sub system, such as different video types, frame rates, size.
- Different cameras/position on Satellite
- **More cameras** around the whole system. Truly get a full VR experience of the satellite.
- Eventually be able to use this as the eyes to the satellite for later **attitude control designs**.
- First demonstration
  - **Power cycling**, **thermal management**, **data processing**, and **data transfer**
- Compression of very large data for optical instruments (e.g. **hyperspectral**)
- AI algorithms to determine which data sets manipulate and send to ground station
- Coupled with **high data rate downlink capability** (e.g. Use of NEN with S-Band and/or X-BAND Capability; Limited laser com)

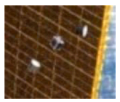

Summary of TechEdSat-8 Mission VR Experiment

- One of the first flight demonstrations of a **COTS graphics GPU** (256-core NVIDIA/TX2) is described
- Flown as a sub-experiment on the **TechEdSat-8 nano-sat** (NASA Ames) and deployed on Jan 31, 2019
- TES-8 is a series nano-sat, with **150W-hr power system** and **8 transmitters** developed as a Nano—Orbital Workshop (**NOW**) to rapidly involve innovative technologies.
- The NVIDIA/TX2 experiment collected **3.3 GB of ISS video data** from the VR experiment and successfully compressed **200:1** using the **H.264 algorithm**.
- The **5.3MB compressed file** was then to be downlinked via an experimental SDR s-band – but **power system** anomaly before the downlink carried out (after 2 successful weeks of operation, partial down link via iridium)
- Minimum use of **high transistor density GPU** appears VIABLE as long as it is used sparingly (due to **radiation effects**, it should be powered 'OFF' unless needed)
- Future tests planned on **TES10, 12** with enhanced SW and revised power subsystem and Lunar Radios

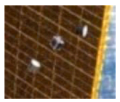

Special Thanks

San Jose State University

AE Department

CS Department

NASA Ames Research Center

Space Project Facility

Small Spacecraft Technology Program

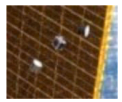

References

- E. J. Wyrwas (Oct 2016) *Proton Testing of nVidia Jetson TX1* https://nepp.nasa.gov/files/28487/NEPP-TR-2016-Wyrwas-16-038-Jetson-TX1-MGH2016Oct-TN44749.pdf
- Nvidia (2017) *Jetson TX2 Developer Kit.* Retrieved from https://developer.nvidia.com/embedded/downloads
- Ffmpeg (2018) *ffmpeg Documentation* Retrieved from https://ffmpeg.org/ffmpeg.html
- ISS Conference 2018-Current Development of the Exo-Brake and Prospects for On-Demand Sample Return from the ISS http://amz.xcdsystem.com/4F14E44B-BC41-E69B-DFAF5A1B1627A0EA_abstract_File10384/PDFUpload_189_0720010951.7.pdf
- ISS Conference 2018-The TechEdSat-N Series: A Collaborative Technology Development Platform in the Nano-Satellite Form Factor http://amz.xcdsystem.com/4F14E44B-BC41-E69B-DFAF5A1B1627A0EA_abstract_File10384/PDFUpload_185_0720010551.4.pdf

Appendix B: Simulation Data at 500 PSI

Model Information

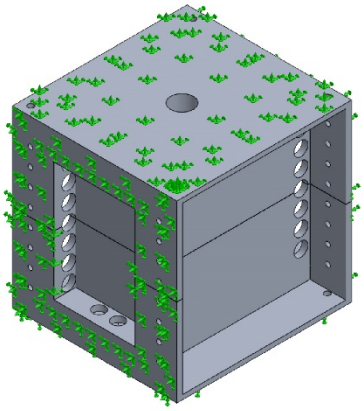

Model name: v1.0 propulsion_tank
Current Configuration: Default

Solid Bodies		
Document Name and Reference	Treated As	Volumetric Properties
v1.0 propulsion_tank A.ipt<1>	Solid Body	Mass:0.261094 kg Volume:9.67016e-05 m^3 Density:2,700 kg/m^3 Weight:2.55872 N
v1.0 propulsion_tank B.ipt<1>	Solid Body	Mass:0.254864 kg Volume:9.43941e-05 m^3 Density:2,700 kg/m^3 Weight:2.49767 N

Study Properties

Study name	Analyze pressure
Analysis type	Static
Mesh type	Solid Mesh
Thermal Effect:	On
Thermal option	Include temperature loads
Zero strain temperature	298 Kelvin
Include fluid pressure effects from SOLIDWORKS Flow Simulation	Off
Solver type	Automatic
Inplane Effect:	Off
Soft Spring:	Off
Inertial Relief:	Off
Incompatible bonding options	Automatic
Large displacement	On
Compute free body forces	On
Friction	Off
Use Adaptive Method:	Off

Units

Unit system:	SI (MKS)
Length/Displacement	mm
Temperature	Kelvin
Angular velocity	Rad/sec
Pressure/Stress	N/m^2

Material Properties

Model Reference	Properties		Components
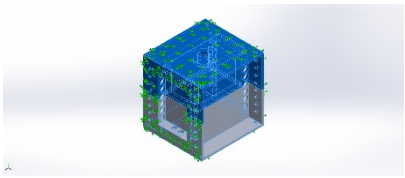	Name: Model type: Default failure criterion: Yield strength: Tensile strength: Elastic modulus: Poisson's ratio: Mass density: Shear modulus: Thermal expansion coefficient:	**6061-T6 (SS)** **Linear Elastic Isotropic** **Max von Mises Stress** **2.75e+08 N/m^2** **3.1e+08 N/m^2** **6.9e+10 N/m^2** **0.33** **2,700 kg/m^3** **2.6e+10 N/m^2** **2.4e-05 /Kelvin**	**SolidBody 1(v1.0 propulsion_tank A.ipt<1>)(v1.0 propulsion_tank.ipt.iam-1/v1.0 propulsion_tank A.ipt-1), SolidBody 1(v1.0 propulsion_tank B.ipt<1>)(v1.0 propulsion_tank.ipt.iam-1/v1.0 propulsion_tank B.ipt-1)**
Curve Data:N/A			

Loads and Fixtures

Fixture name	Fixture Image	Fixture Details
Fixed-1	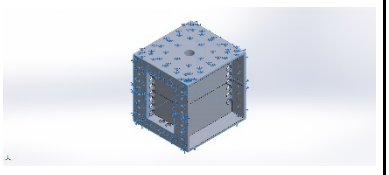	**Entities:** **1 edge(s), 6 face(s)** **Type:** **Fixed Geometry**

Resultant Forces

Components	X	Y	Z	Resultant
Reaction force(N)	**139.701**	**2,027.67**	**-633.231**	**2,128.83**
Reaction Moment(N.m)	**0**	**0**	**0**	**0**

Load name	Load Image	Load Details
Pressure-1	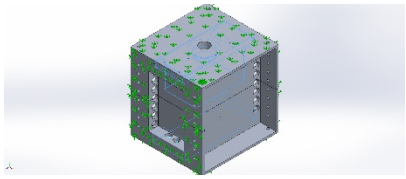	**Entities:** **36 face(s)** **Type:** **Normal to selected face** **Value:** **500** **Units:** **psi** **Phase Angle:** **0** **Units:** **deg**

Contact Information

Contact	Contact Image	Contact Properties
Global Interaction	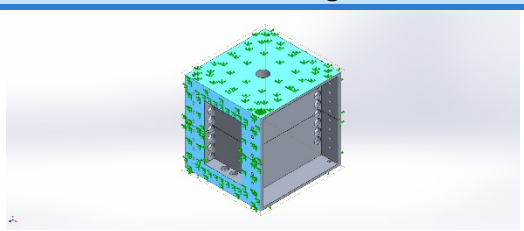	**Type:** Bonded **Components:** 1 component(s) **Options:** Independent mesh

Mesh information

Mesh type	Solid Mesh
Mesher Used:	Standard mesh
Automatic Transition:	Off
Include Mesh Auto Loops:	Off
Jacobian points for High quality mesh	16 Points
Element Size	0.256634 in
Tolerance	0.0128317 in
Mesh Quality	High
Remesh failed parts independently	Off

Mesh information - Details

Total Nodes	34799
Total Elements	17473
Maximum Aspect Ratio	28.288
% of elements with Aspect Ratio < 3	84
Percentage of elements with Aspect Ratio > 10	0.114
Percentage of distorted elements	0
Time to complete mesh(hh;mm;ss):	00:00:02
Computer name:	

Resultant Forces

Reaction forces

Selection set	Units	Sum X	Sum Y	Sum Z	Resultant
Entire Model	N	139.387	1,827.16	-635.662	1,939.59

Reaction Moments

Selection set	Units	Sum X	Sum Y	Sum Z	Resultant
Entire Model	N.m	0	0	0	0

Free body forces

Selection set	Units	Sum X	Sum Y	Sum Z	Resultant
Entire Model	N	0	0	0	0

Free body moments

Selection set	Units	Sum X	Sum Y	Sum Z	Resultant
Entire Model	N.m	0	0	0	0

Study Results

Name	Type	Min	Max
Stress1	VON: von Mises Stress	4.313e-04N/m^2 Node: 13934	2.004e+08N/m^2 Node: 22853

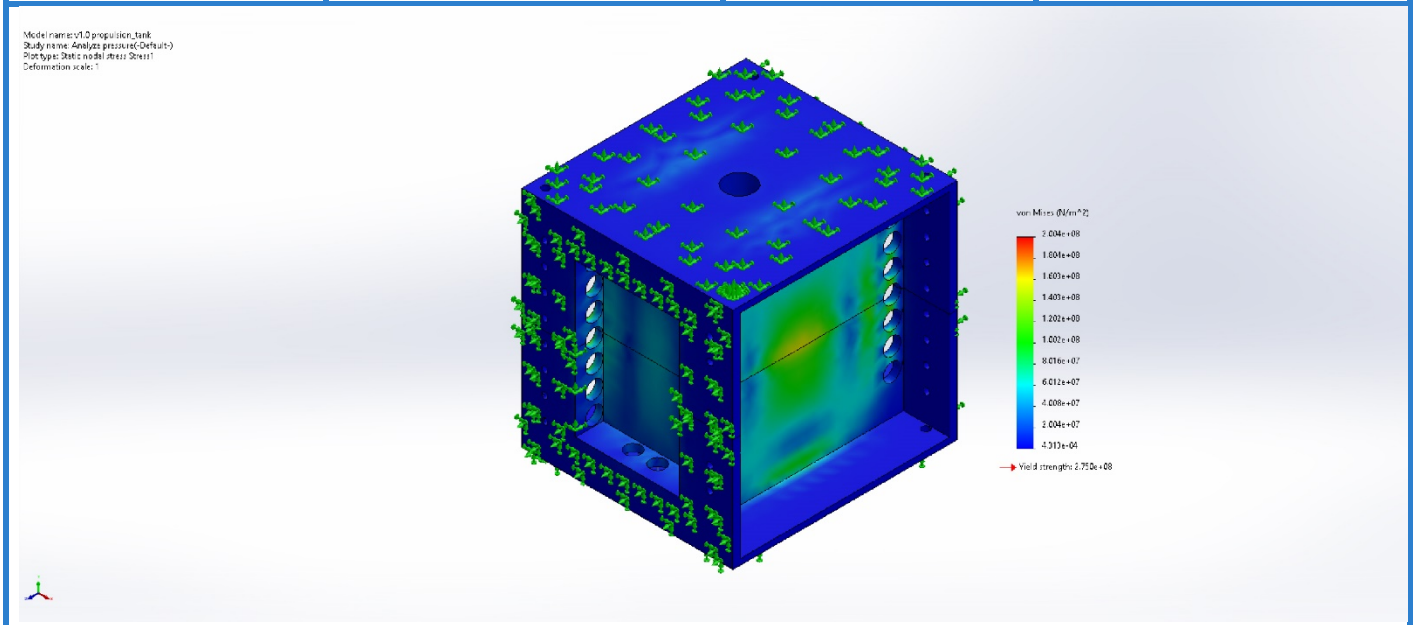

v1.0 propulsion_tank-Analyze pressure-Stress-Stress1

Name	Type	Min	Max
Displacement1	URES: Resultant Displacement	0.000e+00mm Node: 53	2.460e-01mm Node: 2242

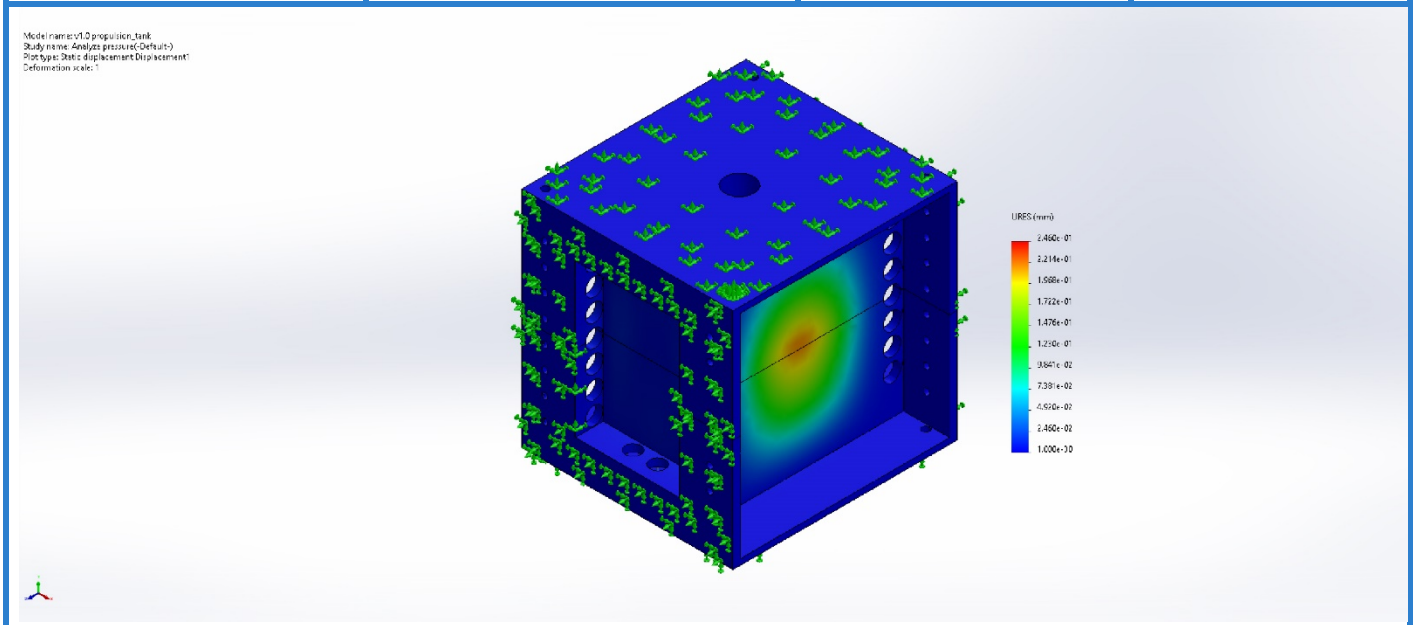

v1.0 propulsion_tank-Analyze pressure-Displacement-Displacement1

Name	Type	Min	Max
Strain1	ESTRN: Equivalent Strain	3.505e-09 Element: 13584	1.854e-03 Element: 12065

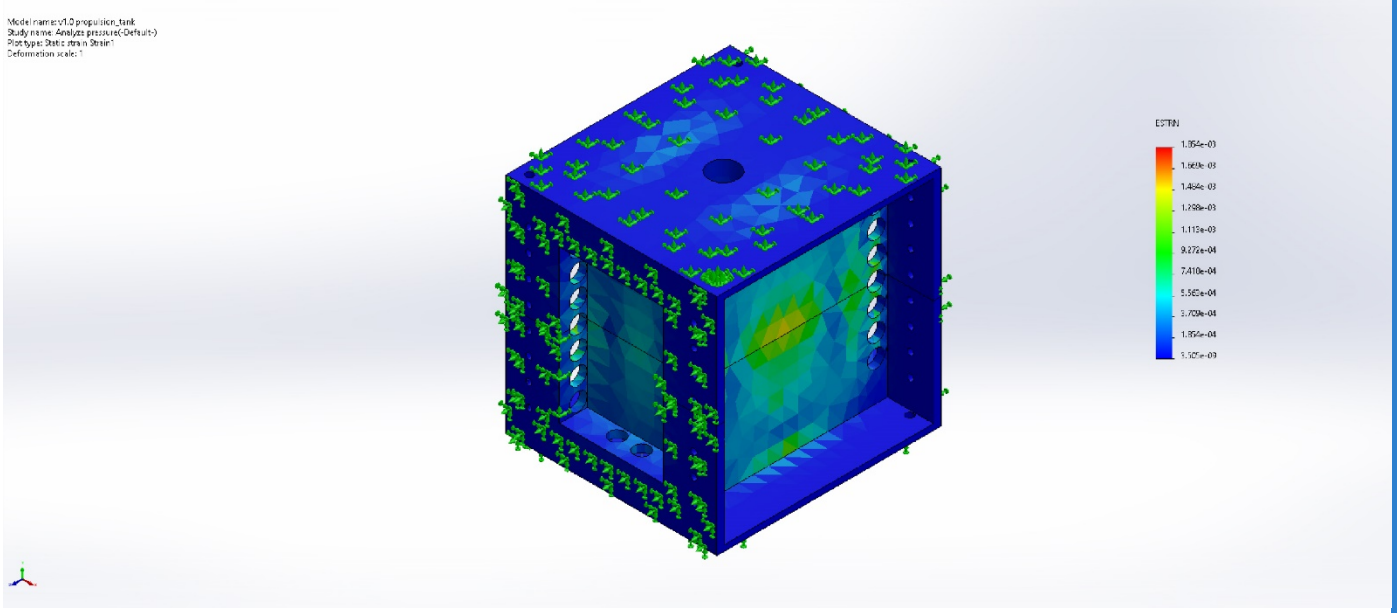

v1.0 propulsion_tank-Analyze pressure-Strain-Strain1

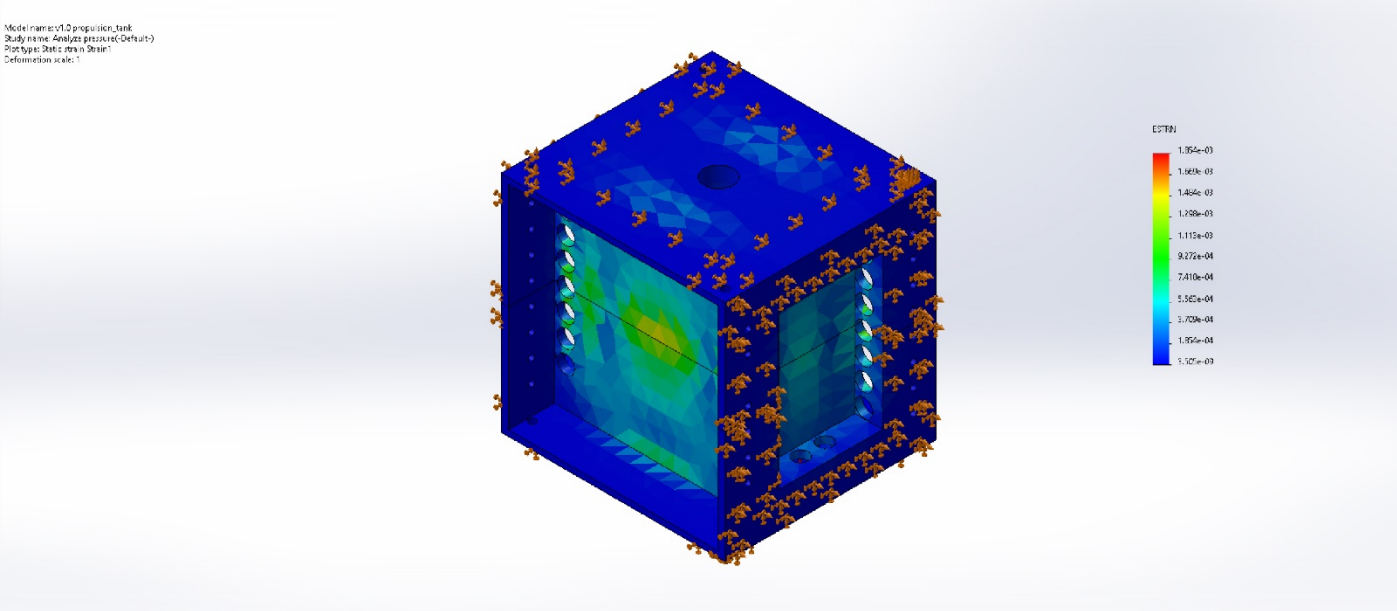

Image-1

Appendix C: Simulation Data at 1000 PSI

Model Information

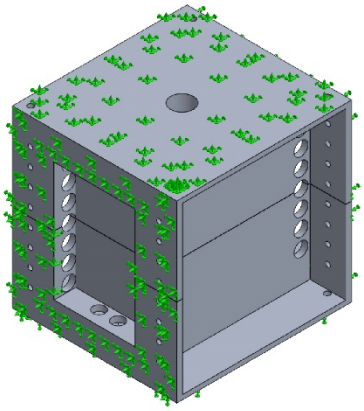

Model name: v1.0 propulsion_tank
Current Configuration: Default

Solid Bodies

Document Name and Reference	Treated As	Volumetric Properties
v1.0 propulsion_tank A.ipt<1>	Solid Body	Mass:0.261094 kg Volume:9.67016e-05 m^3 Density:2,700 kg/m^3 Weight:2.55872 N
v1.0 propulsion_tank B.ipt<1>	Solid Body	Mass:0.254864 kg Volume:9.43941e-05 m^3 Density:2,700 kg/m^3 Weight:2.49767 N

Study Properties

Study name	Static 3 from [Analyze pressure]
Analysis type	Static
Mesh type	Solid Mesh
Thermal Effect:	On
Thermal option	Include temperature loads
Zero strain temperature	298 Kelvin
Include fluid pressure effects from SOLIDWORKS Flow Simulation	Off
Solver type	Automatic
Inplane Effect:	Off
Soft Spring:	Off
Inertial Relief:	Off
Incompatible bonding options	Automatic
Large displacement	On
Compute free body forces	On
Friction	Off
Use Adaptive Method:	Off

Units

Unit system:	SI (MKS)
Length/Displacement	mm
Temperature	Kelvin
Angular velocity	Rad/sec
Pressure/Stress	N/m^2

Material Properties

Model Reference	Properties		Components
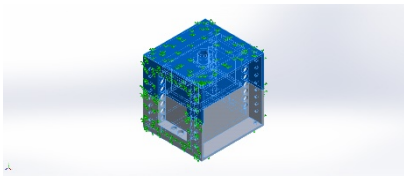	Name: Model type: Default failure criterion: Yield strength: Tensile strength: Elastic modulus: Poisson's ratio: Mass density: Shear modulus: Thermal expansion coefficient:	**6061-T6 (SS)** **Linear Elastic Isotropic** **Max von Mises Stress** **2.75e+08 N/m^2** **3.1e+08 N/m^2** **6.9e+10 N/m^2** **0.33** **2,700 kg/m^3** **2.6e+10 N/m^2** **2.4e-05 /Kelvin**	**SolidBody 1(v1.0 propulsion_tank A.ipt<1>)(v1.0 propulsion_tank.ipt.iam-1/v1.0 propulsion_tank A.ipt-1), SolidBody 1(v1.0 propulsion_tank B.ipt<1>)(v1.0 propulsion_tank.ipt.iam-1/v1.0 propulsion_tank B.ipt-1)**
Curve Data:N/A			

Loads and Fixtures

Fixture name	Fixture Image	Fixture Details
Fixed-1	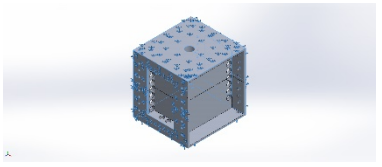	**Entities:** 1 edge(s), 6 face(s) **Type:** Fixed Geometry

Resultant Forces

Components	X	Y	Z	Resultant
Reaction force(N)	**278.982**	**4,056.5**	**-1,265.89**	**4,258.58**
Reaction Moment(N.m)	**0**	**0**	**0**	**0**

Load name	Load Image	Load Details
Pressure-1	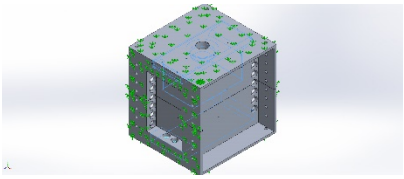	**Entities:** 36 face(s) **Type:** Normal to selected face **Value:** 1,000 **Units:** psi **Phase Angle:** 0 **Units:** deg

Contact Information

Contact	Contact Image	Contact Properties
Global Interaction	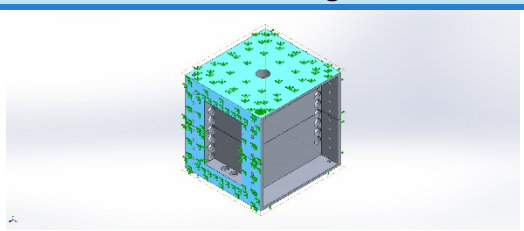	**Type:** Bonded **Components:** 1 component(s) **Options:** Independent mesh

Mesh information

Mesh type	Solid Mesh
Mesher Used:	Standard mesh
Automatic Transition:	Off
Include Mesh Auto Loops:	Off
Jacobian points for High quality mesh	16 Points
Element Size	0.256634 in
Tolerance	0.0128317 in
Mesh Quality	High
Remesh failed parts independently	Off

Mesh information - Details

Total Nodes	34799
Total Elements	17473
Maximum Aspect Ratio	28.288
% of elements with Aspect Ratio < 3	84
Percentage of elements with Aspect Ratio > 10	0.114
Percentage of distorted elements	0
Time to complete mesh(hh;mm;ss):	00:00:02
Computer name:	

Resultant Forces

Reaction forces

Selection set	Units	Sum X	Sum Y	Sum Z	Resultant
Entire Model	N	278.113	3,683.18	-1,270.72	3,906.13

Reaction Moments

Selection set	Units	Sum X	Sum Y	Sum Z	Resultant
Entire Model	N.m	0	0	0	0

Free body forces

Selection set	Units	Sum X	Sum Y	Sum Z	Resultant
Entire Model	N	0	0	0	0

Free body moments

Selection set	Units	Sum X	Sum Y	Sum Z	Resultant
Entire Model	N.m	0	0	0	0

Study Results

Name	Type	Min	Max
Stress1	VON: von Mises Stress	1.565e-03N/m^2 Node: 13934	3.987e+08N/m^2 Node: 22853

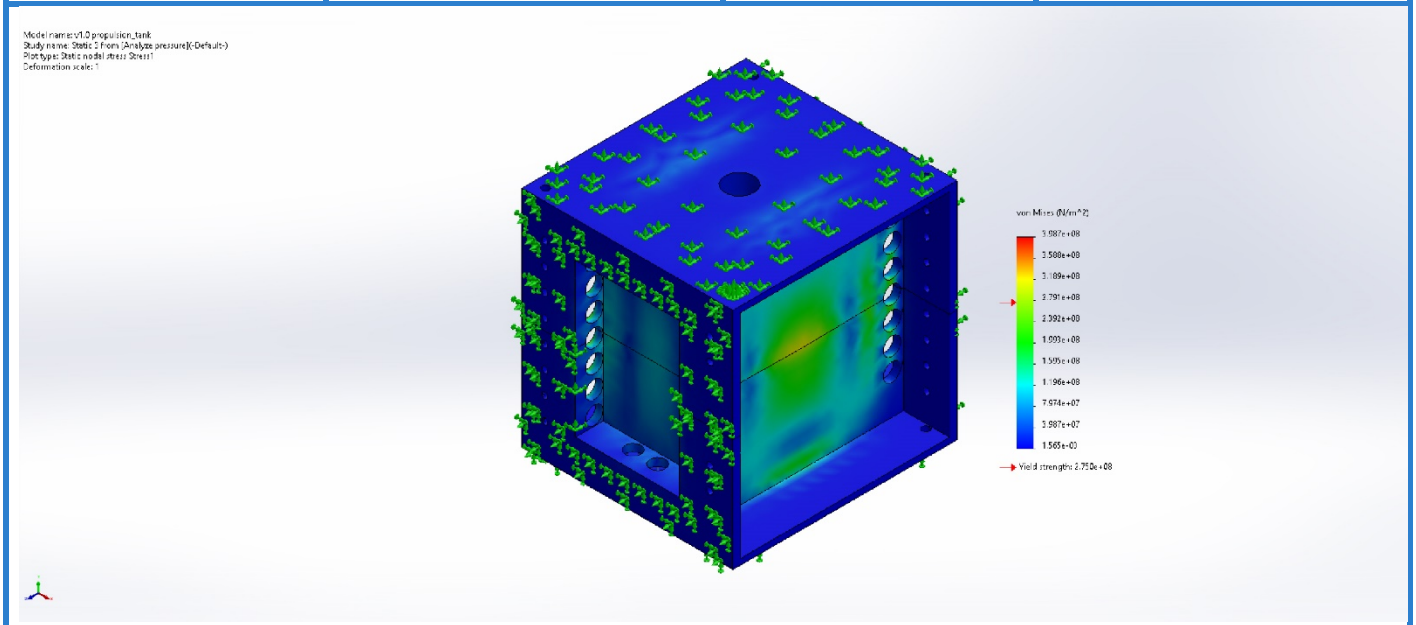

v1.0 propulsion_tank-Static 3 from [Analyze pressure]-Stress-Stress1

Name	Type	Min	Max
Displacement1	URES: Resultant Displacement	0.000e+00mm Node: 53	4.851e-01mm Node: 2242

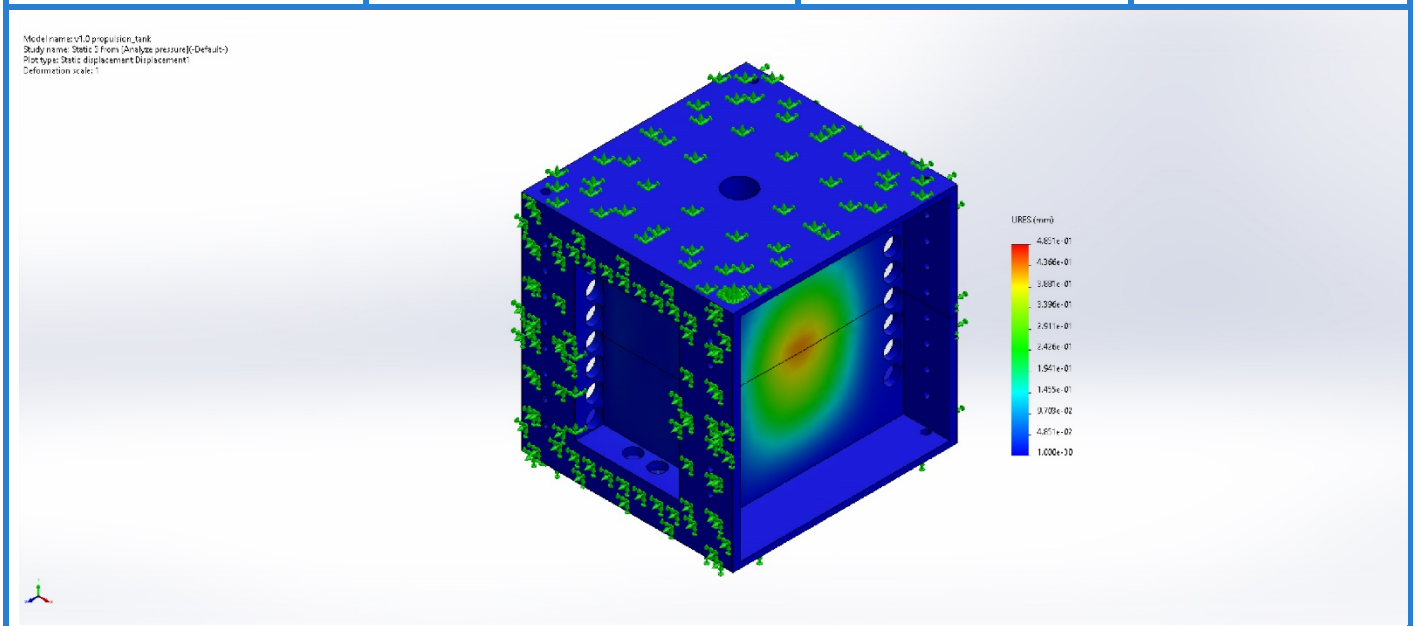

v1.0 propulsion_tank-Static 3 from [Analyze pressure]-Displacement-Displacement1

Name	Type	Min	Max
Strain1	ESTRN: Equivalent Strain	5.270e-09 Element: 13584	3.693e-03 Element: 12065

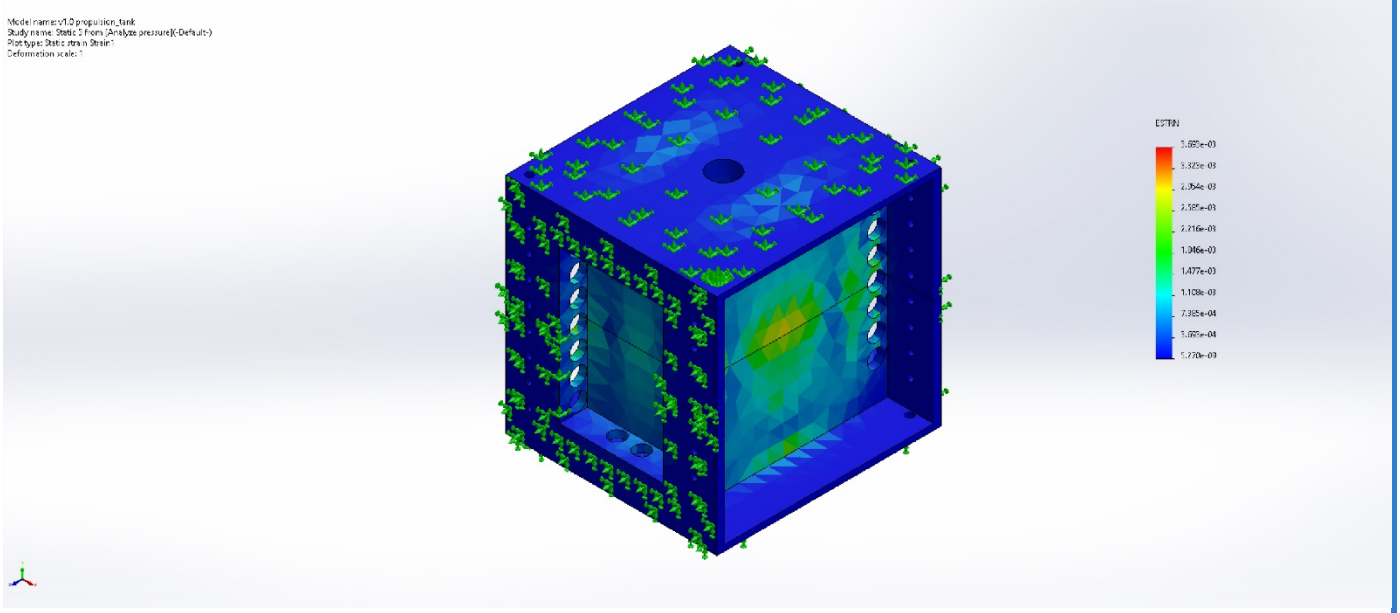

v1.0 propulsion_tank-Static 3 from [Analyze pressure]-Strain-Strain1

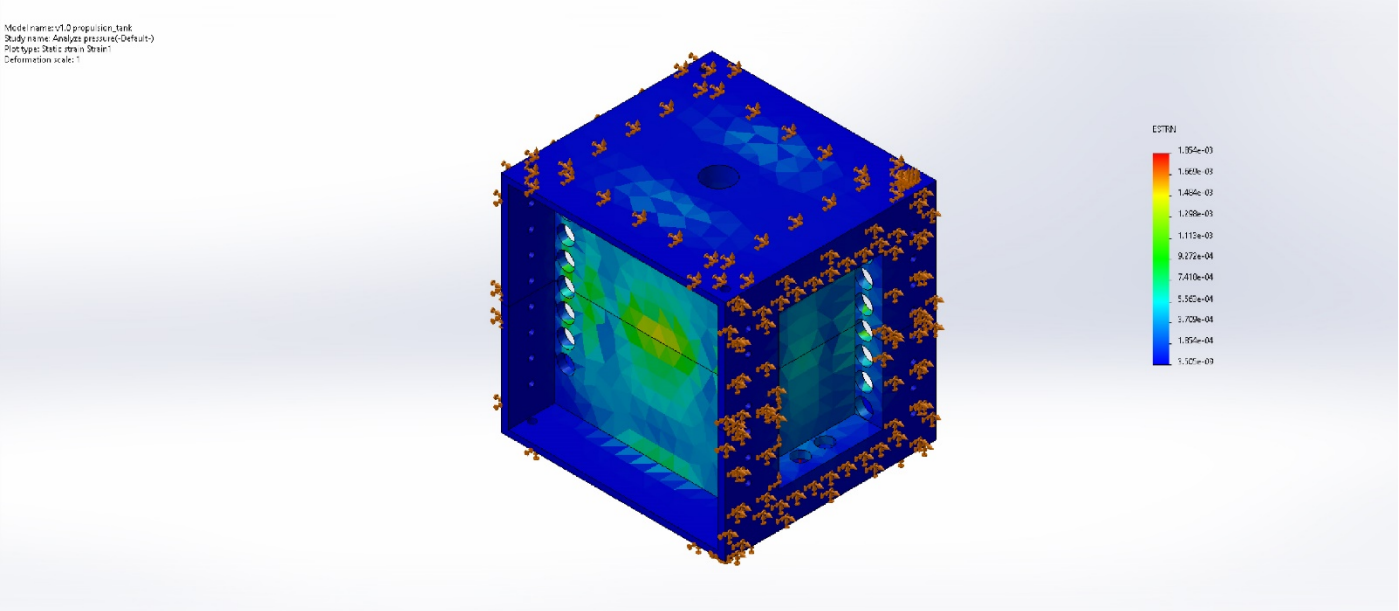

Image-1

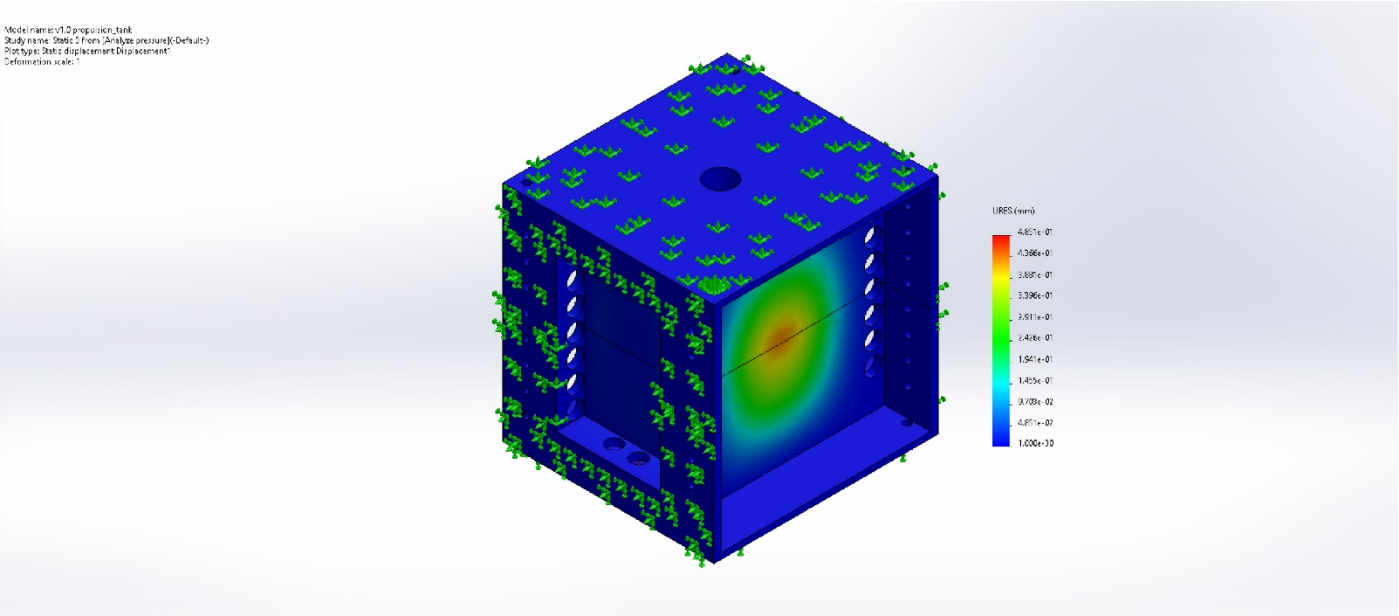
Model name: v1.0 propulsion_tank
Study name: Static 1 From: (Analyze pressure)(-Default-)
Plot type: Static displacement Displacement1
Deformation scale: 1
URES (mm)
4.857e-01
4.368e-01
3.880e-01
3.396e-01
2.911e-01
2.426e-01
1.941e-01
1.455e-01
9.709e-02
4.861e-02
1.000e-30

Image-2

Appendix D: Legend of Symbols, Units, and Abbreviations

Units of Measurement & Common Symbols

- °C (degrees Celsius): A temperature scale where 0°C is the freezing point of water.
- K (Kelvin): The SI base unit for temperature, where 0 K is absolute zero.
- W (Watt): SI unit of power, equivalent to one joule per second.
- mW (milliwatt): 1/1000 of a watt.
- µW (microwatt): 1/1,000,000 of a watt.
- J (Joule): SI unit of energy.
- Pa (Pascal): SI unit of pressure, equal to one newton per square meter.
- psi (pounds per square inch): A unit of pressure commonly used in engineering contexts (non-SI).
- psig (pounds per square inch gauge): Pressure relative to atmospheric pressure.
- g/s (grams per second): A mass flow rate, representing how many grams of mass flow past a point per second.
- mN (millinewton): A unit of force. 1 mN = 0.001 N.
- N (Newton): SI unit of force.
- m/s (meters per second): SI unit of velocity.
- cm (centimeter): 1/100 of a meter.
- mm (millimeter): 1/1000 of a meter.
- nm (nanometer): 1/1,000,000,000 of a meter. Used for wavelength measurements.
- µrad (microradian): An angular measurement. 1 µrad = 10^-6 radians.
- µm (micrometer): A length unit. 1 µm = 10^-6 meters.
- km (kilometer): 1000 meters, used for large distances.
- U (CubeSat Unit): A standardized unit measure for CubeSat dimensions. 1U = 10 cm × 10 cm × 10 cm.
- s (second): SI unit of time.
- Hz (Hertz): Frequency in cycles per second.
- Mbps (Megabits per second): A unit of data rate (1 Mbps = 10^6 bits/s).
- Gbps (Gigabits per second): Data rate (1 Gbps = 10^9 bits/s).
- dB (decibel): A logarithmic unit to express ratios (commonly used in signal strength).

Thermodynamic and Gas Properties

- R (Gas Constant): A constant used in thermodynamics, depends on the gas in question.
- γ (Gamma): The ratio of specific heats (C_p/C_v), commonly 1.4 for diatomic gases.
- Isp (Specific Impulse): A measure of rocket propulsion efficiency, in seconds.

Propulsion & Fluid Dynamics

- Mach number: Ratio of object's speed to the speed of sound in that medium.
- Nozzle throat: The narrowest part of a nozzle, where flow reaches sonic velocity.
- Thrust (N or mN): The force produced by a propulsion system.
- Delta-V (ΔV): Change in velocity, a key measure in orbital mechanics.
- Phase diagram: A chart that shows the state (solid, liquid, gas) of a substance under varying temperature and pressure.

Optical Communication and Related Terms

- FSO (Free-Space Optical) communication: Communication via laser beams transmitted through free space.
- PPM (Pulse Position Modulation): A method of encoding information by varying the position of a pulse in time.
- OOK (On-Off Keying): A simple form of amplitude shift keying in which the presence or absence of a carrier wave indicates binary data.
- QKD (Quantum Key Distribution): A secure communication method using quantum mechanics principles.
- APD (Avalanche Photodiode): A highly sensitive photodiode that provides internal signal gain through avalanche multiplication.
- QPSK (Quadrature Phase-Shift Keying): A modulation method that encodes data by changing the phase of a carrier wave.

Satellite & Aerospace Systems

- CubeSat: A class of nanosatellites built in multiples of a standard 10 cm × 10 cm × 10 cm cubic unit.
- LEO (Low Earth Orbit): An orbit roughly 160 to 2,000 km above Earth.
- ISS (International Space Station): A space station in LEO serving as a microgravity and space environment research laboratory.
- RCS (Reaction Control System): Small thrusters used to maneuver spacecraft.
- MEMS (Microelectromechanical Systems): Miniaturized mechanical and electro-mechanical elements.
- RF (Radio Frequency): Electromagnetic frequencies used in traditional wireless communication.
- ISL (Inter-Satellite Link): A communication link between satellites in space.
- COTS (Commercial Off-The-Shelf): Commercial products ready-made and available for general purchase.
- CCSDS (Consultative Committee for Space Data Systems): International standards organization for space data and information systems.

Organizations and Programs

- NASA (National Aeronautics and Space Administration): The U.S. civil space agency.
- JAXA (Japan Aerospace Exploration Agency): Japan’s national aerospace and space agency.
- ESA (European Space Agency), DLR (German Aerospace Center), CNES (French Space Agency), CSA (Canadian Space Agency): National and international space agencies.
- NICT (National Institute of Information and Communications Technology): A Japanese research institute.

Additional Technical Terms

- TRL (Technology Readiness Level): A measure to assess the maturity level of a technology, from concept to operational system.
- Adaptive optics: A technology used to improve the performance of optical systems by reducing the effect of wavefront distortions.
- Interplanetary: Between planets, referring to space missions beyond Earth orbit.

- SNR (Signal-to-Noise Ratio): A measure comparing the level of a desired signal to the level of background noise.
- Rytov approximation: A model used in optical communication and imaging through atmospheric turbulence.
- LDGM (Low-Density Generator Matrix) codes: A type of forward error correction code.
- Butane, Nitrogen, CO_2, Argon: Various propellants or gases referenced for propulsion tests.
- PSIG: Gauge pressure relative to atmospheric pressure.